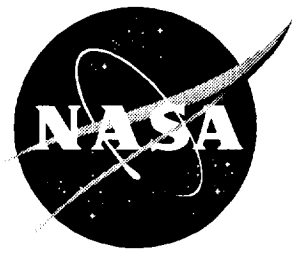

NASA Reference Publication 1376
Volume II

Clouds and the Earth's Radiant Energy System (CERES) Algorithm Theoretical Basis Document

Volume II—Geolocation, Calibration, and ERBE-Like Analyses (Subsystems 1–3)

CERES Science Team

December 1995

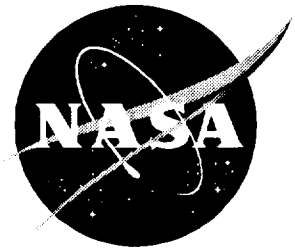

NASA Reference Publication 1376
Volume II

Clouds and the Earth's Radiant Energy System (CERES) Algorithm Theoretical Basis Document

Volume II—Geolocation, Calibration, and ERBE-Like Analyses (Subsystems 1–3)

CERES Science Team
Langley Research Center • Hampton, Virginia

National Aeronautics and Space Administration
Langley Research Center • Hampton, Virginia 23681-0001

December 1995

Available electronically at the following URL address: http://techreports.larc.nasa.gov/ltrs/ltrs.html

Printed copies available from the following:

NASA Center for AeroSpace Information
800 Elkridge Landing Road
Linthicum Heights, MD 21090-2934
(301) 621-0390

National Technical Information Service (NTIS)
5285 Port Royal Road
Springfield, VA 22161-2171
(703) 487-4650

Contents

Preface

The Release-1 CERES Algorithm Theoretical Basis Document (ATBD) is a compilation of the techniques and processes that constitute the prototype data analysis scheme for the Clouds and the Earth's Radiant Energy System (CERES), a key component of NASA's Mission to Planet Earth. The scientific bases for this project and the methodologies used in the data analysis system are also explained in the ATBD. The CERES ATBD comprises 11 subsystems of various sizes and complexities. The ATBD for each subsystem has been reviewed by three or four independently selected university, NASA, and NOAA scientists. In addition to the written reviews, each subsystem ATBD was reviewed during oral presentations given to a six-member scientific peer review panel at Goddard Space Flight Center during May 1994. Both sets of reviews, oral and written, determined that the CERES ATBD was sufficiently mature for use in providing archived Earth Observing System (EOS) data products. The CERES Science Team completed revisions of the ATBD to satisfy all reviewer comments. Because the Release-1 CERES ATBD will serve as the reference for all of the initial CERES data analysis algorithms and product generation, it is published here as a NASA Reference Publication.

Due to its extreme length, this NASA Reference Publication comprises four volumes that divide the CERES ATBD at natural break points between particular subsystems. These four volumes are

I: Overviews
- CERES Algorithm Overview
- Subsystem 0. CERES Data Processing System Objectives and Architecture

II: Geolocation, Calibration, and ERBE-Like Analyses
- Subsystem 1.0. Instrument Geolocate and Calibrate Earth Radiances
- Subsystem 2.0. ERBE-Like Inversion to Instantaneous TOA and Surface Fluxes
- Subsystem 3.0. ERBE-Like Averaging to Monthly TOA

III: Cloud Analyses and Determination of Improved Top of Atmosphere Fluxes
- Subsystem 4.0. Overview of Cloud Retrieval and Radiative Flux Inversion
- Subsystem 4.1. Imager Clear-Sky Determination and Cloud Detection
- Subsystem 4.2. Imager Cloud Height Determination
- Subsystem 4.3. Cloud Optical Property Retrieval
- Subsystem 4.4. Convolution of Imager Cloud Properties With CERES Footprint Point Spread Function
- Subsystem 4.5. CERES Inversion to Instantaneous TOA Fluxes
- Subsystem 4.6. Empirical Estimates of Shortwave and Longwave Surface Radiation Budget Involving CERES Measurements

IV: Determination of Surface and Atmosphere Fluxes and Temporally and Spatially Averaged Products
- Subsystem 5.0. Compute Surface and Atmospheric Fluxes
- Subsystem 6.0. Grid Single Satellite Fluxes and Clouds and Compute Spatial Averages
- Subsystem 7.0. Time Interpolation and Synoptic Flux Computation for Single and Multiple Satellites
- Subsystem 8.0. Monthly Regional, Zonal, and Global Radiation Fluxes and Cloud Properties
- Subsystem 9.0. Grid TOA and Surface Fluxes for Instantaneous Surface Product
- Subsystem 10.0. Monthly Regional TOA and Surface Radiation Budget
- Subsystem 11.0. Update Clear Reflectance, Temperature History (CHR)
- Subsystem 12.0. Regrid Humidity and Temperature Fields

The CERES Science Team serves as the editor for the entire document. A complete list of Science Team members is given below. Different groups of individuals prepared the various subsections that constitute the CERES ATBD. Thus, references to a particular subsection of the ATBD should specify

the subsection number, authors, and page numbers. Questions regarding the content of a given subsection should be directed to the appropriate first or second author. No attempt was made to make the overall document stylistically consistent.

The CERES Science Team is an international group led by 2 principal investigators and 19 coinvestigators. The team members and their institutions are listed below.

CERES Science Team

Bruce A. Wielicki, Interdisciplinary Principal Investigator
Bruce R. Barkstrom, Instrument Principal Investigator

Atmospheric Sciences Division
NASA Langley Research Center
Hampton, Virginia 23681-0001

Coinvestigators

Bryan A. Baum
Atmospheric Sciences Division
NASA Langley Research Center
Hampton, Virginia 23681-0001

Maurice Blackmon
Climate Research Division
NOAA Research Laboratory
Boulder, Colorado 80303

Robert D. Cess
Institute for Terrestrial & Planetary Atmospheres
Marine Sciences Research Center
State University of New York
Stony Brook, New York 11794-5000

Thomas P. Charlock
Atmospheric Sciences Division
NASA Langley Research Division
Hampton, Virginia 23681-0001

James A. Coakley
Oregon State University
Department of Atmospheric Sciences
Corvallis, Oregon 97331-2209

Dominique A. Crommelynck
Institute Royal Meteorologique
B-1180 Bruxelles
Belgium

Richard N. Green
Atmospheric Sciences Division
NASA Langley Research Center
Hampton, Virginia 23681-0001

Robert Kandel
Laboratoire de Meteorologie Dynamique
Ecole Polytechnique
91128 Palaiseau
France

Michael D. King
Goddard Space Flight Center
Greenbelt, Maryland 20771

Robert B. Lee III
Atmospheric Sciences Division
NASA Langley Research Center
Hampton, Virginia 23681-0001

A. James Miller
NOAA/NWS
5200 Auth Road
Camp Springs, Maryland 20233

Patrick Minnis
Atmospheric Sciences Division
NASA Langley Research Center
Hampton, Virginia 23681-0001

Veerabhadran Ramanathan
Scripps Institution of Oceanography
University of California-San Diego
La Jolla, California 92093-0239

David R. Randall
Colorado State University
Department of Atmospheric Science
Foothills Campus, Laporte Avenue
Fort Collins, Colorado 80523

G. Louis Smith
Atmospheric Sciences Division
NASA Langley Research Center
Hampton, Virginia 23681-0001

Larry L. Stowe
NOAA/NWS
5200 Auth Road
Camp Springs, Maryland 20233

Ronald M. Welch
South Dakota School of Mines and Technology
Institute of Atmospheric Sciences
Rapid City, South Dakota 57701-3995

Nomenclature

Acronyms

ADEOS	Advanced Earth Observing System
ADM	Angular Distribution Model
AIRS	Atmospheric Infrared Sounder (EOS-AM)
AMSU	Advanced Microwave Sounding Unit (EOS-PM)
APD	Aerosol Profile Data
APID	Application Identifier
ARESE	ARM Enhanced Shortwave Experiment
ARM	Atmospheric Radiation Measurement
ASOS	Automated Surface Observing Sites
ASTER	Advanced Spaceborne Thermal Emission and Reflection Radiometer
ASTEX	Atlantic Stratocumulus Transition Experiment
ASTR	Atmospheric Structures
ATBD	Algorithm Theoretical Basis Document
AVG	Monthly Regional, Average Radiative Fluxes and Clouds (CERES Archival Data Product)
AVHRR	Advanced Very High Resolution Radiometer
BDS	Bidirectional Scan (CERES Archival Data Product)
BRIE	Best Regional Integral Estimate
BSRN	Baseline Surface Radiation Network
BTD	Brightness Temperature Difference(s)
CCD	Charge Coupled Device
CCSDS	Consultative Committee for Space Data Systems
CEPEX	Central Equatorial Pacific Experiment
CERES	Clouds and the Earth's Radiant Energy System
CID	Cloud Imager Data
CLAVR	Clouds from AVHRR
CLS	Constrained Least Squares
COPRS	Cloud Optical Property Retrieval System
CPR	Cloud Profiling Radar
CRH	Clear Reflectance, Temperature History (CERES Archival Data Product)
CRS	Single Satellite CERES Footprint, Radiative Fluxes and Clouds (CERES Archival Data Product)
DAAC	Distributed Active Archive Center
DAC	Digital-Analog Converter
DB	Database
DFD	Data Flow Diagram
DLF	Downward Longwave Flux

DMSP	Defense Meteorological Satellite Program
EADM	ERBE-Like Albedo Directional Model (CERES Input Data Product)
ECA	Earth Central Angle
ECLIPS	Experimental Cloud Lidar Pilot Study
ECMWF	European Centre for Medium-Range Weather Forecasts
EDDB	ERBE-Like Daily Data Base (CERES Archival Data Product)
EID9	ERBE-Like Internal Data Product 9 (CERES Internal Data Product)
EOS	Earth Observing System
EOSDIS	Earth Observing System Data Information System
EOS-AM	EOS Morning Crossing Mission
EOS-PM	EOS Afternoon Crossing Mission
ENSO	El Niño/Southern Oscillation
ENVISAT	Environmental Satellite
EPHANC	Ephemeris and Ancillary (CERES Input Data Product)
ERB	Earth Radiation Budget
ERBE	Earth Radiation Budget Experiment
ERBS	Earth Radiation Budget Satellite
ESA	European Space Agency
ES4	ERBE-Like S4 Data Product (CERES Archival Data Product)
ES4G	ERBE-Like S4G Data Product (CERES Archival Data Product)
ES8	ERBE-Like S8 Data Product (CERES Archival Data Product)
ES9	ERBE-Like S9 Data Product (CERES Archival Data Product)
FLOP	Floating Point Operation
FIRE	First ISCCP Regional Experiment
FIRE II IFO	First ISCCP Regional Experiment II Intensive Field Observations
FOV	Field of View
FSW	Hourly Gridded Single Satellite Fluxes and Clouds (CERES Archival Data Product)
FTM	Functional Test Model
GAC	Global Area Coverage (AVHRR data mode)
GAP	Gridded Atmospheric Product (CERES Input Data Product)
GCIP	GEWEX Continental-Phase International Project
GCM	General Circulation Model
GEBA	Global Energy Balance Archive
GEO	ISSCP Radiances (CERES Input Data Product)
GEWEX	Global Energy and Water Cycle Experiment
GLAS	Geoscience Laser Altimetry System
GMS	Geostationary Meteorological Satellite
GOES	Geostationary Operational Environmental Satellite
HBTM	Hybrid Bispectral Threshold Method

HIRS	High-Resolution Infrared Radiation Sounder
HIS	High-Resolution Interferometer Sounder
ICM	Internal Calibration Module
ICRCCM	Intercomparison of Radiation Codes in Climate Models
ID	Identification
IEEE	Institute of Electrical and Electronics Engineers
IES	Instrument Earth Scans (CERES Internal Data Product)
IFO	Intensive Field Observation
INSAT	Indian Satellite
IOP	Intensive Observing Period
IR	Infrared
IRIS	Infrared Interferometer Spectrometer
ISCCP	International Satellite Cloud Climatology Project
ISS	Integrated Sounding System
IWP	Ice Water Path
LAC	Local Area Coverage (AVHRR data mode)
LaRC	Langley Research Center
LBC	Laser Beam Ceilometer
LBTM	Layer Bispectral Threshold Method
Lidar	Light Detection and Ranging
LITE	Lidar In-Space Technology Experiment
Lowtran 7	Low-Resolution Transmittance (Radiative Transfer Code)
LW	Longwave
LWP	Liquid Water Path
LWRE	Longwave Radiant Excitance
MAM	Mirror Attenuator Mosaic
MC	Mostly Cloudy
MCR	Microwave Cloud Radiometer
METEOSAT	Meteorological Operational Satellite (European)
METSAT	Meteorological Satellite
MFLOP	Million FLOP
MIMR	Multifrequency Imaging Microwave Radiometer
MISR	Multiangle Imaging Spectroradiometer
MLE	Maximum Likelihood Estimate
MOA	Meteorology Ozone and Aerosol
MODIS	Moderate-Resolution Imaging Spectroradiometer
MSMR	Multispectral, multiresolution
MTSA	Monthly Time and Space Averaging
MWH	Microwave Humidity

MWP	Microwave Water Path
NASA	National Aeronautics and Space Administration
NCAR	National Center for Atmospheric Research
NESDIS	National Environmental Satellite, Data, and Information Service
NIR	Near Infrared
NMC	National Meteorological Center
NOAA	National Oceanic and Atmospheric Administration
NWP	Numerical Weather Prediction
OLR	Outgoing Longwave Radiation
OPD	Ozone Profile Data (CERES Input Data Product)
OV	Overcast
PC	Partly Cloudy
POLDER	Polarization of Directionality of Earth's Reflectances
PRT	Platinum Resistance Thermometer
PSF	Point Spread Function
PW	Precipitable Water
RAPS	Rotating Azimuth Plane Scan
RPM	Radiance Pairs Method
RTM	Radiometer Test Model
SAB	Sorting by Angular Bins
SAGE	Stratospheric Aerosol and Gas Experiment
SARB	Surface and Atmospheric Radiation Budget Working Group
SDCD	Solar Distance Correction and Declination
SFC	Hourly Gridded Single Satellite TOA and Surface Fluxes (CERES Archival Data Product)
SHEBA	Surface Heat Budget in the Arctic
SPECTRE	Spectral Radiance Experiment
SRB	Surface Radiation Budget
SRBAVG	Surface Radiation Budget Average (CERES Archival Data Product)
SSF	Single Satellite CERES Footprint TOA and Surface Fluxes, Clouds
SSMI	Special Sensor Microwave Imager
SST	Sea Surface Temperature
SURFMAP	Surface Properties and Maps (CERES Input Product)
SW	Shortwave
SWICS	Shortwave Internal Calibration Source
SWRE	Shortwave Radiant Excitance
SYN	Synoptic Radiative Fluxes and Clouds (CERES Archival Data Product)
SZA	Solar Zenith Angle
THIR	Temperature/Humidity Infrared Radiometer (Nimbus)

TIROS	Television Infrared Observation Satellite
TISA	Time Interpolation and Spatial Averaging Working Group
TMI	TRMM Microwave Imager
TOA	Top of the Atmosphere
TOGA	Tropical Ocean Global Atmosphere
TOMS	Total Ozone Mapping Spectrometer
TOVS	TIROS Operational Vertical Sounder
TRMM	Tropical Rainfall Measuring Mission
TSA	Time-Space Averaging
UAV	Unmanned Aerospace Vehicle
UT	Universal Time
UTC	Universal Time Code
VAS	VISSR Atmospheric Sounder (GOES)
VIRS	Visible Infrared Scanner
VISSR	Visible and Infrared Spin Scan Radiometer
WCRP	World Climate Research Program
WG	Working Group
Win	Window
WN	Window
WMO	World Meteorological Organization
ZAVG	Monthly Zonal and Global Average Radiative Fluxes and Clouds (CERES Archival Data Product)

Symbols

A	atmospheric absorptance
$B_\lambda(T)$	Planck function
C	cloud fractional area coverage
CF_2Cl_2	dichlorofluorocarbon
$CFCl_3$	trichlorofluorocarbon
CH_4	methane
CO_2	carbon dioxide
D	total number of days in the month
D_e	cloud particle equivalent diameter (for ice clouds)
E_o	solar constant or solar irradiance
F	flux
f	fraction
G_a	atmospheric greenhouse effect
g	cloud asymmetry parameter
H_2O	water vapor

I	radiance
i	scene type
m_i	imaginary refractive index
$\hat{N}$	angular momentum vector
N_2O	nitrous oxide
O_3	ozone
P	point spread function
p	pressure
Q_a	absorption efficiency
Q_e	extinction efficiency
Q_s	scattering efficiency
R	anisotropic reflectance factor
r_E	radius of the Earth
r_e	effective cloud droplet radius (for water clouds)
r_h	column-averaged relative humidity
S_o	summed solar incident SW flux
S_o'	integrated solar incident SW flux
T	temperature
T_B	blackbody temperature
t	time or transmittance
W_{liq}	liquid water path
w	precipitable water
$\hat{x}_o$	satellite position at t_o
x, y, z	satellite position vector components
$\dot{x}, \dot{y}, \dot{z}$	satellite velocity vector components
z	altitude
z_{top}	altitude at top of atmosphere
α	albedo or cone angle
β	cross-scan angle
γ	Earth central angle
γ_{at}	along-track angle
γ_{ct}	cross-track angle
δ	along-scan angle
ε	emittance
Θ	colatitude of satellite
θ	viewing zenith angle
θ_o	solar zenith angle
λ	wavelength
μ	viewing zenith angle cosine

μ_o	solar zenith angle cosine
ν	wave number
ρ	bidirectional reflectance
τ	optical depth
$\tau_{aer}(p)$	spectral optical depth profiles of aerosols
$\tau_{H_2O\lambda}(p)$	spectral optical depth profiles of water vapor
$\tau_{O_3}(p)$	spectral optical depth profiles of ozone
Φ	longitude of satellite
ϕ	azimuth angle
$\tilde{\omega}_o$	single-scattering albedo

Subscripts:

c	cloud
cb	cloud base
ce	cloud effective
cld	cloud
cs	clear sky
ct	cloud top
ice	ice water
lc	lower cloud
liq	liquid water
s	surface
uc	upper cloud
λ	spectral wavelength

Units

AU	astronomical unit
cm	centimeter
cm-sec^{-1}	centimeter per second
count	count
day	day, Julian date
deg	degree
deg-sec^{-1}	degree per second
DU	Dobson unit
erg-sec^{-1}	erg per second
fraction	fraction (range of 0–1)
g	gram
g-cm^{-2}	gram per square centimeter
g-g^{-1}	gram per gram
g-m^{-2}	gram per square meter

h	hour
hPa	hectopascal
K	Kelvin
kg	kilogram
$kg\text{-}m^{-2}$	kilogram per square meter
km	kilometer
$km\text{-}sec^{-1}$	kilometer per second
m	meter
mm	millimeter
μm	micrometer, micron
N/A	not applicable, none, unitless, dimensionless
$ohm\text{-}cm^{-1}$	ohm per centimeter
percent	percent (range of 0–100)
rad	radian
$rad\text{-}sec^{-1}$	radian per second
sec	second
sr^{-1}	per steradian
W	watt
$W\text{-}m^{-2}$	watt per square meter
$W\text{-}m^{-2}sr^{-1}$	watt per square meter per steradian
$W\text{-}m^{-2}sr^{-1}\mu m^{-1}$	watt per square meter per steradian per micrometer

CERES Top Level Data Flow Diagram

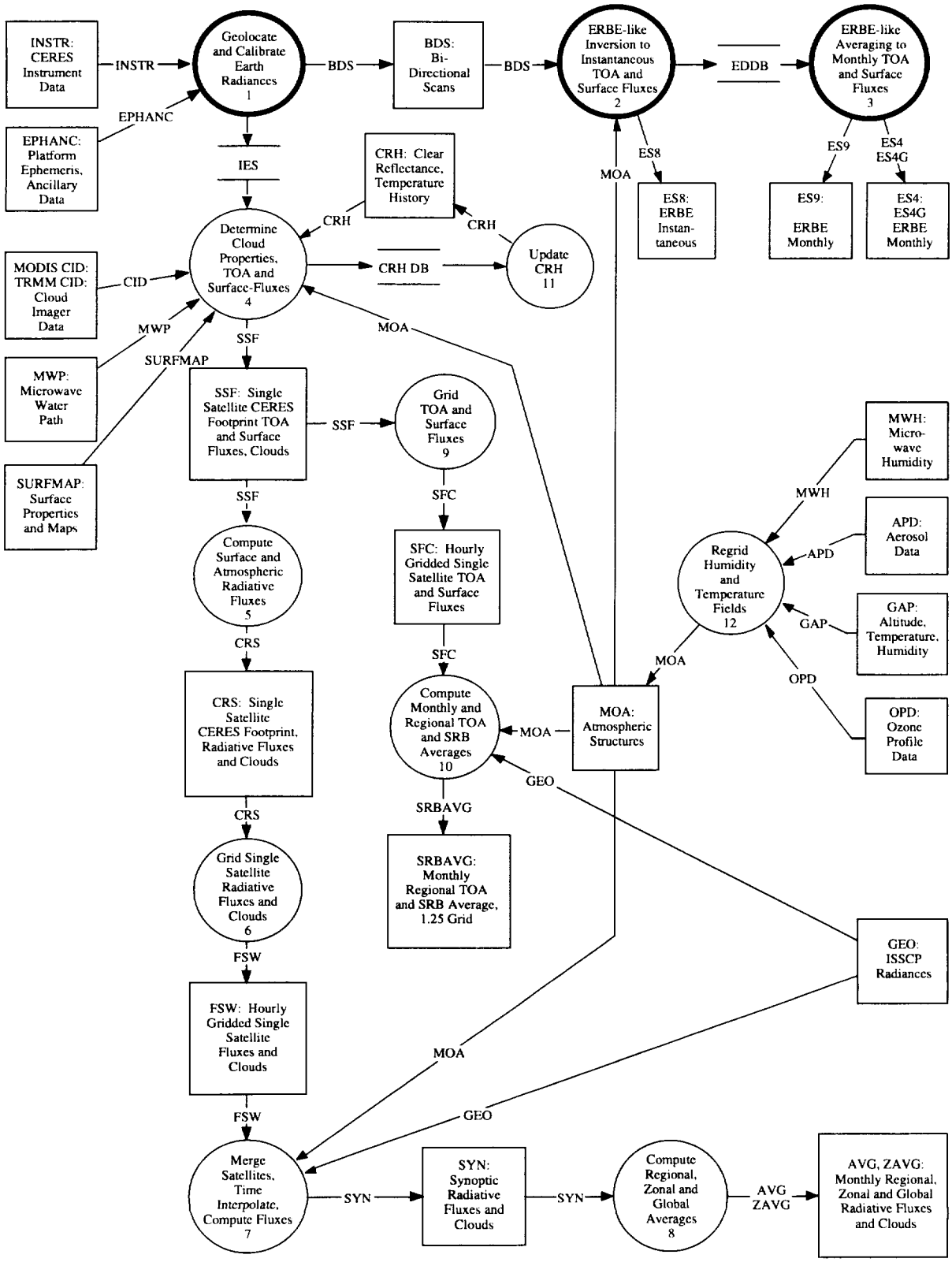

Clouds and the Earth's Radiant Energy System (CERES)

Algorithm Theoretical Basis Document

Instrument Geolocate and Calibrate Earth Radiances

(Subsystem 1.0)

CERES Science Team Cloud Retrieval Working Group

Robert B. Lee III/Group Leader[1]
Brooks A. Childers[1]
Bruce R. Barkstrom/P.I.[1]
G. Louis Smith[1]
Dominique A. Crommelynck[2]

Count Conversion

William C. Bolden[3]
Jack Paden[3]
Dhirendra K. Pandey[3]
Susan Thomas[3]
Robert S. Wilson[3]

Telemetry and Geolocation

Kathy A. Bush[3]
Phillip C. Hess[3]
William L. Weaver[3]

[1]NASA Langley Research Center, Hampton, Virginia 23681-0001
[2]Belgium Royal Meteorological Institute, Avenue Circulaire 3, B-1180 Brussels, Belgium
[3]Science Applications International Corporation (SAIC), Hampton, Virginia 23666

CERES Top Level Data Flow Diagram

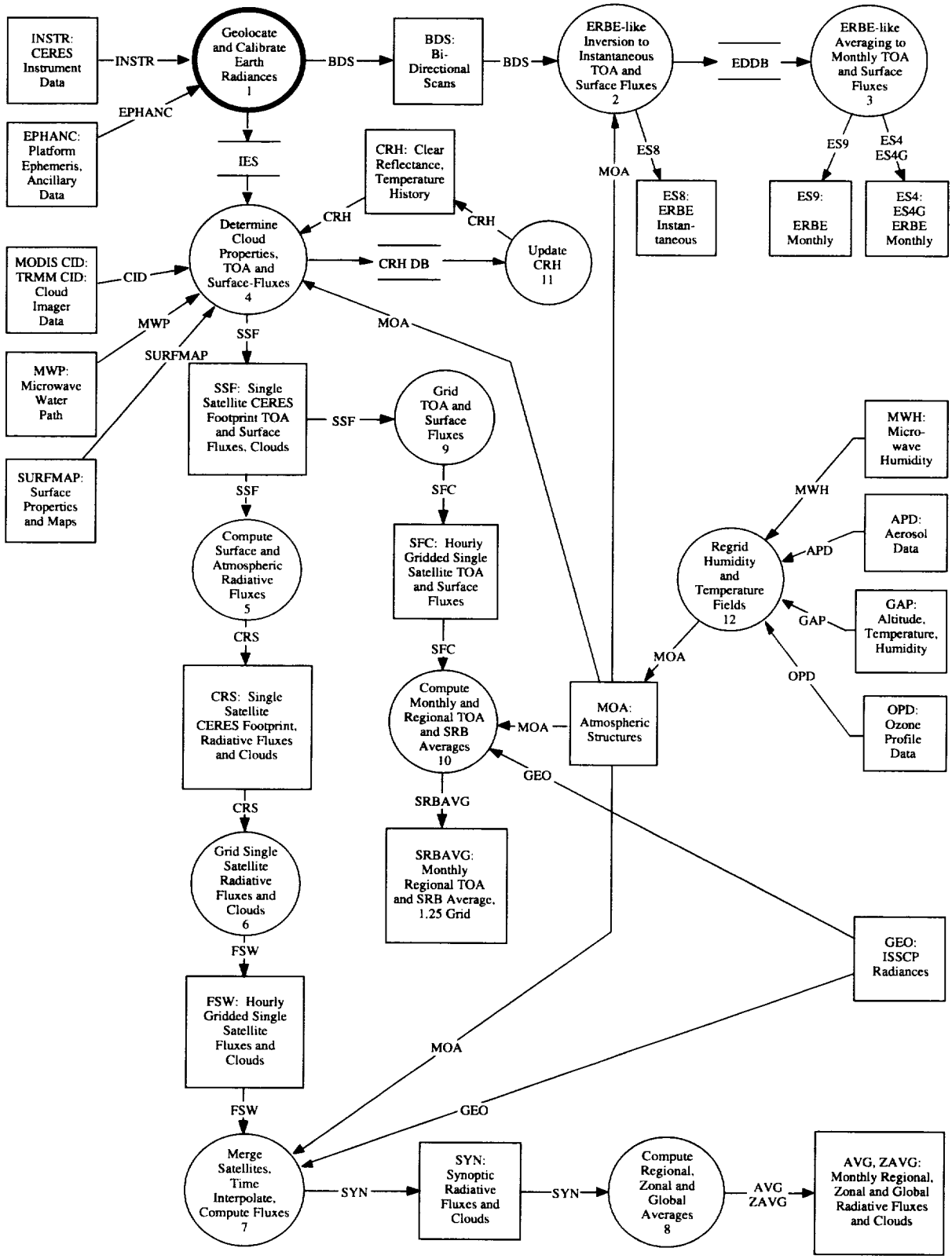

Subsystem 1.0 Top Level Data Flow Diagram

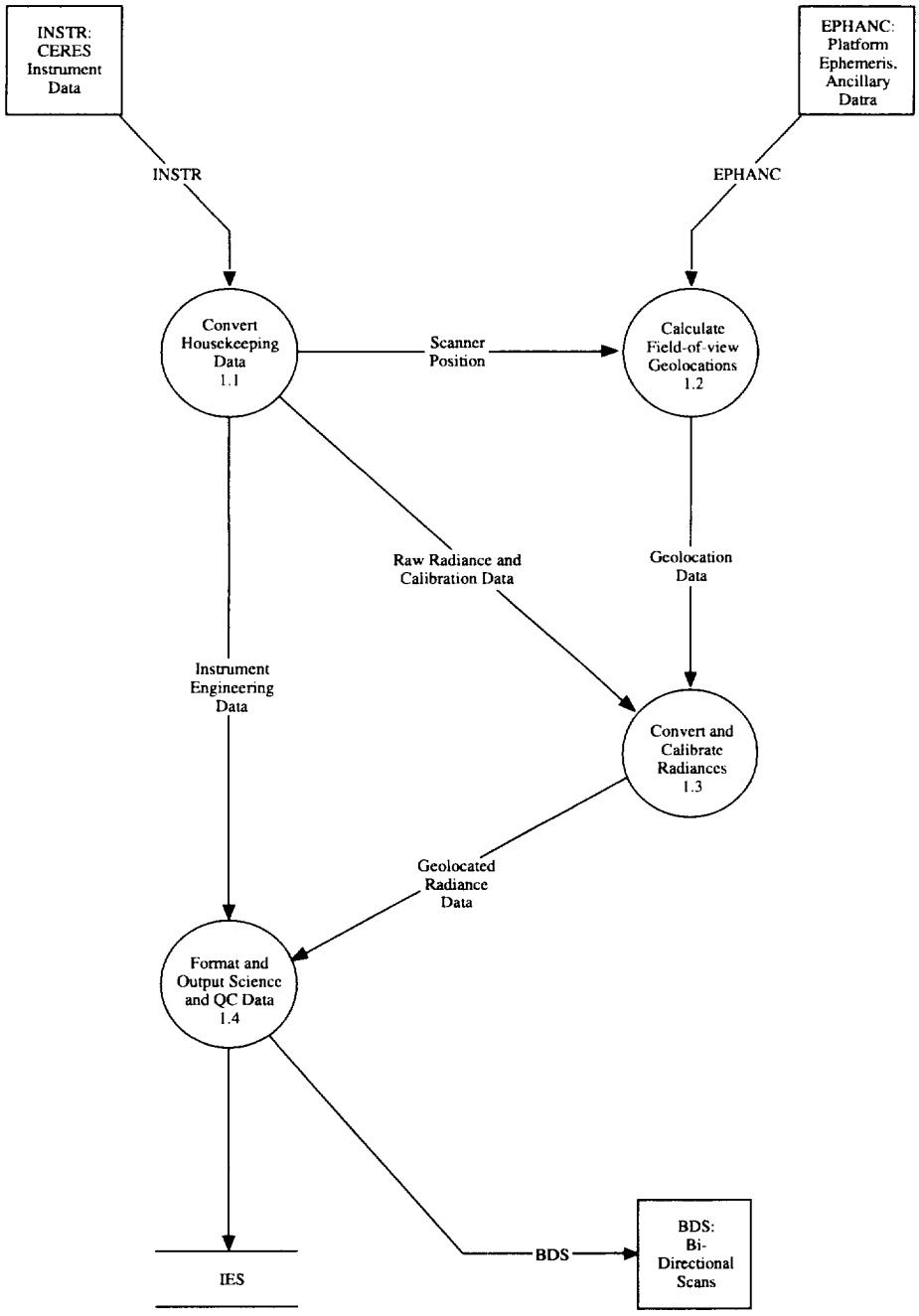

Abstract

The instrument geolocate and calibrate Earth radiance subsystem is the front end of the Clouds and the Earth's Radiant Energy System (CERES) data management system. The spacecraft ephemeris and sensor telemetry are inputs to this subsystem which uses instrument calibration coefficients to convert the spacecraft telemetry inputs into geolocated filtered radiances and housekeeping data into engineering units. These level-1b, chronologically organized standard data products are called the bidirectional scan (BDS) radiances. The BDS product package contains the full set of raw telemetry data along with the converted engineering values. The BDS filtered radiances are converted by the Earth Radiation Budget Experiment (ERBE)-like inversion subsystem into the standard product of unfiltered fluxes at the top of the atmosphere. The instrument subsystem produces nonstandard/ internal radiance products, identified as instrument Earth scan (IES). The IES spatially organized products are inputs to the cloud processing subsystem.

1.0. Instrument Geolocate and Calibrate Earth Radiances

Acronyms

ACA	Azimuth Control Assembly
ADC	Analog-to-Digital Conversion
ADM	Angular Distribution Model
APID	Application Process Identifier
BB	Blackbody
BDS	Bidirectional Scan
CCSDS	Consultative Committee for Space Data Systems, based on octets
CERES	Clouds and Earth's Radiant Energy System
CPU	Central Processing Unit
CRR	Constant Radiance Reference
CSR	Cold Space Reference
DAA	Data Acquisition Assembly
DAC	Digital-to-Analog Converter
DAP	Data Acquisition Processor
ECA	Elevation Control Assembly
EOS	Earth Observing System
ERBE	Earth Radiation Budget Experiment
FOV	Field of View
FTM	Functional Test Model
FTS	Fourier Transform Spectrometer
ICA	Instrument Control Assembly

ICM	Internal Calibration Module
ICP	Instrument Control Processor
ICS	Instrument Coordinate System
ICSBB	Internal Calibration Source Blackbody
IES	Instrument Earth Scan
IPTS-68	International Practical Temperature Scale of 1968
ITS-90	International Temperature Scale of 1990
LW	Longwave
MAM	Mirror Attenuator Mosaic
MEA	Main Electronics Assembly
MODIS	Moderate-Resolution Imaging Spectrometer
NFBB	Narrow Field-of-View Blackbody
PCA	Power Converter Assembly
PFM	Protoflight Model
PRFS	Point Response Function Source
PROM	Programmable Read Only Memory
PRT	Platinum Resistance Thermometer
RAM	Random Access Memory
RAPS	Rotating Azimuth Plane Scan
RCF	Radiometric Calibration Facility
RTM	Radiometric Test Module
S/C	Spacecraft
SEA	Sensor Electronics Assembly
SPS	Solar Presence Sensor
SSA	Sensor Scan Assembly
SW	Shortwave
SWICS	Shortwave Internal Calibration Source
SWRS	Shortwave Reference Source
TACR	Transfer Active Cavity Radiometer
TBD	To Be Defined
TC	Total Channel
TOA	Top of the atmosphere, defined 30 km above the surface of the Earth
TRMM	Tropical Rainfall Measuring Mission
WFBB	Wide Field-of-View Blackbody

Symbols

A_B	Detector bias voltage constant defined by equation (1-21)
A_D	Detector DAC constant defined by equation (1-20)
A_H	Detector heat-sink constant defined by equation (1-19)

A_S	Space observation constant defined by equation (1-18)
A_V	Detector gain expression, defined by equation (1-17)
AB	Detector bias voltage calibration constant
AD	Detector DAC voltage calibration constant
AHA	Detector heat-sink calibration constant
AV	Detector calibration gain
AVA	Detector space observation calibration constant
B	Temperature coefficient of bolometer material, 3400 K
C	Digital-to-analog conversion factor of 409.5 counts per volt
C_1	1.1909×10^{-16} W-m^2
C_2	1.4387×10^{-2} m-K
h	Height of spacecraft above the surface of the Earth
K_{fo}	Post amplification gain
K_T	Housekeeping temperature thermistor coefficient, defined by equation (1-25)
K_1, K_2, K_f, K_{on}, K_{p1}, K_{p2}, K	Housekeeping temperature coefficients defined in table 1-2
L	Filtered radiance
$L(\lambda)$	Unfiltered spectral radiance
m	Detector output signal at time t
m_s	Detector output signal, observing cold space
$o(t)$	Detector offset dependent upon scan geometry (elevation angle)
P	Point spread function
p	Roll angle around the spacecraft X-axis
Q	Heat transfer
q	Pitch angle about spacecraft Y-axis
R	Bolometer resistivity at temperature T
R_e	Earth radius at the equator
R_0	Bolometer resistivity at reference temperature T_0, 250 ohm-cm
R_p	Earth radius at either pole
r	Yaw angle about spacecraft Z-axis
S	Detector response
$S(\lambda)$	Spectral response
$S(\theta,\phi,x,y)$	Detector angular and spatial response
T	Temperature
T_H	Detector heat-sink temperature
T_m	Thermistor temperature
T_0	Reference temperature
T_{PRT}	Detector temperature
T_s	Sensor heater control temperature, defined by equation (1-23)

t	Time
t_k	Time of the reference space observations
t_{ki}	$t_k + i$ (10 msec)
t_0	Time of space observation
V_{bias}	Bolometer bias and bridge voltage
V_D	Detector DAC drift voltage
$V(t)$	Detector output signal voltage at time t
$V(t_k)$	Detector output signal voltage at time t_k space observation
X_I	Instrument fixed X-axis, figure 1-22
X_S	Spacecraft fixed X-axis, figure 1-22
X_β	Detector X-axis, perpendicular to elevation plane
Y_I	Instrument fixed Y-axis, figure 1-22
Y_S	Spacecraft fixed Y-axis, figure 1-22
Y_β	Detector Y-axis, in elevation plane and perpendicular to detector optical axis
Z_I	Instrument fixed Z-axis, figure 1-22
Z_S	Spacecraft fixed Z-axis, figure 1-22
Z_β	Detector Z-axis, aligned with the detector optical axis
α	Azimuthal angle of rotation, between Y_β and Y_α axes
α_b	Absorptance of bolometer black paint layer
β	Elevation angle of rotation
γ	Average time lag between the instantaneous detector optical field of view and point spread function centroid
Δ_t	6.6-sec total scan period
δ_k	Estimate of unaccounted detector drift during the kth scan period
ε	Emittance
η	Heading angle defined between north and the projection of the spacecraft velocity vector in the local horizon plane
θ	Polar angle aligned with optical axis of telescope
Λ	Geodetic longitude of detector measurement
λ	Wavelength, μm
ρ_m	Reflectance of telescope silvered mirrors
σ_k	Noise variance estimate during space measurements
τ	Filter transmission
Φ_G	Geodetic latitude of the detector measurement
ϕ	Azimuthal angle aligned with the scan direction
Ω	FOV solid angle

1.1. Introduction

1.1.1. Algorithm Purpose

The geolocate algorithms are required to identify the geographic scenes emitting the measured filtered radiances and to define the solar and observational geometries of the radiances. The identification of the geographical scenes allows the radiances to be correlated with the cloud coverage of the scene. Scene cloud coverage and solar/observational geometries are vital in the inversion processes in which the filtered radiances are converted into unfiltered fluxes.

In order to determine accurately the scene radiances, the radiometric count conversion algorithms must be adjusted for changes in specific detector housekeeping temperatures and voltages. These specific housekeeping parameters are used as inputs into the radiometric algorithms and calibration processes.

The detectors output signals are fed into the telemetry stream as digital counts, which are converted into voltages. The radiometric count conversion algorithms convert the detector voltages into the level-1 product of radiances, using calibration (count conversion) coefficients which are derived in ground laboratory measurements. The detector radiance conversion algorithms are represented by equations (1-15) through (1-21), while the detector housekeeping algorithms are outlined by equations (1-22) through (1-25). The geolocate algorithms are summarized by equations (1-26) through (1-34).

The "Geolocate and Calibrate Earth Radiances" processing bubble on the Clouds and the Earth's Radiant Energy System (CERES) Top Level Data Flow Diagram, found on page 2, is outlined on page 3. As illustrated in the Geolocate and Calibrate Earth Radiances processing level flow diagram, this instrument subsystem (1) converts the raw housekeeping telemetry into engineering units (temperatures, voltages, etc.), (2) calculates the geographical location of the CERES footprints, (3) merges the raw spacecraft ephemeris and detector point knowledge telemetry, converted housekeeping data, and raw radiometric detector telemetry, (4) revises the radiometric detector count conversion coefficients when required, (5) converts the detector radiometric signals into filtered radiances, and (6) archives the BDS standard products and generates the nonstandard/internal IES products. The CERES instrument pointing knowledge requirement for the geolocated measurements is ±0.1 angular degree per 10 msec, at the spacecraft.

1.1.2. Historical Perspective

The basic geolocate and calibrate algorithms were developed in the Earth Radiation Budget Experiment (Barkstrom et al. 1990) and the Nimbus-7 (Kyle et al. 1993) spacecraft missions. The specific algorithms for the Earth Radiation Budget Experiment (ERBE) thermistor bolometers are outlined by Halyo et al. (1987) and Lee et al. (1989), while geolocate algorithms are summarized by Hoffmann et al. (1987). The geolocate, housekeeping, and radiometric count conversion algorithms are discussed briefly in the sections to follow.

To provide a better understanding of the physical and operational processes vital to these algorithms, the CERES detector characteristics and measurement operational modes are discussed before the algorithms are presented. The input and output products of the instrument subsystem are listed in Appendixes A and B, respectively.

1.2. Instrument Description

1.2.1. General Description

The CERES experiment concepts are built upon the successful legacy of the Earth Radiation Budget Experiment (ERBE) spacecraft mission (Barkstrom et al. 1990). The CERES experiment has challenging goals of defining the Earth-emitted longwave and Earth-reflected solar radiances, with

Table 1-1. Accuracy Requirements (1 σ)

Detector	Shortwave		Total		Window
Spectral Region	0.3 → < 5.0 μm		0.3 → < 100 μm		8 → < 12 μm
Scene Levels	< 100 W-m^{-2}sr^{-1}	> 100 W-m^{-2}sr^{-1}	< 100 W-m^{-2}sr^{-1}	> 100 W-m^{-2}sr^{-1}	All levels
Accuracy Requirements	0.8 W-m^{-2}sr^{-1}	1.0%	0.6 W-m^{-2}sr^{-1}	0.5%	0.3 W-m^{-2}sr^{-1}

precisions (1σ) approaching 0.5 percent and 1.0 percent, respectively, at the instrument level, and measuring narrowband longwave (8-μm to 12-μm) radiances. In table 1-1, the CERES instrument accuracy requirements are listed. The ground calibrations of the CERES sensors are described by Lee et al. (1996).

In addition, the CERES spacecraft investigation is designed to define the physical properties of clouds, define the surface radiation budget, and determine the divergence of energy throughout the atmosphere (Barkstrom 1990, Wielicki and Barkstrom 1991). The CERES instrument packages are scheduled for launch on the NASA Tropical Rainfall Measuring Mission (TRMM) spacecraft as early as 1997 and on the Earth Observing System (EOS) spacecraft platforms starting in 1998. The TRMM spacecraft will be launched into a low-inclination 35°, 350-km altitude orbit by a National Space Development Agency (Japan) launch vehicle. The EOS spacecraft platforms will be launched into a Sun-synchronous polar, 705-km orbit using NASA Atlas IIC launch vehicles.

CERES will focus upon cloud studies and initiate new studies on the surface radiation budget. The work of Ramanathan et al. (1989), based on ERBE detector measurements, has demonstrated that clouds serve to cool the Earth's climate. The higher spatial and spectral resolution cloud pixel measurements from instruments such as the Moderate-Resolution Imaging Spectrometer (MODIS) will be merged with the CERES footprint radiance measurements to provide the best identification of the cloud properties. Along with the continuation of the ERBE-like measurements of reflected solar fluxes and emitted terrestrial fluxes, the CERES instruments will provide angular radiance measurements that will be used to build better Angular Distribution Models (ADM).

The CERES instrument package, as shown in figure 1-1, contains three scanning thermistor bolometer detector units (Lee et al. 1993a) indicated in the figure as total, window, and shortwave detectors. The detectors measure the radiation in the near-visible through far-infrared spectral region. The main electronics assembly (MEA) access connector is shown in the upper portion of the figure, while the mirror attenuator mosaic (MAM) baffles are shown to the right. The CERES detectors are being designed, manufactured, and tested by TRW's Space and Electronics Group, Spacecraft and Technology Division (Redondo Beach, CA) under NASA contract number NAS1-19039. The shortwave detector measures Earth-reflected solar radiation in the wavelength region of 0.3 μm to 5.0 μm; the window detector measures Earth-emitted longwave radiation in the water vapor window wavelength region of 8 μm to 12 μm; and the total detector measures radiation in the range of 0.2 μm to 200 μm. In figure 1-2, the spectral responses of the detectors are shown. The responses represent the spectral throughput of the individual detector optical elements, illustrated in figure 1-3. The detectors are coaligned and mounted on a spindle that rotates about the elevation axis. The detectors fields of view overlap about 98 percent.

1.2.2. Detector Element

Each CERES detector unit consists of telescope baffle, telescope, and thermistor bolometer detector modules as shown in figure 1-3. The detector module consists of an active and a reference thermistor bolometer flake with time constants less than 9 and 12 milliseconds, respectively. The telescope baffle prevents radiation from striking the active bolometer flake at angles greater than 16° off the telescope optical axis. The f/1.8 Cassegrainian telescope module has an 18-mm diameter silvered primary mirror

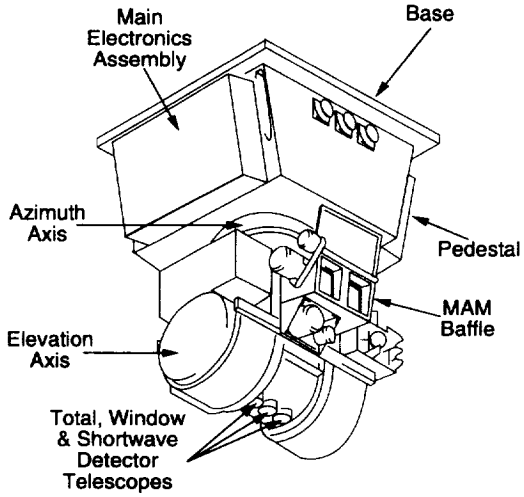

Figure 1-1. CERES instrument.

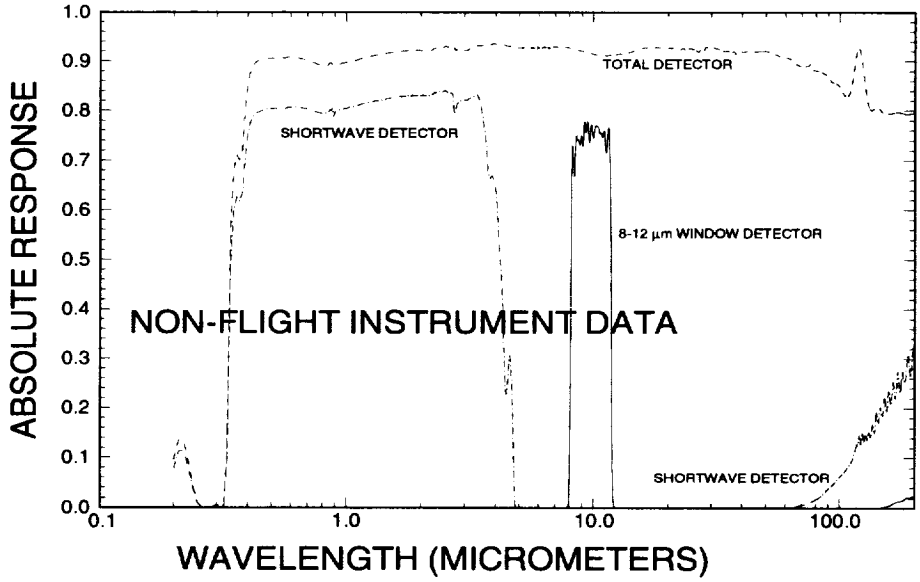

Figure 1-2. Spectral responsivity of CERES detectors.

and a silvered secondary mirror. In the shortwave and window detectors, the filters are located before the secondary mirror spider and in front of the active bolometer flake. The shortwave detector has a filter made of Dynasil, fused, waterless quartz. The 8 μm–12 μm window detector has 1-mm-thick zinc sulfide and 0.5-mm-thick cadmium telluride filter elements. The total detector does not have an optical filter. The active and the reference flakes are arranged on a heat sink, which is maintained at a constant temperature of 38°C using 1.9-watt electrical heaters. The surfaces of both the active flake and the reference bolometers are covered with an 11-μm-thick absorptive black paint layer of Aeroglaze Z-306 that is doped with 10-percent carbon black. The absorptance of the paint layer is greater than 85 percent out to 100 μm (Jarecke et al. 1991). The cross-sectional view of a bolometer detector element assembly is given in figure 1-4.

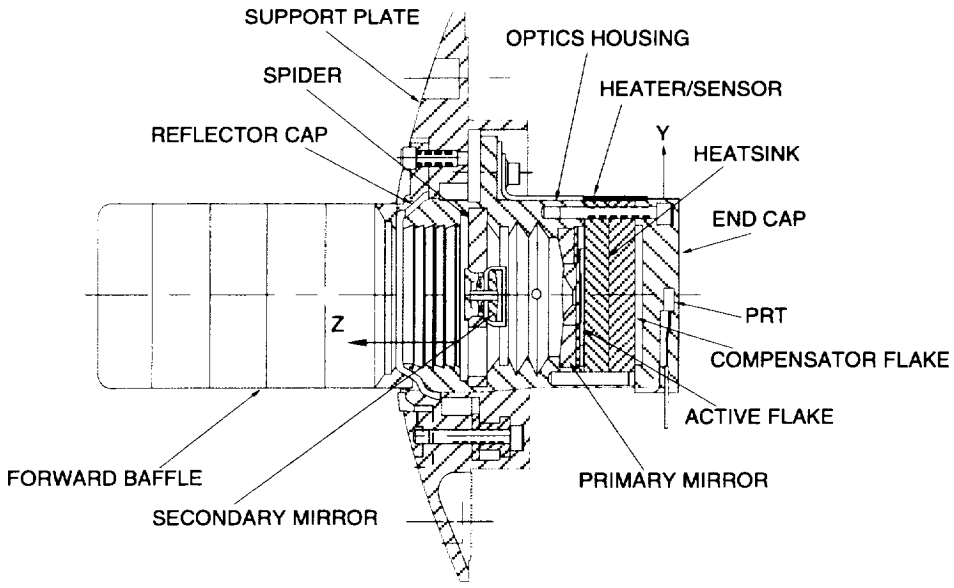

Figure 1-3. CERES baffle, telescope, and detection modules.

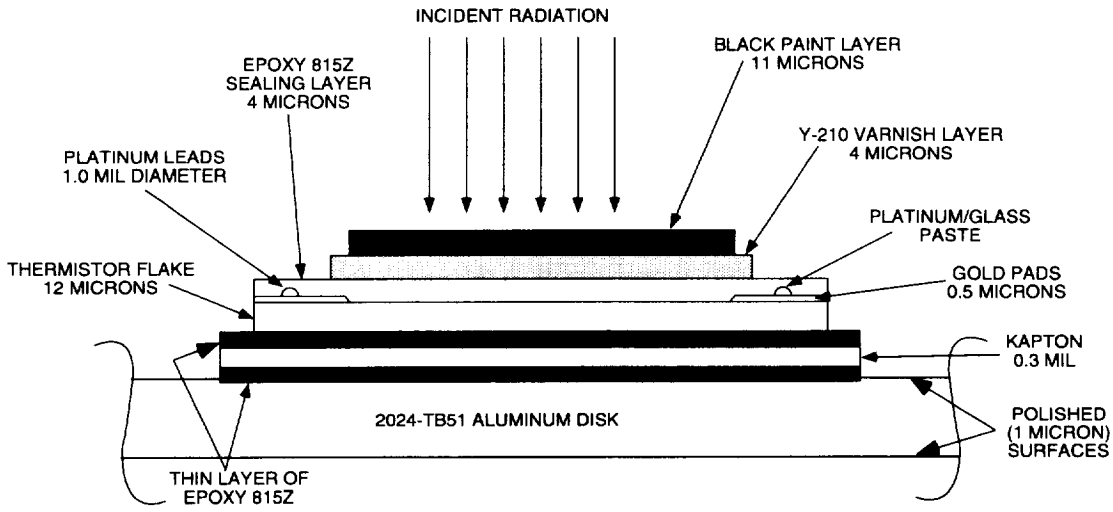

Figure 1-4. Detector element assembly cross-section.

The black paint layer on the active flake absorbs and converts the target scene energy into heat, which causes a measurable change in the bolometer electrical resistance. The bolometer consists of a sintered semiconductor material with a high negative coefficient of resistance. The bolometer electrical resistivity, R, can be represented as a function of the temperature, T, by the following equation (Astheimer 1983)

$$R = R_0 \exp\left[B\left(\frac{1}{T} - \frac{1}{T_0}\right)\right] \tag{1-1}$$

where R_o is the resistance at the reference temperature T_0 (293 K), and B (3400 K) is the temperature coefficient of the bolometer material. The sintered semiconductor bolometer material is a mixture of

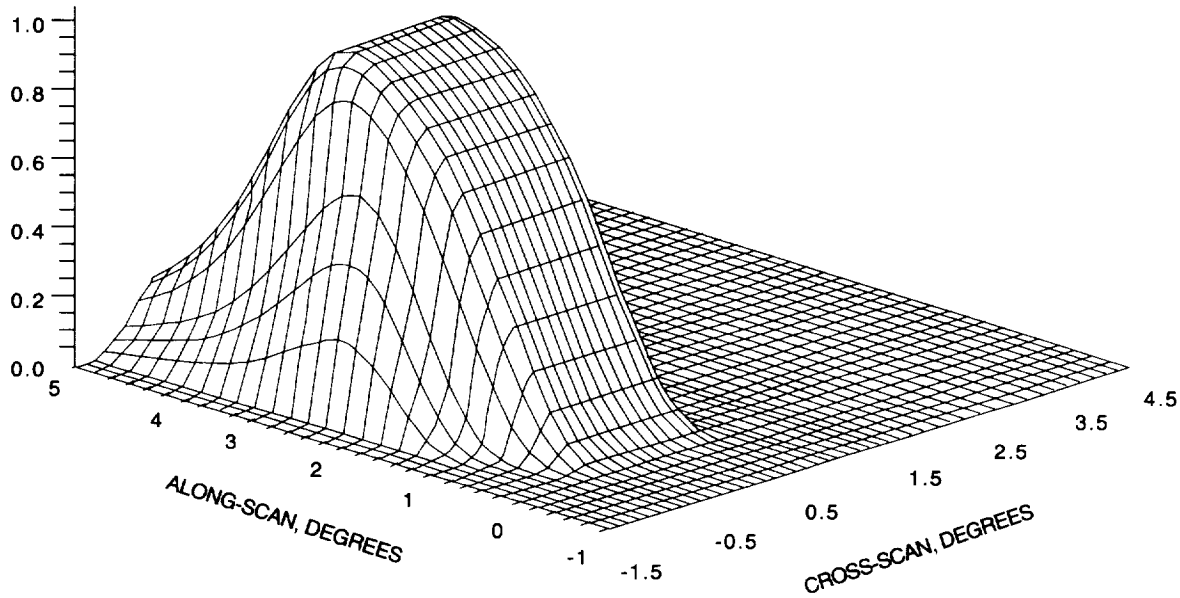

Figure 1-5. Illustration of point spread function.

manganese, nickel, and cobalt oxides having a resistivity, R_0, of approximately 250 ohm-cm at 25°C. Note that Astheimer's Equation and equation (1-1) are equivalent except for a geometric constant factor associated with the thermistor that relates resistivity and resistance. Because the temperature of the bolometer responses to both incoming radiation and heat conducted from the heat sink, we used a compensator bolometer flake to follow thermal changes in the heat sink. The active and compensator bolometer flakes are elements of a Wheatstone bridge. Thus, the bridge output is determined by the scene dependent energy that is absorbed and sensed by the active flake.

The radiometric measurements are sampled from the detectors every 10 milliseconds. The radiation being sampled enters the telescope and strikes the 0.75-mm by 1.50-mm hexagonal precision field stop. The field stop aperture restricts the detector field of view to 1.3° by 2.6°; the small angular dimension is in the elevation plane and the larger dimension is perpendicular to the elevation plane. The bolometer signal is then passed through a noise filter and a 4-pole Bessel filter. The filter further delays and smooths the analog signal before the electronics sample it. The field of view footprints of the CERES detectors are approximately 10- and 20-km squares at nadir for the instruments on the TRMM and EOS spacecraft, respectively. Portions of the Earth near the center of the optical axis will contribute more strongly to the measurements than those off center. Quantitatively, each part of the field of view contributes according to the point spread function (P) as shown in figure 1-5 (Smith 1994); the normalized detector response is plotted as functions of along-scan and cross-scan angles, which are found perpendicular to and in the elevation plane, respectively. If the half power point is considered to be the footprint, the CERES footprint measured in Earth central angle is about 4 degrees along track and 2.6 degrees cross track. The point spread function is used in the data reduction algorithms, as described later in sections 1.3.2, Algorithms/Theoretical Basis and 1.3.3, Flight Algorithms/Practical Basis. The TRMM and EOS detector pointing requirements are presented in tables 1-2 and 1-3.

1.2.3. Instrument Operations

1.2.3.1. General. The CERES instrument has an operational cycle of 6.6 seconds and several different operational modes, shown in table 1-4. The outputs of the detectors are sampled every 10 milliseconds in all operational modes. While the detectors rotate in the vertical (elevation scan) and horizontal

Table 1-2. TRMM Pointing Requirements

Science requirement	Mission requirement	Boresight requirement	CERES instrument capability	TRMM capability	CERES/TRMM capability
Sensor coalignment	98 percent common FOV	98 percent common FOV	>98 percent common FOV	N/A	N/A
Pointing knowledge	10 percent effective FOV	9.8 arc-min	3 arc-min (0.05°)	12 arc-min	12.4 arc-min
Pointing accuracy	Earth/Sun knowledge	<30 arc-min	3 arc-min (0.05°)	24 arc-min	24.2 arc-min
Coregistration	0.75 km	7.4 arc-min	3 arc-min (0.05°)	6 arc-min	6.7 arc-min
Jitter	2 percent of FOV	2.0 arc-min/Earth Scan	0.6 arc-min (0.01°)	6 arc-min/ 1 sec	6 arc-min/ 1 sec

Table 1-3. EOS-AM Pointing Requirements

Science requirement	Mission requirement	Boresight requirement	CERES instrument capability	EOS-AM capability	CERES/EOS-AM capability
Sensor coalignment	98 percent common FOV	98 percent common FOV	>98 percent common FOV	N/A	N/A
Pointing knowledge	10 percent effective FOV	588 arc-sec	180 arc-sec (0.05°)	114 arc-sec	215 arc-sec
Pointing accuracy	Earth/Sun knowledge	<1800 arc-sec	180 arc-sec (0.05°)	312 arc-sec	360 arc-sec
Coregistration	0.75 km	215 arc-sec	180 arc-sec (0.05°)	215 arc-sec	215 arc-sec
Jitter	2 percent of FOV	120 arc-sec/Earth Scan	36 arc-sec (0.01°)	36 arc-sec/ 6.6 sec	79 arc-sec/ 6.6 sec

Table 1-4. Operational Modes and Configurations of CERES Instrument

	Fixed azimuth scan mode	Rotating azimuth plane scan mode	Solar calibration mode	Standby mode	Diagnostic mode	Safe mode
Nominal profile	Normal Earth scan	Normal Earth scan	MAM scan	Scan head stowed	Scan head stowed	Scan head stowed
Secondary profile	N/A	Short scan	N/A	N/A	N/A	N/A
Azimuth angle	Crosstrack (180°)	Uprange-downrange (90°–270°)	At predicted Sun angle	Braked at arbitrary angle	TBD	Braked at arbitrary angle
Inflight calibration sources	OFF or alternate: ON and OFF for internal vals	OFF or alternate: ON and OFF for internal cals	OFF	OFF	OFF	OFF
Data type	Science	Science	Calibration	Diagnostic	Diagnostic	Diagnostic
Data output format	Science	Science	Science	Science	Diagnostic	Science or diagnostic

(azimuth rotation) planes, the instrument makes Earth science measurements. The scanning geometry for the CERES detectors is illustrated in figure 1-6. The instrument has built-in calibration sources, for performing flight calibrations, and can be calibrated by measuring solar radiances reflected by a solar diffuser plate into the instrument field of view.

There are two basic elevation scan profiles associated with the fixed-azimuth and rotating-azimuth plane scan (RAPS) modes: the normal Earth scan and the short Earth scan profile. Figure 1-6 identifies

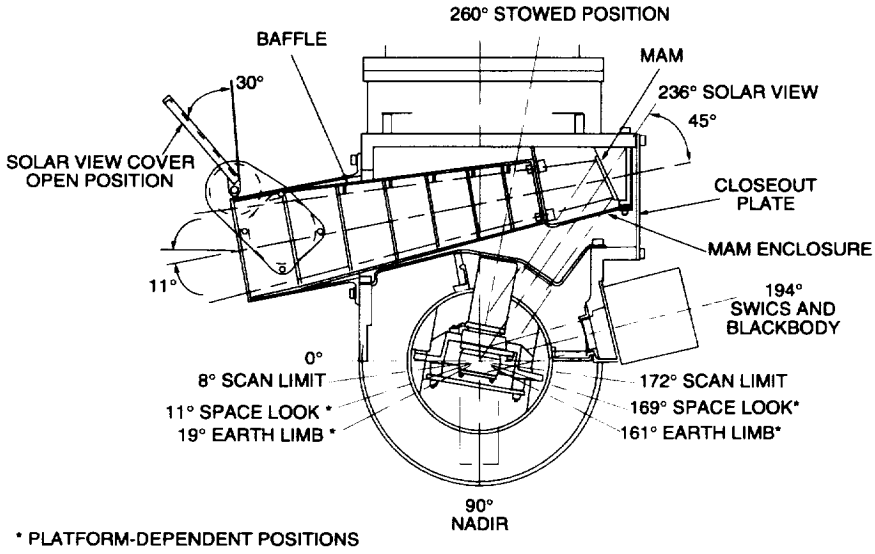

Figure 1-6. Elevation scan positions for instrument on TRMM platform.

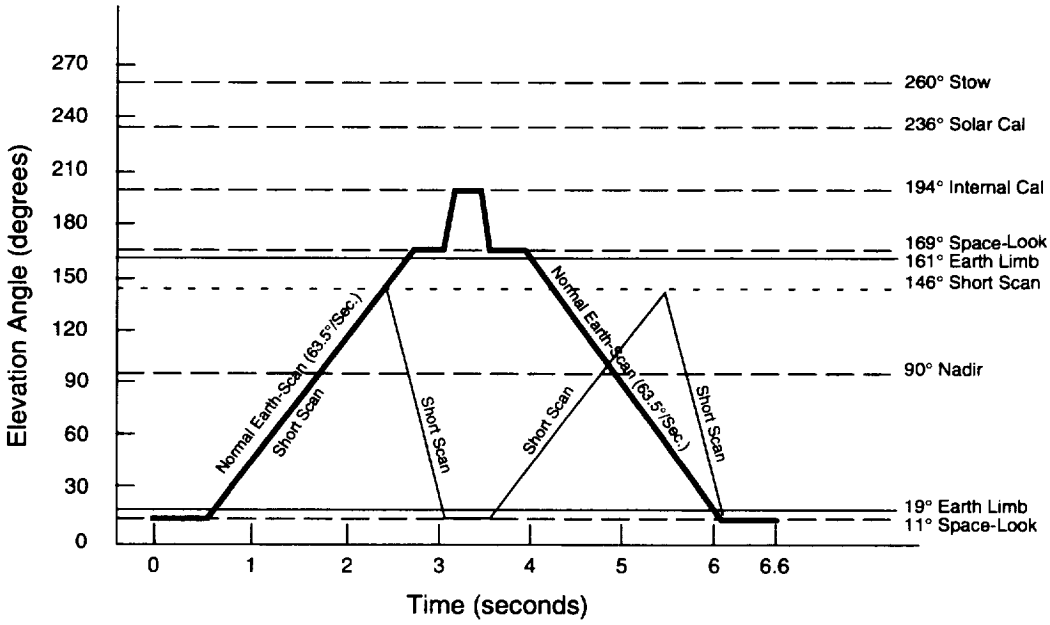

Figure 1-7. Normal and short Earth scan profiles for instrument on TRMM platform.

scenes observed at some specific elevation angles, and figure 1-7 shows the elevation angle with time during a 6.6 second scan period for the normal and short scan profiles of the instrument on the TRMM spacecraft. Figure 1-7 illustrates the uniform motion of the detectors across the Earth and the time spent at several of the fixed scan positions illustrated in figure 1-6. The internal calibration sources are not active (turned on) during normal science operations. The short scan profile restricts the detectors to elevation angles below the Earth limb and is used primarily during rotating azimuth plane scan operation to prevent the detectors from scanning the Sun.

1.2.3.2. Science operations. The most important science operational configuration is crosstrack, fixed-azimuth scan mode and the normal Earth scan profile. In this configuration, the detectors scan perpendicular to the spacecraft orbit plane in a whiskbroom fashion. Data collected and archived chronologically are referred to as bidirectional scan (BDS) measurements. Data internally stored spatially is referred to as instrument Earth scan (IES) measurements. The crosstrack, fixed-azimuth measurements will be the primary data used by the CERES science team for performing Earth radiation budget studies.

As with fixed-azimuth, cross track operation, the primary rotating azimuth plane scan operation also includes the normal Earth scan profile. In this configuration, the detector elevation scan plane normally oscillates through an azimuth angle of 180° with the end points being uprange and downrange. At the nominal azimuthal rotation rate of 6° per second, a complete azimuth scan cycle is completed in 1 minute. During rotating azimuth operations, the detectors measure radiances from all geographical scenes with varying incident solar radiation and observing geometry. The resulting angular radiance measurements will be used to compute new angular distribution models for use in converting radiances to radiant fluxes.

The alternate configuration during rotating azimuth plane scan includes the short Earth scan profile, which is used to prevent the detectors from scanning the Sun during sunrise and sunset. The scan operation is changed to the short scan profile at the beginning of sunrise and sunset events, and is changed back to the normal scan profile at the end of these events. Changes between scan profiles will be made via stored commands whose times of execution are based on ephemeris predictions. The instrument will perform normal and short scan profiles about 75 and 25 percent of the time, respectively, during RAPS operation.

1.2.3.3. Calibrations. The instrument can perform flight calibrations while operating in the fixed-azimuth, crosstrack or rotating azimuth plane scan mode. During flight calibrations, the internal calibration sources are cycled on and off via a programmed sequence of commands while the instrument continues to perform a normal Earth scan profile. Earth measurement data taken during internal calibrations are also included in the archival science data.

The solar calibration mode incorporates a special scan profile in which solar radiances, reflected by the mirror attenuator mosaic (MAM), are measured by the detectors. In this profile, the detectors alternate between making measurements at space (169°), the internal calibration sources, and the MAM. The solar calibration procedure requires that the instrument be rotated to the predicted azimuth angle at which the Sun drifts through the MAM field of view.

1.2.3.4. Other operational modes. The diagnostic mode will be used primarily for handling microprocessor memory loads. The safe mode is incorporated to protect the instrument during emergencies or high-risk situations. The safe mode can be entered at any time from any operational mode via a command from either the instrument or the spacecraft. It can be exited only by a real-time ground command. The standby mode is essentially the same as the safe mode, except that it can be entered only via a few operational commands, but the instrument will respond to most operational commands during the standby mode. Diagnostic instrument parameters are listed in table A-4.

1.2.3.5. Operational plans. There will be two CERES instruments aboard the EOS-AM (morning) spacecraft. The current plan is to operate one instrument in the crosstrack/normal Earth scan configuration and the other in the rotating azimuth plane mode with the instrument switching between the normal and short scan profiles as described above. The EOS-PM (afternoon) and TRMM spacecraft will each have a single CERES instrument. The current plan is to operate the instrument in the crosstrack/normal Earth scan configuration for 2 days and in the rotating azimuth plane mode for 1 day out of every 3 days. The internal flight and solar calibrations are performed on each instrument during the same orbit about every 2 weeks.

1.3. Earth Radiance Count Conversion Algorithms

1.3.1. Math Model

In figure 1-3, the silvered primary and secondary telescope mirrors, the filters, and the black paint layer on the active bolometer flake represent the sensor optical elements that reflect, absorb, or transmit scene energy. The spectral response or sensitivity, S, of these sensor elements can be represented as

$$S(\lambda) = \tau_f(\lambda)\rho_m^2(\lambda)\alpha_b(\lambda) \tag{1-2}$$

where τ_f represents the combined transmittance of the filters, ρ_m represents the reflectance of the telescope secondary or primary mirrors, and α_b is the effective absorptance of the black paint layer on the bolometer. A Fourier transform spectrometer (FTS) and a pyroelectric reference detector (Frink et al. 1993) are used primarily to spectrally characterize the optical elements of each detector, using witness samples. Using equation (1-2) and the spectral characterizations of the optical component elements, the spectral responses were derived for the shortwave, total, and 8-μm to 12-μm window detector units. The resulting responses are presented in figure 1-2. For the flight detectors, end-to-end spectral characterizations (Jarecke et al. 1994) of each detector will be conducted using the Fourier spectrometer and the reference detector. The filtered radiance sensed at the bolometer surface can be represented as

$$\tilde{L} = \int_0^\infty L(\lambda)S(\lambda)d\lambda \tag{1-3}$$

where $L(\lambda)$ is the unfiltered radiance from a target scene before the radiance enters the telescope. During ground or flight calibrations, the unfiltered spectral radiance $L(\lambda)$ from a blackbody target (Sparrow and Cess 1978) is calculated as a function of the temperature T and is expressed as

$$L(\lambda) = \frac{C_1}{\lambda^5(e^{C_2/\lambda T} - 1)} \tag{1-4}$$

where C_1 (1.1909×10^{-16} W-m^2) and C_2 (1.4387×10^{-2} m-K) are the constants. The filtered radiance $\tilde{L}$ can be described as the average filtered radiance over the point spread function (P). Thus, $\tilde{L}$ is expressed as

$$\tilde{L} = \int d\Omega P(\Omega) \int_0^\infty d\lambda S(\lambda)L(\lambda\Omega) \tag{1-5}$$

where $d\Omega$ is the increment of solid angle and is given as

$$d\Omega = d\phi d\theta \sin(\theta) \tag{1-6}$$

where θ is the polar angle aligned with the optical axis and ϕ is the azimuthal angle aligned with the scan direction. The symbols θ and ϕ define the right-handed, spherical polar coordinate system.

A simplified version of the basic sensor data reduction equation for filtered radiance is

$$\tilde{L} = \frac{AV[m(t) - m_s(t_0)]}{CV_{\text{bias}}} \tag{1-7}$$

where AV is the detector gain, V_{bias} represents the bias voltage in counts applied to the bolometers at time t, $m(t)$ is the detector output voltage signal, in counts, at time t, $m_s(t_0)$ is the detector output voltage

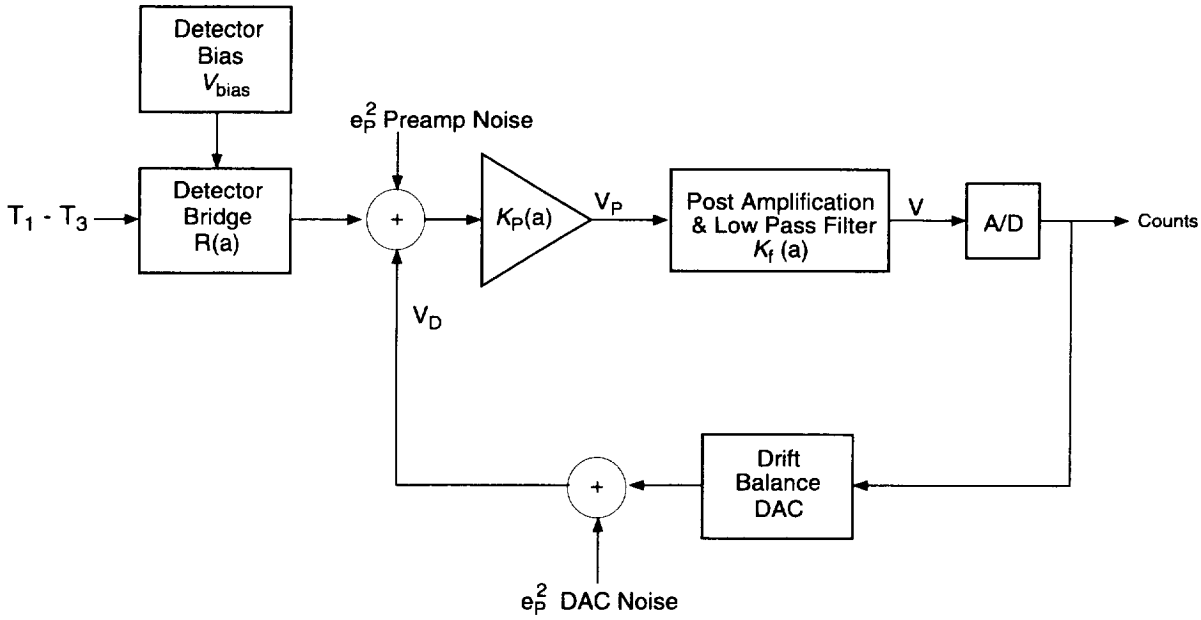

Figure 1-8. Scanner electronics block diagram.

signal, in counts, when exposed to cold space (3 K radiance source) at time t_0, and C is the digital-to-analog conversion factor of 409.5 counts/volt. Thus, the gain can be expressed as

$$AV = \frac{CV_{\text{bias}}(\tilde{L} - \tilde{L}_{\text{cold dark source}})}{m - m_{\text{cold dark source}}} \tag{1-8}$$

where gain is a function of the bias voltage. For the ERBE thermistor bolometer detectors, equations (1-7) and (1-8) are described by Halyo et al. (1987, 1989). The CERES sensor gains are derived from observations of the standard radiometric sources described in section 1.4.

1.3.2. Algorithms/Theoretical Basis

As shown in figure 1-3, the radiation from the target scenes passes through the filters (except for the total channel) and falls on the 18-mm diameter primary telescope mirror and is then reflected to the secondary mirror, which reflects the radiation through the primary insert, the precision field stop (aperture), and through the corresponding filters. Finally, the radiation is absorbed by the active flake paint layer. The absorbed target radiation causes a change in temperature between active and reference flakes that is detected by a balanced bridge. Figure 1-8 shows the block diagram for the detector electronics. The difference in active and reference flake resistances produces a signal that is amplified in the preamp and processed through a low pass filter. The filtered output is sampled, digitized into counts, and telemetered to Earth as the radiometric output of the detector.

The detector output, illustrated in figure 1-9 and resulting from the combined interaction of the incoming radiation, conduction, and electrical modes of heat transfer, Q, can be written under steady state conditions as

$$Q_{\text{conduction}} + Q_{\text{radiation}} + Q_{\text{electrical}} = 0 \tag{1-9}$$

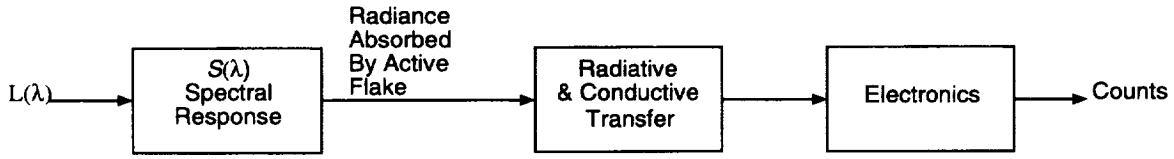

Figure 1-9. Detector output.

The CERES estimation equation for filtered radiance is of the same form as that for the ERBE thermistor bolometers, described by Halyo et al. (1987, 1989). The radiance estimation equation for the CERES sensors can be expressed as

$$\tilde{L}(t-\gamma) = A_V[m(t)-m(t_k)] + A_H[T_H(t)-T_H(t_k)] + A_\delta \delta_k \frac{t-t_k}{\Delta t} \tag{1-10}$$

for

$$t_{k-1} \le t \le t_k$$

The coefficient gain terms A_V and A_H are determined using the detector voltage and heatsink temperature measurements, respectively. The coefficient A_V is the gain expression. The term A_δ can be given as

$$A_\delta = CK_{f_o} A_V \tag{1-11}$$

The time t_k is given as

$$t_k = t_{k-1} + \Delta t \tag{1-12}$$

The average of the scan points during space clamp is given as

$$\bar{m}(t_k) = \frac{1}{n}\sum_{i=1}^{n} m(t_{ki}) \text{ where } n = 12 \tag{1-13}$$

The mean variance of the counts compared with the space clamp during a scan cycle is obtained by the equation

$$\sigma_k^2 = \frac{1}{n}\sum_{i=1}^{n} [m(t_k)-\bar{m}(t_k)]^2 \tag{1-14}$$

The constants in the above equations are defined as

$\bar{m}(t_k)$ = detector signal, in digital counts, corresponding to space measurement at time t_k

$m(t_{ki})$ = detector signal, in digital counts, when viewing space at $t_{ki} = t_k + i\,(10\,ms)$

σ_k^2 = noise variance estimate during space look

$m(t)$ = detector output signal, in counts, at time t

$T_H(t)$ = heat sink temperature measurement at t or most recent value (K)

Δt = total scan period (6.6 sec)

t_k = time of space measurement (sec)

t = time of detector measurement (sec)

$V_{\text{bias}}(t)$ = detector bridge bias voltage, in digital counts, measurement at time t

$V_D(t_k)$ = drift balance digital to analog conversion (DAC) voltage, in counts, measurement at time t_k

δ_k = estimate of unaccounted drift during t_kth scan period (v)

γ = average time lag between the instantaneous detector optical field of view and point spread function centroid (sec)

K_{f_o} = post amplification gain

C = digital to analog conversion factor, 409.5 digital counts/volt

1.3.3. Flight Algorithms/Practical Basis

From the standpoint of computational time, it is desirable to have as simple an algorithm as possible. Based on equation (1-10), the following algorithm (Lee et al. 1989) has been selected to interpret the CERES detector's radiometric output voltage in digital counts at time t, $m(t)$:

$$\begin{aligned}\tilde{L}(t-\gamma) = {} & A_V[m(t)-\bar{m}(t_k)-o(t)]+\frac{t-t_k}{\Delta t}[A_S(\bar{m}(t_{k+1})-m(t_k)) \\ & + A_H(T_H(t_{k+1})-T_H(t_k))+A_D(V_D(t_{k+1})-V_D(t_k)) \\ & + A_B(V_{\text{bias}}(t_{k+1})-V_{\text{bias}}(t_k))]\end{aligned} \tag{1-15}$$

where

$$t_k = t_{k+1}+\Delta t \tag{1-16}$$

and $\bar{m}(t_k)$ is the average detector output signal during the reference space measurements at the beginning of the scan and at time t_k, Δt is the scan duration of 6.6 sec, $o(t)$ is an offset dependent on the scan geometry during the scan. The housekeeping data $T_H(t_k)$ and $V_D(t_k)$ are transmitted to Earth once every scan and are not available during the scan. The symbol $T_H(t)$ is the heatsink temperature used to drive the heatsink controller, and $V_D(t)$ is the digital to analog conversion drift voltage. The symbol $V_{\text{bias}}(t)$ is the detector bridge bias voltage.

The coefficients A_V, A_S, A_H, A_D, and A_B are defined as

$$A_V = \frac{AV}{CV_{\text{bias}}(t)} \tag{1-17}$$

$$A_S = \frac{AVA}{CV_{\text{bias}}(t)} \tag{1-18}$$

$$A_H = \frac{AHA}{CV_{\text{bias}}(t)} \tag{1-19}$$

$$A_D = \frac{AD}{CV_{\text{bias}}(t)} \tag{1-20}$$

$$A_B = \frac{AB}{CV_{\text{bias}}(t)} \tag{1-21}$$

where AV, AVA, AHA, AD, and AB are constants determined using the ground calibration data (Lee et al. 1989, Halyo et al. 1989, and Jarecke et al. 1993), and C is the digital-to-analog conversion factor and is equal to 409.5 digital counts/volt.

The first term, A_V, in equation (1-15) is the most important term, while the remaining terms are relatively small. It is important to point out that the A_B term in ERBE ground calibration data analysis was

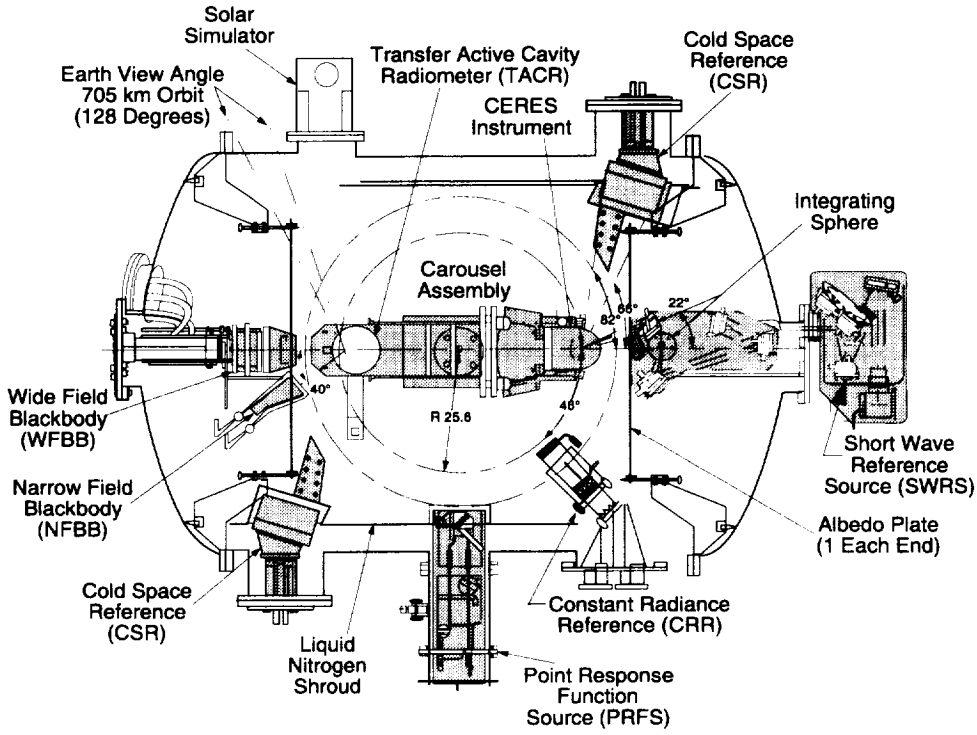

Figure 1-10. Radiometric calibration facility (RCF).

found to be negligible. The ground calibrations of the detectors are outlined in the following section, along with descriptions of the in-flight calibrations.

1.4. Ground and Flight Calibrations

The CERES radiometric test model (RTM) and functional test model (FTM) detectors were calibrated in the TRW radiometric calibration facility (RCF), which is illustrated in figure 1-10. The radiometric calibration facility is 2.44 meters in diameter and 3.66 meters in length. In the early 1980's, the facility was used to calibrate the Earth Radiation Budget Experiment (ERBE) scanning thermistor bolometer detectors (Lee et al. 1989). During the ERBE detector calibrations, the wide field of view blackbody (WFBB) was the primary calibration standard for the TRW facility. The blackbody was formerly called the master reference blackbody (Carman 1983). The blackbody consists of a 12.7-cm-diameter, concentric-groove, anodized black aluminum blackbody. Presently, its emitted radiances are based upon the international temperature scale of 1990 (ITS-90) using six platinum resistance thermometers (PRT), and it is operated over the 200 K and 370 K temperature range. One of its six thermometers is used for temperature control, while the remaining five PRT's are used for temperature knowledge with measurement precisions of the order of ±0.1 K. During the ERBE calibrations, the TRW radiometric calibration facility employed the cold space reference (CSR) blackbodies, a solar simulator, a 50.8-cm-diameter integrating sphere with associated optics (Hesser and Carman 1983), liquid nitrogen cooled shroud walls, and Earth visible and infrared albedo radiation simulators.

Since the 1980's, TRW has expanded the facility to include a very accurate reference narrow field of view blackbody (NFBB), an accurate shortwave reference source (SWRS) with minimum longwave variations and better spectral characterizations, a point response function source (PRFS), a blackbody mask for the narrow field of view blackbody that is used as an out of field response mechanism, a constant radiance reference (CRR), curved strip blackbody that is an offset variation measuring instrument, an improved solar simulator, and a cryogenically cooled transfer active cavity radiometer (TACR). The TACR is identical to the reference active-cavity radiometer used by the National Institute of Standards

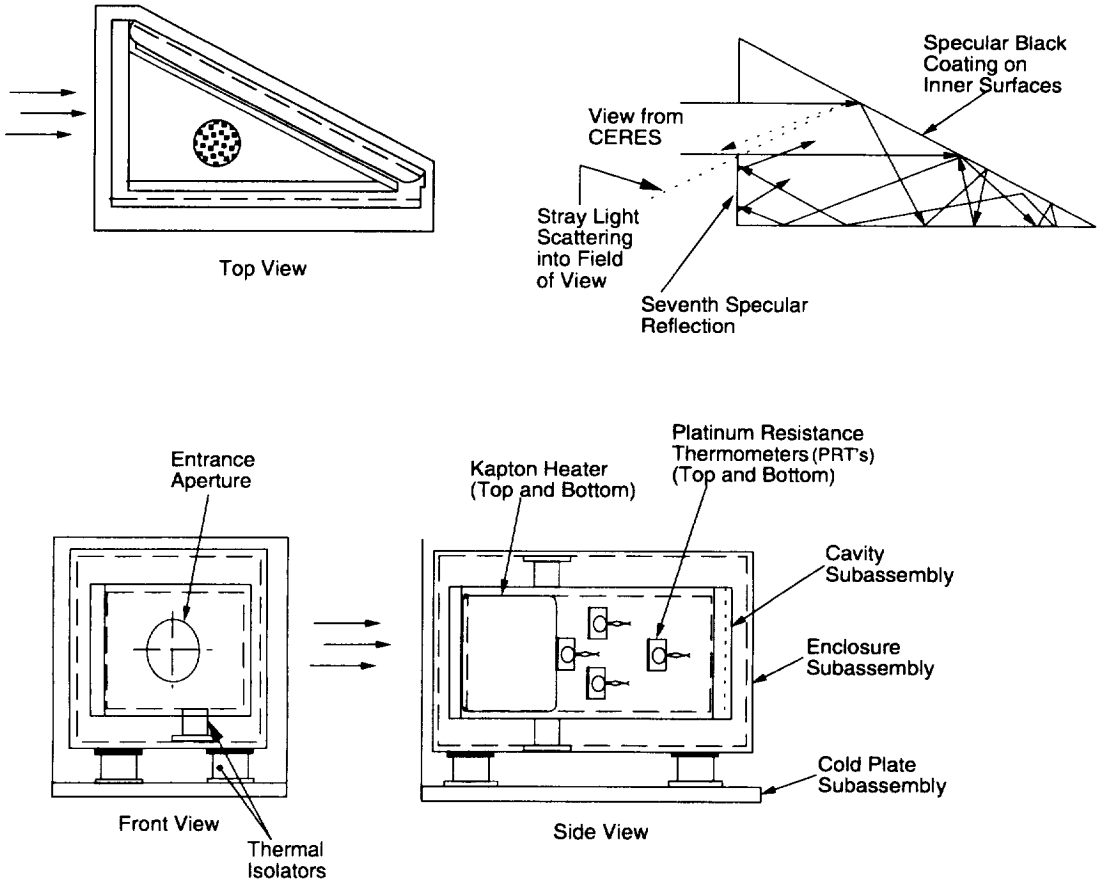

Figure 1-11. Schematic of narrow field of view blackbody (NFBB).

and Technology (NIST). Detailed descriptions of the radiometric calibration facility are given by Folkman et al. (1991), Jarecke et al. (1991), and Lee et al. (1993a). The May 1992 longwave calibration results and equations for the CERES radiometric test model total detectors are presented by Jarecke et al. (1993). The CERES functional test model shortwave, window, and total detectors were calibrated during December 1993. The functional test model calibration analyses will be released by September 1994. The TRMM protoflight model (PFM) detectors are scheduled to be calibrated before August 1995.

1.4.1. Longwave Calibrations

The narrow field of view blackbody is the reference source for the CERES longwave and shortwave calibrations (detector gain and offset determinations). The narrow field of view blackbody was selected as the CERES reference standard because it has more accurate spectral characterizations and a higher emittance than the wide field of view blackbody. The NFBB has an aperture opening that is 3.8 cm by 4.7 cm. The aperture is shown in the front view of figure 1-11. The narrow field of view blackbody has copper walls that are coated with an Aeroglaze Z-302 specular black paint. The blackbody is approximately 21.45 cm deep with an estimated emittance of 0.999952 (Jarecke et al. 1993). It has seven platinum resistance thermometers that are used for temperature knowledge, and it has one thermometer that is used for temperature control. The PRT's exhibit less than ±0.033 K uncertainty in temperature knowledge. The aperture of the blackbody is covered by a thermally controlled, diffused black mask. The mask permits the CERES detector out of field response to be determined and the longwave out of field radiances to be known and held constant during longwave calibrations. The mask covers the detector out of field view between the telescope module field of view and the location of the telescope detector

baffle, 16° off the detector optical axis. The blackbody temperature is varied at different levels between 200 K and 320 K, while the blackbody aperture mask temperature is typically maintained at 170 K. The mask temperature is set at 170 K, 200 K, 250 K, 300 K, 350 K, and 380 K during out of field response tests.

The longwave gain determination of CERES detectors consists of alternating staring observations at the narrow field of view blackbody and staring observations at the cold space reference blackbody identified in figure 1-10. The cold space reference blackbody is a 12.7-cm-diameter, concentric groove, anodized black aluminum emitting surface. It has two platinum resistance thermometers, which can be used for either temperature control or knowledge. It is cooled by liquid nitrogen to a constant temperature near 85 K. The narrow field of view blackbody radiances are calculated using a temperature-based model. The model is tied to the international temperature scale of 1990 using platinum resistance thermometers. The blackbody radiances are measured by CERES detectors when the NFBB is operated at 11 different temperature levels in the 200 K to 320 K range. Using a form of equation (1-8), the detector gains are determined from regression analyses of the differences in the filtered radiances from the NFBB and the CSR, and of the differences in the detectors output signals corresponding to measurements of the NFBB and CSR. Since the detectors are sensitive to the out of field radiances as well as in field radiances, the detector out of field response has to be considered in the gain determinations. The out of field response is determined from measurements of the narrow field of view blackbody with its temperature held constant near 200 K, while the NFBB aperture mask temperature is varied between 170 K and 380 K at the difference levels listed previously. Regression analyses of the mask data indicate an out of view response as much as 1 percent of the in field response.

To determine the variation of the detector zero-radiance offset signal, the detector output signal is sampled as a function of scan position with low emittance caps on the telescope module in place of the telescope baffles. The observed systematic offset variations are used to adjust the near zero-radiance measurement of the cold space reference source as a function of scan position. The detectors are sensitive to gravity forces during the offset determination processes. The low-emittance telescope caps allow the offsets to be determined in the same gravitational environment as the detector gains. In its present gravitational orientation, the constant radiance reference (CRR) generated offsets are affected by gravity in an unpredictable manner. Therefore, the CRR is not as reliable as the low-emittance telescope caps in determining the offsets.

In figure 1-12, the uncertainty allocations in percent for the NFBB radiances are presented (Jarecke et al. 1993). The blackbody irradiances are scheduled for cross-comparisons with the cryogenically cooled transfer active cavity radiometer (TACR), shown in figure 1-10. The cross-comparisons will define the linearity of the NFBB.

The wide field of view blackbody is observed in the staring and operational scanning cycle modes to define calibration differences that may be caused by observational geometry and scan rate.

In figure 1-13, the longwave uncertainty allocations in percent are presented for the total detector ground and flight calibrations (Jarecke et al. 1993). In the upper panel of figure 1-13, the ground longwave percent uncertainty allocations are presented for the total detector. The delta from ground block represents the uncertainty error due to differences in the radiant and thermal environments between the ground calibration in the radiometric calibration facility and flight in space, which result in an offset error in the internal calibration source blackbodies (ICSBB). A 0.3-percent ICSBB drift value was observed during the 5-year ERBE bolometer flight calibration time series (Lee et al. 1990, 1993b). The symbol $\Delta S(\lambda)$ represents the longwave percent uncertainty in characterizing the spectral throughput of each detector. The symbol $S(\theta,\phi,x,y)$ represents the angular and spatial detector response. The point response function source (PRFS) device is used to define the spatial response function $S(x,y)$ and the point spread function. The internal calibration source blackbody uncertainty is represented by the transfer uncertainty block, and RANCOM is the random error. In the lower panel, the flight longwave percent uncertainty requirements are presented for the total detector.

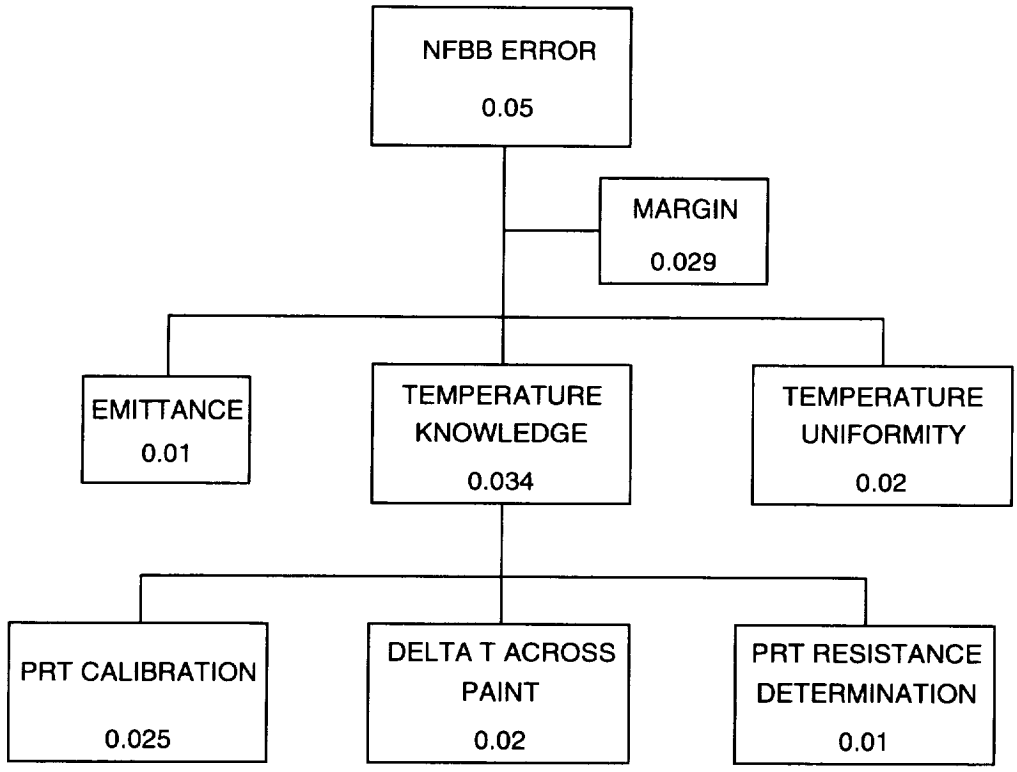

Figure 1-12. Narrow field of view blackbody (NFBB) percent uncertainty allocations.

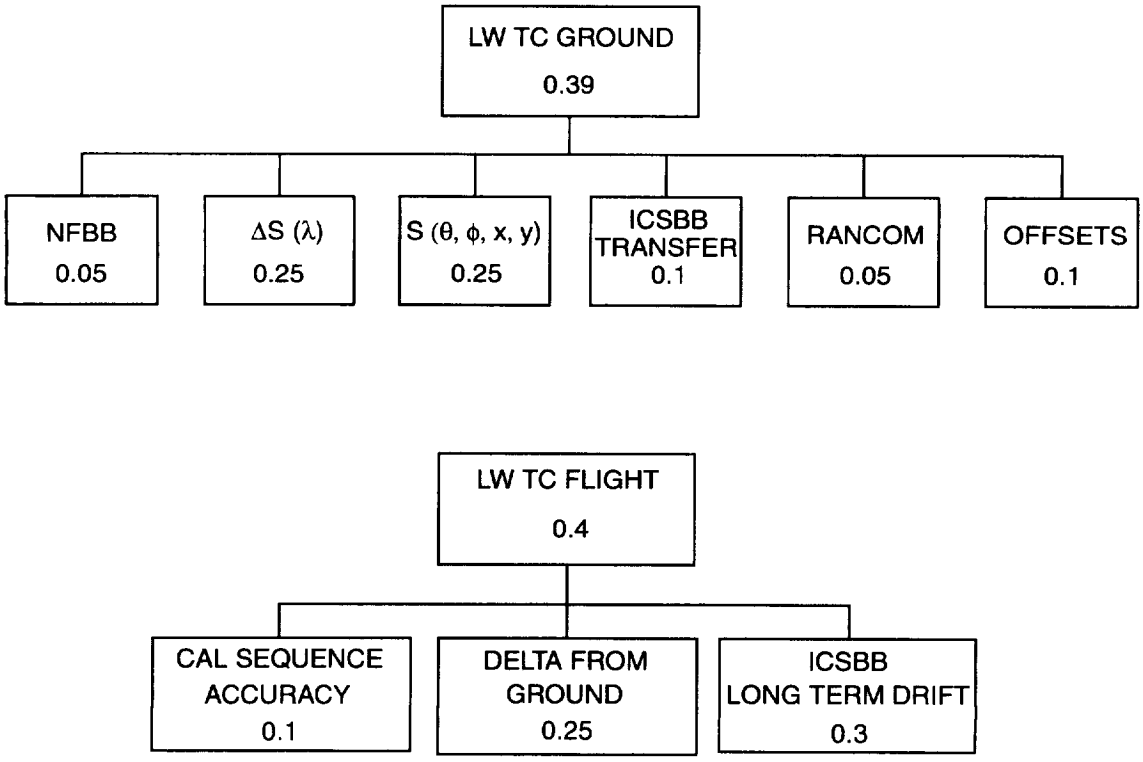

Figure 1-13. Longwave (LW) ground and flight calibration percent uncertainty allocations.

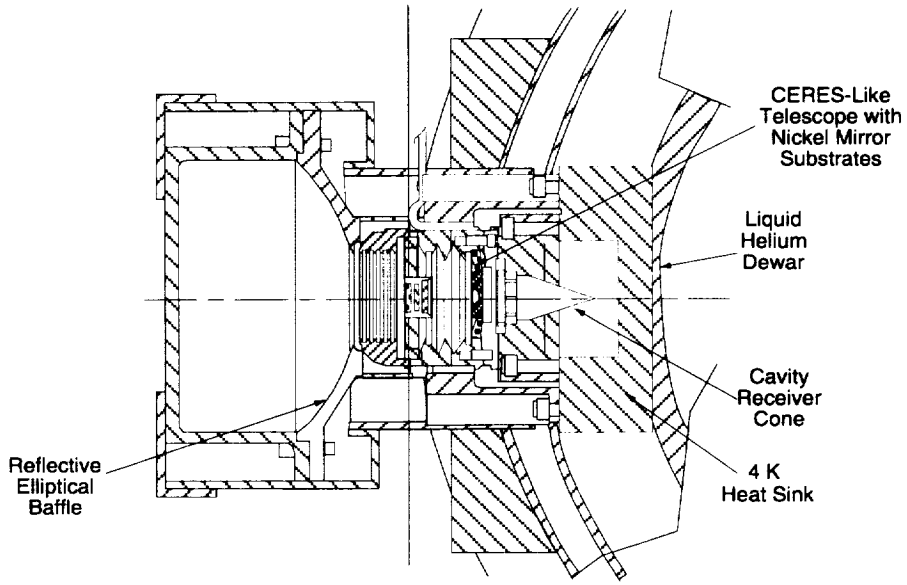

Figure 1-14. Transfer active cavity radiometer (TACR).

1.4.2. Shortwave Calibrations

For the ERBE calibrations, the total and longwave bolometer detectors were used to transfer the wide field of view blackbody temperature-based radiometric scale to the radiometric calibration facility integrating sphere. The total detector was used to measure the longwave and shortwave radiances from the integrating sphere. The longwave detector was used to measure longwave radiances from the integrating sphere. The properly corrected differences between the total and longwave detector measurements were used to characterize the shortwave radiances from the integrating sphere. For the CERES calibrations, a new shortwave system was developed that minimizes the heating of the integrating sphere and uses a radiometer to transfer the NFBB temperature-based radiometric scale to the new shortwave reference source. The absolute radiometer is called the transfer active cavity radiometer, identified in figure 1-10. The TACR (Foukal et al. 1990) operates near 5 K. In figure 1-14, a schematic of the TACR is presented. The radiometer is equipped with the same telescope and field stop aperture design geometries as the CERES detectors, to duplicate the CERES detector field of view and aperture area. The radiometer makes power measurements with uncertainties approaching 0.2 nW. The product of the radiometer aperture area and field of view was calculated from the TACR power measurements of the NFBB divided by the modeled NFBB target radiances. Folkman et al. (1994) describe the calibration of the SWRS using the TACR. The uncertainty allocations in percents for the radiometer are presented in figure 1-15.

The shortwave reference source is used to determine the shortwave detector and shortwave portion of the total detector gains and offsets. The SWRS consists of a 250 Watt quartz tungsten halogen source lamp, 17 narrow band optical filters, relay reflective optics, an 11-cm diameter Spectralon integrating sphere, and associated optics. The SWRS lamp output is maintained at the 0.1-percent stability level over several hours. The radiant exitance from the sphere has been measured at the 0.5-percent uniformity level over the exit port, which subtends approximately 6 angular degrees at the CERES detectors observational positions.

In the upper portion of figure 1-16, the shortwave calibration percent uncertainty allocations are presented. The uncertainty in the shortwave internal calibration source (SWICS) is considered in the error budget.

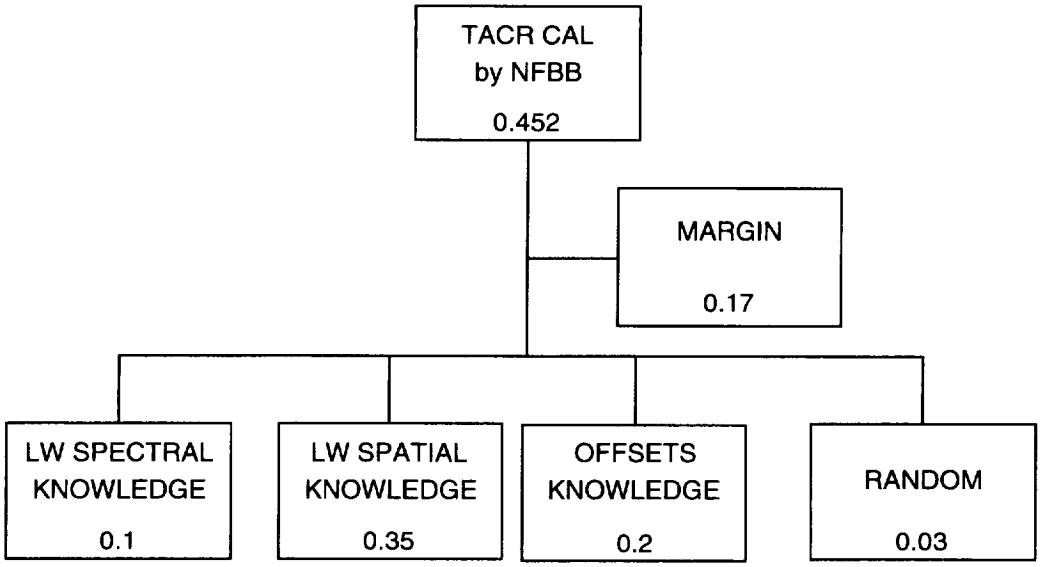

Figure 1-15. Transfer active cavity radiometer (TACR) percent uncertainty allocations.

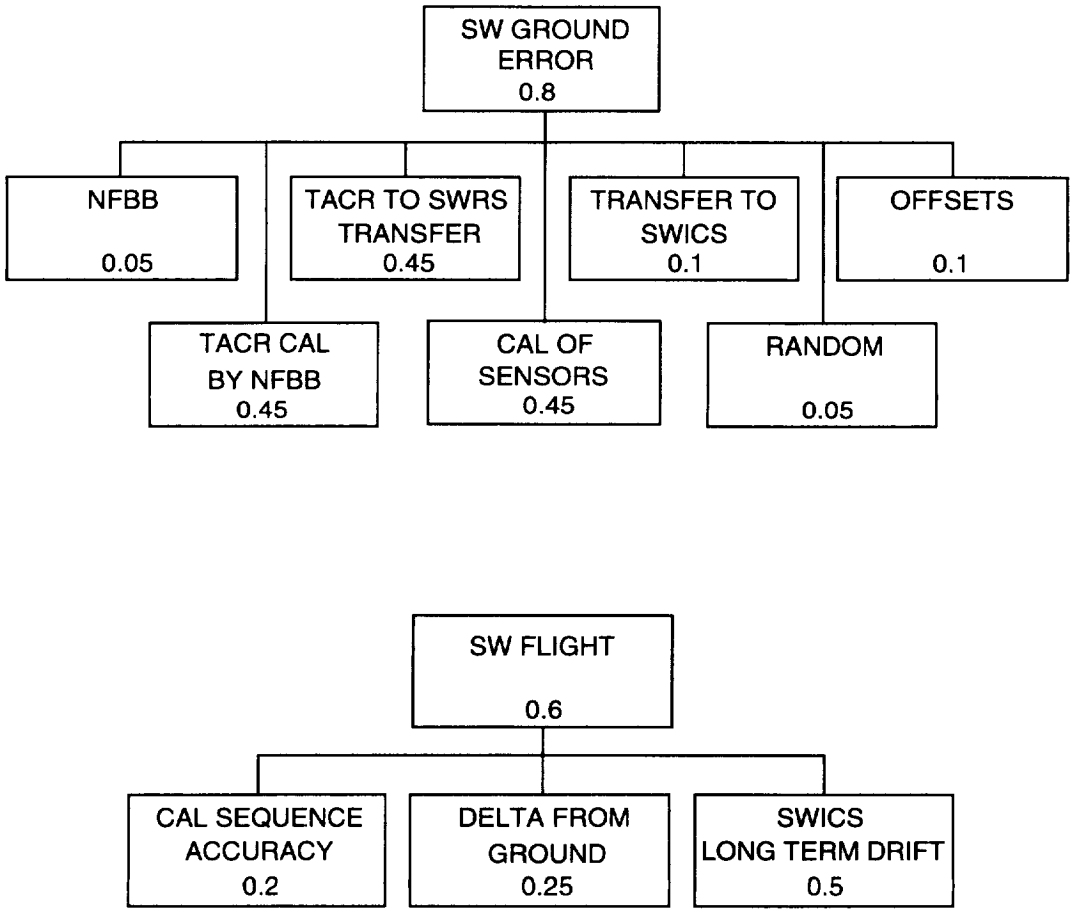

Figure 1-16. Shortwave ground and flight percent uncertainty allocations.

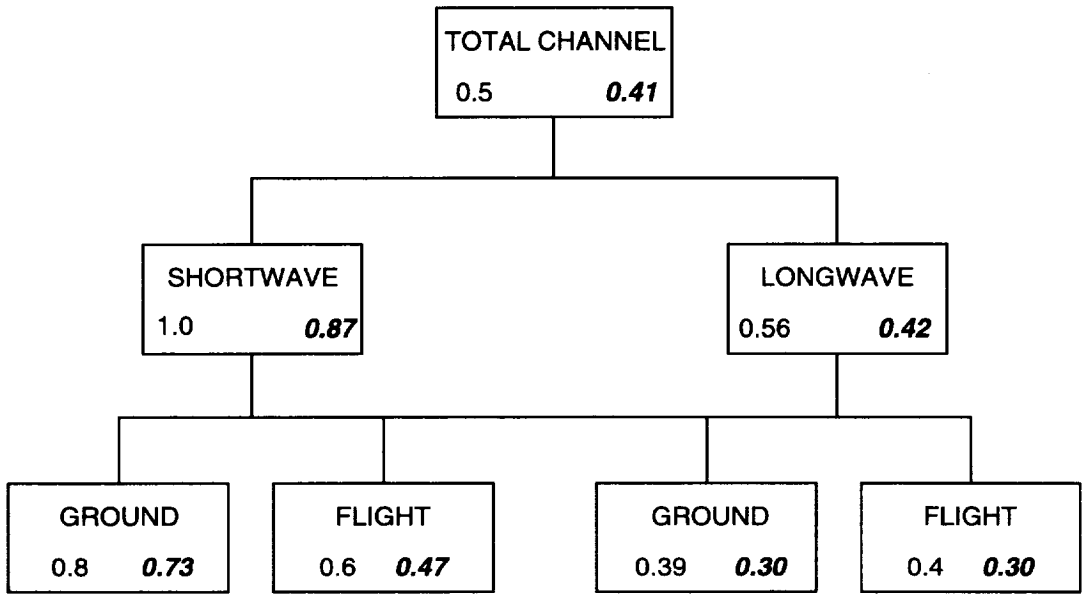

Figure 1-17. Total detector ground and flight percent uncertainty allocations.

In figure 1-17, the uncertainty allocations for the total detector are presented. The numbers in italics represent the predicted performance levels.

1.4.3. In-Flight Calibrations

In-flight calibration systems are built into the CERES instrument. The three detectors are calibrated using the internal calibration module (ICM), shown in figure 1-18. The module consists of concentric grooved blackbody sources for the total and longwave detectors and an evaluated tungsten lamp source system, known as the shortwave internal calibration source (SWICS), for the shortwave detector. The basic SWICS design is described by Lee et al. (1993b). The ICM was used to calibrate thermistor bolometers and active-cavity radiometers aboard the Earth Radiation Budget Satellite (ERBS), NOAA-9, and NOAA-10 spacecraft platforms. In figure 1-19, ERBS flight calibration measurements demonstrate the maturity of the CERES ICM design. The measurements represent raw output signals from the shortwave, longwave, and total thermistor bolometers. The dropouts in the measurements were caused by misalignments between the bolometers and the calibration sources. The misalignments occurred when the sensor scanning mechanism became sluggish (Kopia and Lee 1992). The measurements show that the bolometers and flight calibration sources (evacuate tungsten lamp and blackbodies) were stable to approximately 0.3 percent (Lee and Barkstrom 1991, Lee et al. 1993b). The shortwave and total channels are calibrated using the solar radiances reflected from a solar diffuser plate, referred to as the mirror attenuator mosaic (MAM). The locations of the MAM baffle and reflecting surface are identified in figure 1-6. The MAM solar radiance reflecting surface consists of an array of spherical aluminum mirror segments that are separated by a black paint reflecting surface. The CERES MAM design should yield calibration precisions approaching 1 percent for the total and shortwave detectors (Folkman et al. 1993). The CERES basic solar calibration approach and flight data reduction algorithms are similar to those for ERBE, described by Lee et al. (1992). The ERBE MAM calibration approach, flight data reduction algorithms, and in-flight performances have yielded measurement precisions at the 3-percent level (Lee et al. 1992) as shown in figure 1-20. Using the ICM, the CERES total, window, and shortwave detectors will be calibrated to define revisions in the count conversion coefficients, used in equations 1-17 to 1-21, and to monitor the gain stability of these detectors (Lee et al. 1990, Gibson et al.

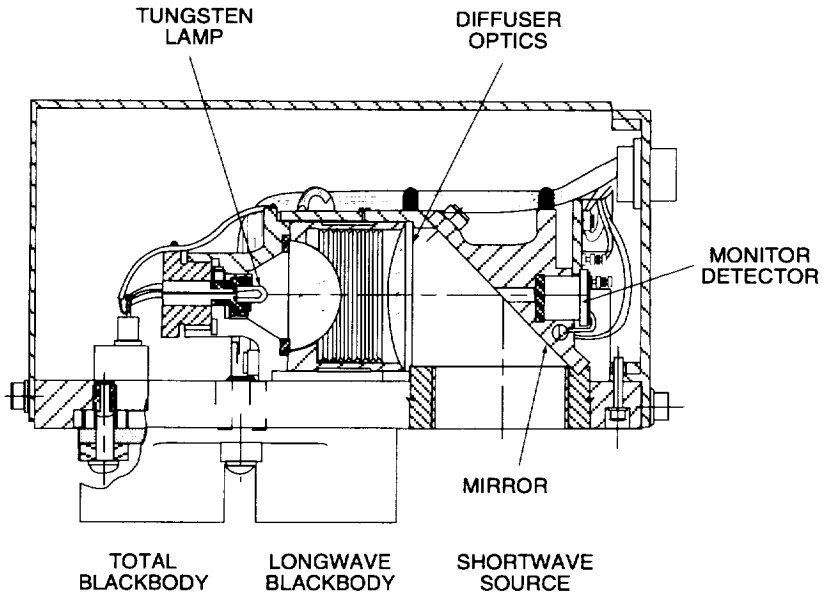

Figure 1-18. Internal calibration module (ICM).

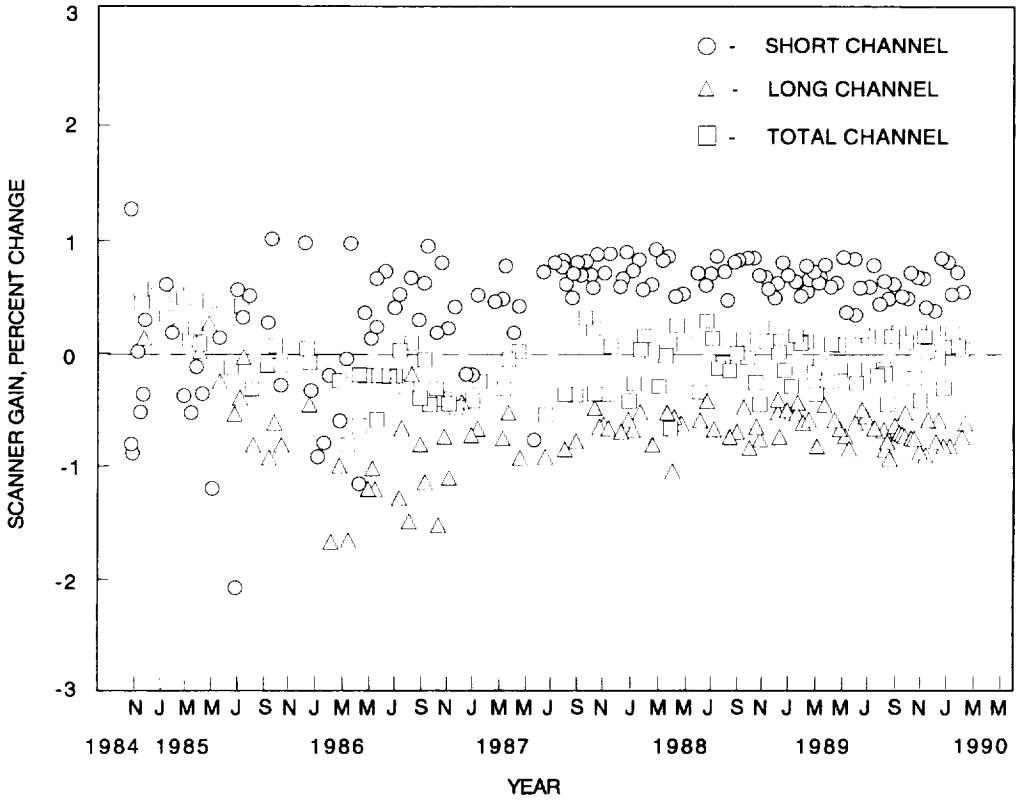

Figure 1-19. ERBS scanner calibration.

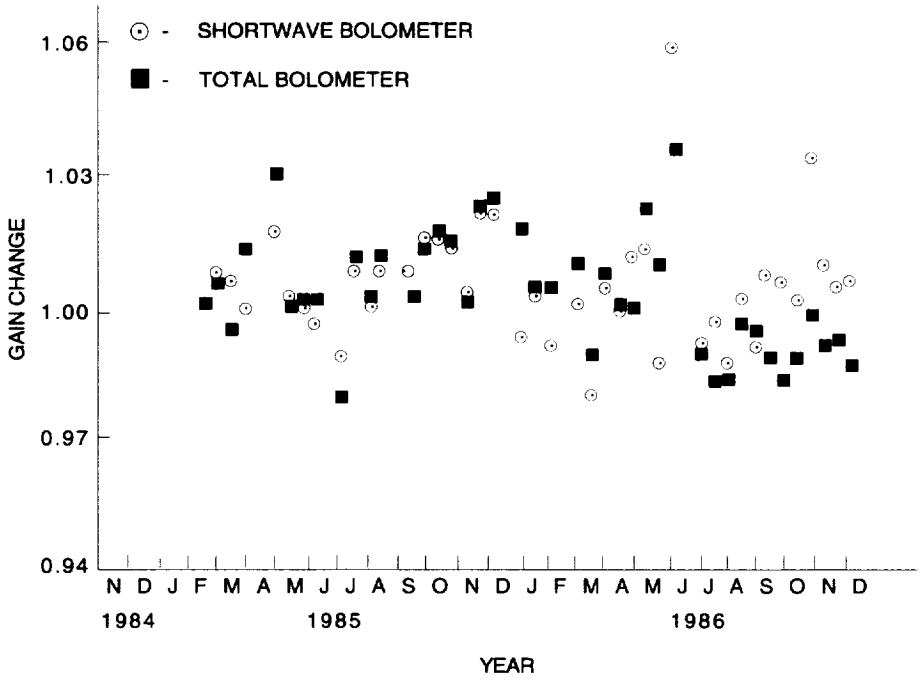

Figure 1-20. NOAA-9 thermistor bolometer solar calibrations.

1992). The nighttime radiance time series for each shortwave detector will be produced on a daily basis to modify the detector offset. By definition, the nighttime shortwave radiance should be zero.

The uncertainty requirements for the flight calibrations are presented in the lower portions of figures 1-13 and 1-16.

1.5. Input Data

The primary data stream is a 24-hour data file or set of archival science data packets containing CERES instrument science measurements and associated engineering data. The contents of these packets are listed in appendix A, table A-2. Each packet consists of instrument data acquired during a 6.6-sec scan period when the instrument is operating in one of the primary science modes. The packet headers contain a time stamp and an application process identifier (APID) that identifies the data as archival science data from a specific CERES instrument.

The archival science data packets from the instruments aboard the EOS platforms also contain orbit ephemeris and spacecraft attitude data for computing the geolocations of the science measurements. The corresponding ancillary data are contained in separate data sets from the TRMM spacecraft. These data are listed in appendix A, table A-4, and section 1.7 describes how these data are used to calculate the Earth locations of the CERES instrument measurements.

The Instrument Subsystem is also capable of dealing with production calibration and diagnostic data sets that consist of data packets when the instrument is acquiring solar calibration data and generating diagnostic data, respectively. The structure of these packets is nearly identical to that of the archival data packets, but the data content is different, and they are identified with the CERES calibration and diagnostic application identifiers, respectively. These data sets consist of all packets generated with the calibration and diagnostic application identifiers during a 24-hour period, but the actual data periods are normally only a fractional part of a day.

1.6. Housekeeping Data Conversions to Engineering Units

The basic engineering data provided by the CERES instrument package are elevation and azimuth positions, voltage and temperature measurements, and instrument status information. The temperature and voltage measurements and the status data are essential in monitoring the health and safety of the instruments and in studying the instrument condition during emergencies.

The elevation and azimuth positions, along with the ephemeris and attitude data, determine the location of instrument measurements at the top of the atmosphere. The bias voltage, digital to analog (DAC) drift voltage, and heat-sink temperature are used in the calculation of filtered radiances. The blackbody temperatures and shortwave internal calibration source output voltage are needed in analyzing the calibration data. The instrument status words identify the instrument's operational state.

The data conversion equations for transforming temperature measurements in counts to degrees Celsius are outlined by the CERES Science Team and by TRW. The following relationships are used to calculate the CERES radiometric test model instrument, sensor heater control, and thermistor temperatures.

Detector Temperature:

$$T_{PRT} = 32 + \frac{(K_T - 572.53)}{1.895} \tag{1-22}$$

Sensor Heater Control Temperature:

$$T_s = 32 + \frac{(K_T - 1012.62)}{4.51333} \tag{1-23}$$

Thermistor Temperature:

$$T_m = [9.354 \times 10^{-4} + 2.211 \times 10^{-4} \ln(K_T) + 1.275 \times 10^{-7} (\ln(K_T))^3]^{-1} - 273.15 \tag{1-24}$$

where K_T is given as

$$K_T = \frac{K_1}{1 + \frac{K_f}{K_p} + \frac{K_f}{K_2}\left(\frac{\left(16 \times \frac{\text{Counts}}{4095} - 8\right)}{V_{\text{ref}} + \frac{K_f}{K_p}} - 1\right)} - K_{on} \tag{1-25}$$

The numerical constant values required in the above equations for the CERES radiometric test model (RTM) are given in table 1-5. The corresponding constant values for the functional test model, proto-flight model, and the flight model instruments will be defined at a later date.

Table 1-5. Temperature Coefficients for CERES RTM Instrument

Constants	Detector	Control Sensor	Thermistor
K_1	2538.7	4995.8	30 900
K_2	2635.7	2613.8	91 434
K_f	39 1196	348 292	20 000
K_{on}	0	0	180
K_{p1}	4872	76 865	N/A
K_{p2}	1484	14 850	N/A
K_p	$1/(1/Kp_1 + 1/Kp_2)$		14 956
V_{ref}	10	10	10

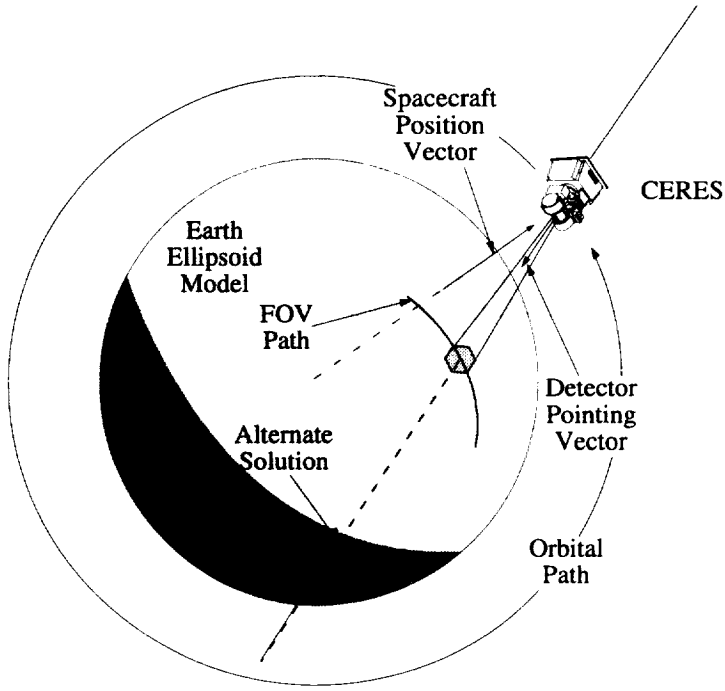

Figure 1-21. Geometry of the detector field of view and Earth ellipsoid intersection.

1.7. Field-of-View Location

It is essential in interpreting the CERES radiance measurements that the geographic location falling within the detector field of view be accurately determined for each measurement (Hoffman et al. 1987). The input data required to perform the geolocation procedure include the spacecraft ephemeris and attitude, the detector pointing knowledge, an ellipsoid model of the Earth, and the time. First, the spacecraft position vector and the detector pointing vector are transformed into an Earth fixed coordinate system. The equation of the line passing through the spacecraft position and parallel to the detector pointing vector is then determined and combined with the Earth ellipsoid equation to form a system of equations. Finally, the solution of the system determines the points of intersection between the line and the ellipsoid. The geometry of the procedure is illustrated in figure 1-21. The geographic location observed in the detector field of view is the intersection point closest to the spacecraft. The alternate intersection solution on the far side of the Earth is also shown.

The orientation of the Earth's equatorial plane with respect to the plane of its orbit about the Sun is illustrated in figure 1-22. The axes of the geocentric-equatorial coordinate system (designated by X_I, Y_I, and Z_I) are defined with respect to these planes. The X_I-axis is the intersection of the planes, and the Z_I-axis is normal to the equatorial plane. The positive direction of the X_I-axis is from the Sun to the Earth during the autumnal equinox, as illustrated in figure 1-22. The positive direction of the Z_I-axis is from the Earth's center to the north pole. The positive Y_I-axis completes a right handed coordinate system. This coordinate system does not rotate with the Earth and makes up the inertial frame that is used to report the spacecraft ephemeris. The position vector for the spacecraft reported in the ephemeris data is designated by X_I, Y_I, and Z_I.

The Earth's rotation causes the Earth fixed coordinate system (designated by X_F, Y_F, and Z_F) to rotate with respect to the inertial system as a function of time. The rotation of the Earth fixed frame is illustrated in figure 1-22. The spacecraft position vector is transformed into Earth fixed coordinates by

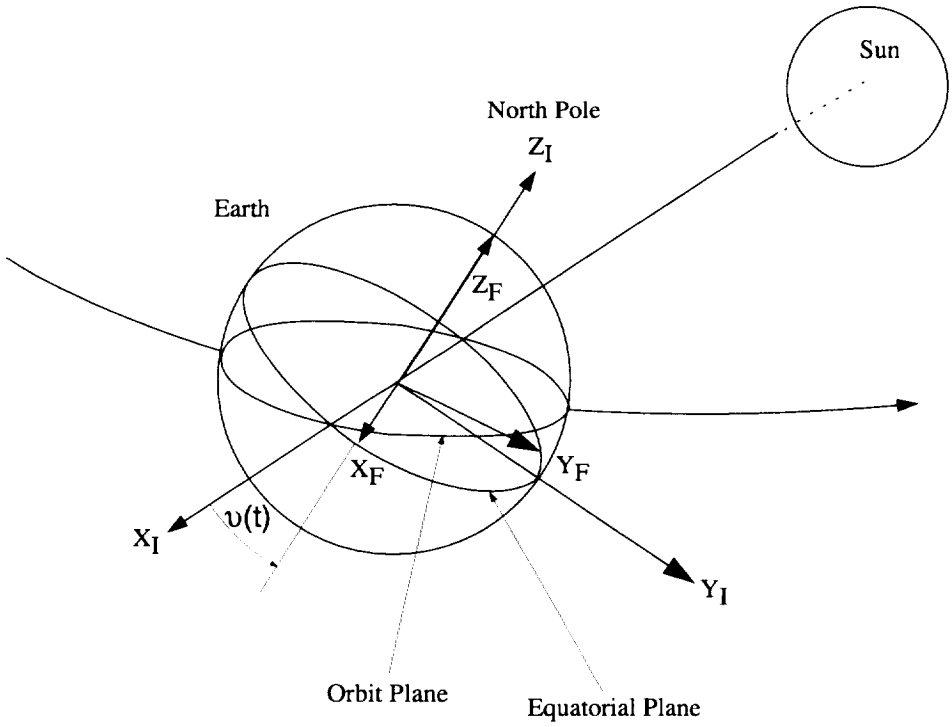

Figure 1-22. Orientation of the inertial and Earth fixed coordinate systems with respect to the equatorial and orbital planes.

$$\begin{bmatrix} X_F \\ Y_F \\ Z_F \end{bmatrix} = \begin{bmatrix} \cos\nu(t) & \sin\nu(t) & 0 \\ -\sin\nu(t) & \cos\nu(t) & 0 \\ 0 & 0 & 1 \end{bmatrix} \begin{bmatrix} X_I \\ Y_I \\ Z_I \end{bmatrix} \tag{1-26}$$

which is a rotation about the Z_I-axis, where $\nu(t)$ is the time dependent rotation angle of the Earth fixed frame with respect to the inertial frame and is given by

$$\nu = 99.6909833° + 36000.7689°t + 0.00038708°t^2 + 360.9856463°\Delta d \tag{1-27}$$

where t is in Julian centuries since 1900 and Δd is fractional days between the measurement time and midnight universal time.

The orientation of the instrument in the spacecraft coordinate system (designated by X_S, Y_S, and Z_S) is illustrated in figure 1-23, for the cross-track mode, at the instant of nadir viewing. During nominal operations, the spacecraft coordinate system is aligned with the local horizon coordinate system (designated by X_H, Y_H, and Z_H). Therefore, X_S and X_H point along the projection of the spacecraft velocity vector in the local horizon plane, Z_S and Z_H point to the geodetic nadir, and Y_S and Y_H complete the right handed coordinate systems, pointing along the negative orbit momentum vector. The detector has two degrees of freedom relative to the instrument. The instrument is aligned during integration with the spacecraft so that values of zero for the azimuth and elevation angles will point the detector along the orbit momentum vector of the spacecraft. If the alignment is done perfectly, the detector pointing vector in spacecraft coordinates is given by

$$\begin{bmatrix} X_S \\ Y_S \\ Z_S \end{bmatrix} = \begin{bmatrix} \cos\alpha & -\sin\alpha\cos\beta & -\sin\alpha\sin\beta \\ \sin\alpha & \cos\beta\cos\alpha & \sin\alpha\cos\alpha \\ 0 & -\sin\beta & \cos\beta \end{bmatrix} \begin{bmatrix} 0 \\ -1 \\ 0 \end{bmatrix} \tag{1-28}$$

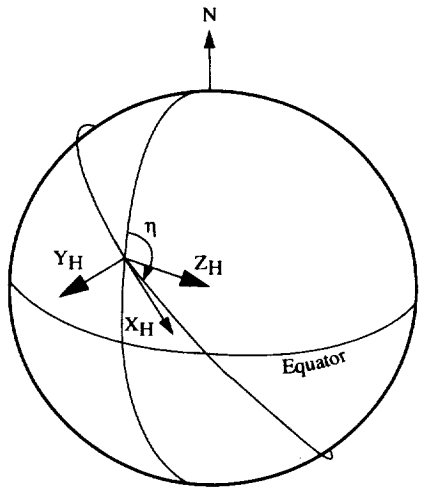

Figure 1-23. Orientation of the detector field of view with respect to the spacecraft and local horizon coordinate systems.

where α is the azimuth angle and β is the elevation angle. The orientation of the detector as shown in figure 1-23 is for α = 180° and β = 90°.

The roll, pitch, and yaw angles of the spacecraft in orbit will not generally be zero, so the spacecraft will be rotated with respect to the local horizon. The equation that transforms the detector pointing vector from the spacecraft coordinate system to the local horizon coordinate system is

$$\begin{bmatrix} X_H \\ Y_H \\ Z_H \end{bmatrix} = \begin{bmatrix} \cos q\cos r - \sin p\sin q\sin r & -\sin r\cos p & \sin p\sin r\cos q \\ \sin r\cos q + \sin p\sin q\cos r & \cos p\cos r & \sin q\sin r - \sin p\cos q\cos r \\ -\sin q\cos p & \sin p & \cos p\cos q \end{bmatrix} \begin{bmatrix} X_S \\ Y_S \\ Z_S \end{bmatrix} \tag{1-29}$$

where p, q, and r represent roll, pitch, and yaw angles of the spacecraft about the X_H, Y_H, and Z_H axes, respectively.

The local horizon coordinate system is rotated about nadir with respect to the local geodetic coordinate system as a result of the inclination of the orbit, as shown in figure 1-24. The rotation angle η, called the heading angle, is the angle between geodetic north and the projection of the spacecraft velocity vector onto the local horizon coordinate system. The detector pointing vector is both rotated by the heading angle and transformed to the Earth fixed geocentric-equatorial coordinate system by

$$\begin{bmatrix} X_F \\ Y_F \\ Z_F \end{bmatrix} = \begin{bmatrix} -\cos\eta\cos\Lambda\sin\Phi_G + \sin\eta\sin\Lambda & -\sin\eta\cos\Lambda\sin\Phi_G - \cos\eta\sin\Lambda & -\cos\Lambda\cos\Phi_G \\ -\cos\eta\sin\Lambda\sin\Phi_G - \sin\eta\cos\Lambda & -\sin\eta\sin\Lambda\sin\Phi_G + \cos\eta\cos\Lambda & -\sin\Lambda\cos\Phi_G \\ \cos\eta\cos\Phi_G & \sin\eta\cos\Phi_G & -\sin\Phi_G \end{bmatrix} \begin{bmatrix} X_H \\ Y_H \\ Z_H \end{bmatrix} \tag{1-30}$$

where Λ and Φ_G are the Earth fixed longitude and geodetic latitude of the spacecraft. The Earth fixed longitude and geocentric latitude are derived from equation 1-26. The geodetic latitude is determined from the geocentric latitude Φ_C by

$$\Phi_G = \tan^{-1}(\tan\Phi_C R_e^2/R_p^2) \tag{1-31}$$

where R_e and R_p are the equatorial and polar radii, respectively.

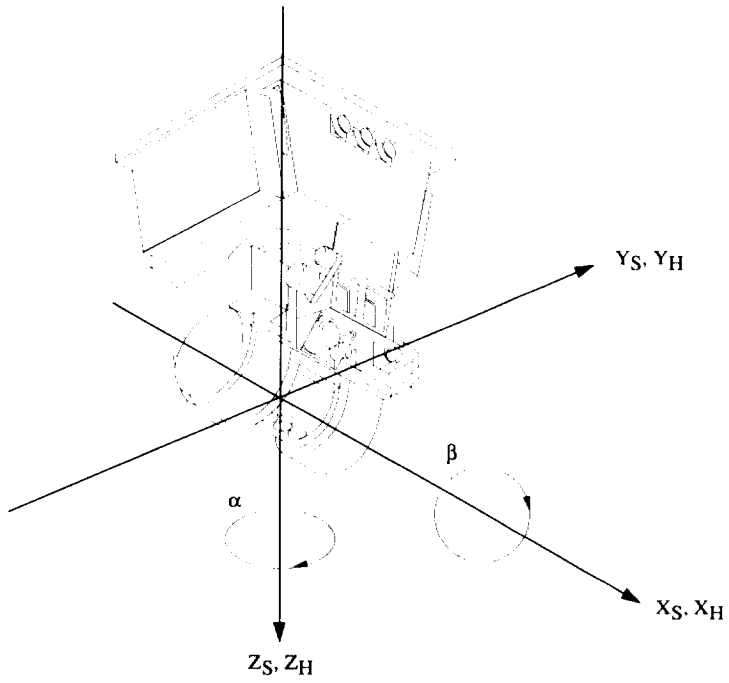

Figure 1-24. Rotation of the local horizon coordinate system with respect to local geodetic north by the spacecraft heading angle η.

The Earth ellipsoid model is given by

$$\frac{X^2}{(R_e+h)^2}+\frac{Y^2}{(R_e+h)^2}+\frac{Z^2}{(R_p+h)^2}=1 \tag{1-32}$$

where h is a top of atmosphere reference height above the Earth of 30 kilometers. The equation for the line passing through the spacecraft position and parallel to the detector pointing vector is

$$\frac{X-X_0}{a}=\frac{Y-Y_0}{b}=\frac{Z-Z_0}{c} \tag{1-33}$$

where a, b, and c are the components of the detector pointing vector from equation (1-29), and X_0, Y_0, and Z_0 are the Earth fixed coordinates of the spacecraft from equation (1-26). The solutions of system of equations 1-32 and 1-33 are the Earth fixed coordinates of the detector field-of-view intersection point (designated as X_F, Y_F, and Z_F) and an alternate intersection point on the far side of the Earth ellipsoid from the spacecraft.

Finally, the latitude and longitude of the Earth located measurement in Earth fixed geocentric coordinates are:

$$\begin{aligned}\Phi_C &= \sin^{-1}\left(\frac{Z_F}{|\vec{R}_F|}\right)\\ \Lambda_C &= \tan^{-1}\left(\frac{Y_F}{X_F}\right)\end{aligned} \tag{1-34}$$

1.8. Quality Control Schemes

1. Monitoring the behavior of housekeeping measurements, such as temperatures and voltages, is very essential. Time histories of all flight housekeeping measurements in terms of minimum, mean, and maximum values will be graphically displayed daily.

2. Limit tests: flight edit routines will be used to justify/verify the set of converted data (detector housekeeping, attitude, spacecraft housekeeping, and radiometric). The tables for limits can be prepared accordingly.

3. Special flight algorithms will be used to detect possible abnormal space zero-radiance measurements.

4. Revision of count conversion coefficients.

During the first 30 days in orbit, the sensor contamination doors will be closed. During this period, the sensors will be calibrated using the internal calibration module at least weekly. After the doors are opened, the ICM and MAM in-flight calibrations will be performed daily during the first week of Earth radiance measurements, every other day during the second week, once a week for the third and fourth weeks, and thereafter every 14 days.

For CERES total-wave, window, and shortwave sensors, the resulting time series plots will be analyzed to monitor the gain stability of these sensors (Lee et al. 1993b). In addition, the difference between the total-wave and longwave sensor nighttime radiance will be monitored on a daily basis to determine any drifts in the sensor coefficients.

The sensors' flight gains and offsets will be evaluated using in-flight calibrations and validation studies. The preflight sensor gains and offsets will be used to initially convert the CERES sensor output signals into radiances. The in-flight calibrations will be used to detect drifts or abrupt shifts in the sensors' responses. Validation measurements of the Earth radiances will be used to verify sensor response changes, indicated by in-flight calibrations. The CERES science team will conduct detailed analyses of the first 6 months of in-flight calibrations and of the validations before the sensor gains or offsets are revised. Thereafter, the gains or offsets will be revised only if the sensors' responses degrade by more than 0.5 percent in the longwave region or 1 percent in the shortwave region.

5. Special flight algorithms and approaches will be used to determine the scanner offsets as derivatives of scanning geometry.

Basically, the sensors' measurements of cold space will be used to define the sensor flight zero-radiance offset. The nighttime Earth shortwave radiance is zero by definition. During each orbit, the nighttime Earth radiances for each shortwave sensor will be used to define the sensor zero-radiance offsets as a function of elevation angle. During the next series of day side measurements, these offset determinations will be used to adjust the cold space determined offsets as a function of elevation angle. In the case of the total-wave and window sensors, the variations of the offsets will be derived from measurements of space during the 180° deep space spacecraft pitch maneuver. The sensor offsets can also be determined from comparisons with different spacecraft calibrated/validation radiance measurements of the same geographical scenes using the techniques of Avis et al. (1994).

6. ERBE developed validation techniques will be used to verify the geolocation accuracies.

The TRMM and EOS sensor pointing requirements are presented in tables 1-2 and 1-3. Coregistration refers to pointing knowledge between the CERES sensor optical axis and the axes of visible and infrared imaging sensors such as the TRMM visible imaging radiometer sounder (VIRS) and EOS AM platform MODIS. The pointing knowledge for the CERES footprints will be checked using coastline crossings (Hoffmann et al. 1987). The crossings were used to verify the ERBE pointing knowledge

with average geographical local errors less than 6.1 km from the Earth Radiation Budget Satellite orbital altitude of 610 km.

1.9. Output Data

There are two output data products, the bidirectional scans (BDS) and the instrument Earth scan (IES). Appendix B lists these output products. Each BDS product is a time-ordered 24-hour bidirectional scan data product that is used in the production of the ERBE like products. The BDS product contains both the raw and converted values of radiometric, engineering, digital status, and location data. The IES product consists of 1-hour data of spatially organized footprints that are sent to the cloud subsystem. The IES products contain only the converted filtered radiance for the three channels with each footprint location data, along with associated viewing geometries and quality flags.

1.10. References

Astheimer, R. W. 1983: Thermistor Infrared Detectors. *Infrared Detectors: Proceedings of SPIE*, William L. Wolfe, ed., vol. 443, SPIE, pp. 95–109.

Avis, L. M.; Paden, J.; Lee, R. B. III; Pandey, D. K.; Stassi, J. C.; Wilson, R. S.; Tolson, C. J.; and Bolden, W. C. 1994: NOAA-9 Earth Radiation Budget Experiment (ERBE) Scanner Offsets Determination. NASA TM 109086.

Barkstrom, Bruce R. 1990: Earth Radiation Budget Measurements—Pre-ERBE, ERBE, and CERES. *SPIE*, pp. 52–60.

Barkstrom, Bruce R.; Harrison, Edwin F.; and Lee, Robert, B., III 1990: Earth Radiation Budget Experiment—Preliminary Seasonal Results. *EOS*, vol. 71, p. 297 and 304.

Carman, Stephen L. 1983: Deep Concentric Grooves Enhance Blackbody Spectral and Spatial Uniformity. *Applications of Optical Metrology: Techniques and Measurements II—Proceedings of SPIE*, John J. Lee, Jr., ed., vol. 416, pp. 178–186.

Folkman, Mark A.; Jarecke, Peter J.; and Darnton, Lane A. 1991: Enhancements to the Radiometric Calibration Facility for the Clouds and the Earth's Radiant Energy System (CERES) Instruments. *Calibration of Passive Remote Observing Optical and Microwave Instrumentation—Proceedings of SPIE*, Bruce W. Guenther, ed., SPIE, vol. 1493, pp. 255–266.

Folkman, Mark A.; Jarecke, Peter J.; Hedman, Ted R.; Yun, John S.; and Lee, Robert B., III 1993: Design of a Solar Diffuser for On-Orbit Calibration of the Clouds and the Earth's Radiant Energy System (CERES) Instruments. *Sensor Systems for the Early Earth Observing System Platforms—Proceedings of SPIE*, William E. Barnes, ed., SPIE, vol. 1939, pp. 72–81.

Folkman, Mark; Jarecke, Peter; Hedman, Ted; Carman, Steve; Avis, Lee; Barkstrom, Bruce; Cooper, Jack; Kopia Leonard; Lawrence, Wes; Lee, Robert; and Smith, Lou 1994: Calibration of a Shortwave Reference Standard by Transfer From a Blackbody Standard Using a Cryogenic Active Cavity Radiometer. *IGRASS '94—Surface and Atmospheric Remote Sensing: Technologies, Data Analysis and Interpretation*, Volume IV, IEEE, pp. 2298–2300.

Foukal, Peter V.; Hoyt, C.; Kochling, H.; and Miller, P. 1990: Cryogenic Absolute Radiometers as Laboratory Irradiance Standards. *Remote Sens. Detect., & Pyroheliometers. Appl. Opt.*, vol. 29, pp. 988–993.

Frink, M. E.; Jarecke, P. J.; Folkman, M. A.; and Wright, R. E. 1993: Far-IR Spectral Measurements of the Clouds and the Earth's Radiant Energy System (CERES) Sensors Using a Fourier Transform Spectrometer and Pyro-Electric Reference Detector. *Sensor Systems for the Early Earth Observing System Platforms—Proceedings of SPIE*, William E. Barnes, ed., SPIE, vol. 1939, pp. 82–91.

Gibson, Michael A.; Lee, Robert B., III; and Thomas, Susan 1992: Evaluation of the Earth Radiation Budget Experiment Shortwave Channel's Stability Using In-Flight Calibration Sources. *Instrumentation for Planetary and Terrestrial Atmospheric Remote*, SPIE, pp. 108–216.

Halyo, Nesim; Choi, Dan A., Jr.; and Samms, Richard W. 1987: *Development of Response Models for the Earth Radiation Budget Experiment (ERBE) Sensors. I—Dynamic Models and Computer Simulations for the ERBE Nonscanner, Scanner and Solar Monitor Sensors*. NASA CR-178292.

Halyo, Nesim; Pandey, Dhirendra K.; and Taylor, Deborah B. 1989: *Modeling and Characterization of the Earth Radiation Budget Experiment (ERBE) Nonscanner and Scanner Sensors*. NASA CR-181818.

Hesser, R. J.; and Carman, S. L. 1983: Integrating Sphere as a Precision Radiometer Calibration Source. *Proceedings of SPIE*, vol. 416, pp. 111–118.

Hoffman, Lawrence H.; Weaver, William L.; and Kibler, James F. 1987: *Calculation and Accuracy of ERBE Scanner Measurement Locations*. NASA TP-2670.

Jarecke, P. J.; Folkman, M. A.; and Darnton, L. A. 1991: Radiometric Calibration Plan for the Clouds and the Earth's Radiant Energy System (CERES) Scanning Instruments. *Calibration of Passive Remote Observing Optical and Microwave Instrumentation—Proceedings of SPIE*, Bruce W. Guenther, ed., vol. 1493, pp. 244–254.

Jarecke, P. J.; Folkman, M. A.; and Hedman, T. R. 1993: Clouds and the Earth's Radiant Energy System (CERES): Long-Wave Calibration Plan and Radiometric Test Model (RTM) Calibration Results. *Metrologia.*, vol. 30, no. 4, p. 223.

Jarecke, Peter; Frink, Mark; Folkman, Mark; Carman, Steve; Baliga, Shankar; Doctor, Alan; Avis, Lee; Bardstrom, Bruce; Cooper, Jack; Kopia, Leonard; Lawrence, Wes; Lee, Robert; and Smith, Lou: End-to-End Spectral Response Characterization of the Clouds and the Earth's Radiant Energy System Sensors From 0.3 to 200 Microns. *IGRASS '94—Surface and Atmospheric Remote Sensing: Technologies, Data Analysis and Interpretation,* Volume IV, IEEE, pp. 2007–2009.

Kopia, Leonard P.; and Lee, Robert B., III 1992: Thermistor Bolometer Scanning Radiometer—Applications and Flight Experience. *Opt. Eng.*, vol. 31, pp. 156–165.

Kyle, H. L. 1993: The Nimbus Earth Radiation Budget (ERB) Experiment—1975 to 1992. *Bull. Am. Meteorol. Soc.*, vol. 74, no. 5, p. 815.

Kyle, H. L.; Hickey, J. R.; Ardanuy, P. E.; Jacobowitz, H.; Arking, A.; Cambell, G. G.; House, F. B.; Maschhoff, R.; Smith, G. L.; Stowe, L. L.; and Vonder Haar, T. 1933: The Nimbus Earth Radiation Budget (ERB) Experiment: 1975 to 1992. *Bull. American Meteorol. Soc.*, vol. 74, pp. 815–830/

Lee, Robert B., III; Barkstrom, Bruce R.; Avis, Lee M.; Halyo, Nesim; and Gibson, Michael A. 1989: Characterization of the Earth Radiation Budget Experiment (ERBE) Scanning Radiometers. *SPIE*, pp. 186–194.

Lee, Robert B., III; Gibson, M. A.; Thomas, Susan; Meekins, Jeffrey L.; and Mahan, J. R. 1990: Earth Radiation Budget Experiment Scanner Radiometric Calibration Results. Society of Photo-Optical Instrumentation Engineers, pp. 80–91.

Lee, R. B., III; and Barkstrom, B. R. 1991: Characterization of the Earth Radiation Budget Experiment Radiometers. *Metrologia*, vol. 28, p. 183–187.

Lee, Robert B.; Avis, Lee M.; Gibson, M. Alan; and Kopia, Leonard P. 1992: Characterization of the Mirror Attenuator Mosaic: Solar Diffuser Plate. *Appl. Opt.*, vol. 31, no. 31, pp. 6643–6652.

Lee, Robert B., III; Barkstrom, Bruce R.; Carman, Steve L.; Cooper, John E.; Folkman, Mark A.; Jarecke, Peter J.; Kopia, Leonard P.; and Wielicki, Bruce A. 1993a: *Sensor Systems for the Early Earth Observing System Platforms—Proceedings of SPIE,* William E. Barnes, ed., SPIE, vol. 1939, pp. 61–71.

Lee, R. B., III; Avis, L. M.; and Gibson, M. A. 1993b: In-Flight Evaluations of Tungsten Calibration Lamps Using Shortwave Thermisotr Bolometers and Active-Cavity. *Metrologia.*, vol. 30, no. 4, p. 389.

Lee, R. B., III; Barkstrom, B. R.; Smith, G. L.; Cooper, J. E.; Kopia, L. P.; Lawrence, R. W.; Folkman, M. A.; Jarecke, P. J.; Thomas, S.; Pandey, D. K.; Gibson, M. A.; Degnan, K. T.; Weaver, W. L.; and Crommelynck, D. A. H. 1996: The Clouds and the Earth's Radiant Energy System (CERES) Sensors and Preflight Calibration Plans, *J. Atmos. & Ocean. Technol.*, (submitted).

Ramanathan, V.; Barkstrom, Bruce R.; and Harrison, Edwin F. 1989: Climate and the Earth's Radiation Budget. *Phys. Today*, vol. 42, pp. 22–32.

Smith, G. Louis 1994: Effects of Time Response on the Point Spread Function of a Scanning Radiometer. *Appl. Opt.*, vol. 33, no. 30, p. 7031.

Sparrow, E. M.; and Cess, R. D. 1978: *Radiation Heat Transfer*. Hemisphere Publ., Corp.

Wielicki, Bruce A.; and Barkstrom, Bruce R. 1991: Clouds and the Earth's Radiant Energy System (CERES)—An Earth Observing System Experiment. *Second Symposium on Global Change Studies —Preprints* Am. Meteorol. Soc., pp. 11–16.

Appendix A

Input Data Products

Geolocate and Calibrate Earth Radiances (Subsystem 1.0)

This appendix describes the data products which are used by the algorithms in this subsystem. Table A-1 below summarizes these products, listing the CERES and EOSDIS product codes or abbreviations, a short product name, the product type, the production frequency, and volume estimates for each individual product as well as a complete data month of production. The product types are defined as follows:

Archival products:	Assumed to be permanently stored by EOSDIS
Internal products:	Temporary storage by EOSDIS (days to years)
Ancillary products:	Non-CERES data needed to interpret measurements

The following pages describe each product. An introductory page provides an overall description of the product and specifies the temporal and spatial coverage. The table which follows the introductory page briefly describes every parameter which is contained in the product. Each product may be thought of as metadata followed by data records. The metadata (or header data) is not well-defined yet and is included mainly as a placeholder. The description of parameters which are present in each data record includes parameter number (a unique number for each distinct parameter), units, dynamic range, the number of elements per record, an estimate of the number of bits required to represent each parameter, and an element number (a unique number for each instance of every parameter). A summary at the bottom of each table shows the current estimated sizes of metadata, each data record, and the total data product. A more detailed description of each data product will be contained in a user's guide to be published before the first CERES launch.

Table A-1. Input Products Summary

Product code		Name	Category	Frequency	Size, MB	Monthly size, MB
CERES	EOSDIS					
INSTR_PDS	none	Instrument production data set	archival	1/day	87.0	2697
INSTR_QLKD	none	Instrument quicklook data set	archival	1/day	3.3	102
EPH_ANC	none	Satellite ephemeris/ancillary data	archival	1/day	0.1	3

Instrument Production Data Set (INSTR_PDS)

The instrument production data set (INSTR_PDS) is the level 0 raw data from the CERES instrument as structured by the instrument itself, and is programmed by the instrument developer, TRW, Inc. All CERES instrument output is formatted according to the CCSDS packet concept, and all CERES instrument packets contain the same data output formatting options, although some instrument data packets contain data unique to a particular spacecraft. The seven basic pieces of information contained in a normal CERES data packet (i.e., science output format) are

1. Packet header
2. Time (in secondary header)
3. Radiometric detector outputs
4. Instrument gimbal pointing knowledge
5. Instrument engineering data (temperatures and voltages)
6. Instrument digital status

There are several packet content variations possible for the CERES instruments; some of these variations are due to spacecraft differences and some are due to instrument output differences. These differences are noted in the following table as selections. The data structure labelled EOS_Quicklook_Statword represents an 8-bit piece of the secondary header on the EOS platform that will contain a one bit quicklook flag, and seven bits of user-definable flags. Data packets from the TRMM spacecraft do not contain these extra 8 bits in the secondary header, so the EOS_Quicklook_Statword structure is not valid for TRMM packets.

Another selection shown in the following table is the INSTR_Digital_Status_Block. One and only one of the two selection possibilities can be present in any given CERES data packet; either the actual instrument digital status information is present, or a "fixed pattern" of bits is present. This fixed pattern will be present when the instrument is outputting data in the fixed pattern data format.

The INSTR_Science_Data data structure is another selection where one and only one of the selection possibilities can be present in any given CERES data packet. The selection options here are based on the different data output formats of the instrument: science, memory dump, gimbal operation, processor operation, and fixed pattern.

Finally, the INSTR-EOS_Ancillary_Data structure shown in the following table is a spacecraft-dependent structure. The spacecraft ancillary data is only appended to data packets output by a CERES instrument on an EOS spacecraft; the data packets output by a CERES instrument on a TRMM spacecraft will not have this information.

Level: 0
Type: Archival
Frequency: 1/day

Time Interval Covered
File: 1 day
Record: Single 6.6-sec scans

Portion of Globe Covered
File: Satellite swath
Record: N/A

Portion of Atmosphere Covered
File: N/A

Table A-2. Instrument Production Data Set (INSTR_PDS)

Description	Parameter Number	Units	Range	Elements/ Record	Bits/ Elem	Elem Num
INSTR_PDS						
INSTR_PDS File Header		N/A		1	256	
INSTR_PDS_Data_Packets is Array[13091] of:						
INSTR_PDS_Data_Packet						
INSTR_Data_Packet						
INSTR_Packet_Hdr						
INSTR_Packet_Header_Data						
Version Number	1	N/A	0..7	1	3	1
Packet Type	2	N/A	0..1	1	1	2
Secondary Header Flag	3	N/A	0..1	1	1	3
Application Identifier	4	N/A	0..2047	1	11	4
Segment Flags	5	N/A	0..3	1	2	5
Source Sequence Count	6	N/A	0..16383	1	14	6
Packet Length	7	N/A	0..65535	1	16	7
Packet Time Code	8	day	Mission Life	1	64	8
EOS_Supplem_Secondary_Hdr is selection of						
EOS_Supplem_Flags						
EOS Quicklook Flag	9	N/A	0..1	1	1	9
EOS User Flag	10	N/A	0..127	1	7	10
INSTR_Data						
INSTR_Digital_Status_Block is selection of						
Instrument Digital Status - see DRL64, Rev B. (TRW) for details	11	-	-	1	2288	11
Instrument Digital Status Fixed Pattern	12	count	N/A	1	2288	12
INSTR_Measurement_Data is selection of						
INSTR_Science_Data is Array[660] of:						
INSTR_Science_Record						
Elevation Position Count	13	count	0..65535	660	16	13
Azimuth Position Count	14	count	0..65535	660	16	673
Total Detector Output	15	count	0..4095	660	12	1333
SW Detector Output	16	count	0..4095	660	12	1993
Window Detector Output	17	count	0..4095	660	12	2653
Instrument Analog Data - see DRL64, Rev. B (TRW) for details	18	-	-	660	12	3313
INSTR_Memory_Data is Array[660] of:						
INSTR_Memory_Record						
Elevation Position Count	19	count	0..65535	660	16	3973
Azimuth Position Count	20	count	0..65535	660	16	4633
DAP Memory Dump Data	21	N/A	0..65535	660	16	5293
ICP Memory Dump Data	22	N/A	0..65535	660	16	5953
Fill Data	23	N/A	0..15	660	4	6613
Instrument Analog Data - see DRL64, Rev. B (TRW) for details	24	-	-	660	12	7273
INSTR_Gimbal_Operation_Data is Array[660] of:						
INSTR_Gimbal_Record						
Elevation Position Count	25	count	0..65535	660	16	7933
Azimuth Position Count	26	count	0..65535	660	16	8593
Elevation Error	27	count	0..55535	660	16	9253
Azimuth Error	28	count	0..65535	660	16	9913
Fill Data	29	N/A	0..15	660	4	10573
Instrument Analog Data - see DRL64, Rev. B (TRW) for details	30	-	-	660	12	11233
INSTR_Processor_Operation_Data is Array[660] of:						
INSTR_Processor_Op_Record						
Elevation Position Count	31	count	0..65535	660	16	11893
Azimuth Position Count	32	count	0..65535	660	16	12553
DAP Timing	33	N/A	0..65535	660	16	13213
ICP Timing	34	N/A	0..65535	660	16	13873

Table A-2. Concluded

Description	Parameter Number	Units	Range	Elements/ Record	Bits/ Elem	Elem Num
Fill Data	35	N/A	0..15	660	4	14533
Instrument Analog Data - see DRL64, Rev. B (TRW) for details	36	-	-	660	12	15193
INSTR_Diagnostic_Pattern_Data is Array[660] of:						
INSTR_Fixed_Record						
Fixed Pattern in Elevation Field	37	N/A	0..65535	660	16	15853
Fixed Pattern for Azimuth Field	38	N/A	0..65535	660	16	16513
Fixed Pattern for Total Channel Field	39	N/A	0..4095	660	12	17173
Fixed Pattern for Window Channel Field	40	N/A	0..4095	660	12	17833
Fixed Pattern for Shortwave Channel Field	41	N/A	0..4095	660	12	18493
Fixed Pattern for Analog Field	42	N/A	0..4095	660	12	19153
INSTR-EOS_Ancillary_Data is selection of						
INSTR_Ancillary_Data						
Ancillary Time Stamp	43	count	$0..1.84x10^{19}$	1	64	19813
GPS/UTC Time Conversion	44	count	$0..4.29x10^{9}$	1	32	19814
Solar Array Current	45	count	0..255	1	8	19815
Mag Coil Current X	46	count	0..255	1	8	19816
Mag Coil Current Y	47	count	0..255	1	8	19817
Mag Coil Current Z	48	count	0..255	1	8	19818
Satellite Position (X) Count	49	count	$0..4.29x10^{9}$	1	32	19819
Satellite Position (Y) Count	50	count	$0..4.29x10^{9}$	1	32	19820
Satellite Position (Z) Count	51	count	$0..4.29x10^{9}$	1	32	19821
Satellite Velocity (X) Count	52	count	$0..4.29x10^{9}$	1	32	19822
Satellite Velocity (Y) Count	53	count	$0..4.29x10^{9}$	1	32	19823
Satellite Velocity (Z) Count	54	count	$0..4.29x10^{9}$	1	32	19824
Satellite Attitude (Roll) Count	55	count	0..65535	1	16	19825
Satellite Attitude (Pitch) Count	56	count	0..65535	1	16	19826
Satellite Attitude (Yaw) Count	57	count	0..65535	1	16	19827
Satellite Attitude Rate (Roll) Count	58	count	0..65535	1	16	19828
Satellite Attitude Rate (Pitch) Count	59	count	0..65535	1	16	19829
Satellite Attitude Rate (Yaw) Count	60	count	0..65535	1	16	19830
Solar X Position	61	count	0..255	1	8	19831
Solar Y Position	62	count	0..255	1	8	19832
Solar Z Position	63	count	0..255	1	8	19833
Lunar X Position	64	count	0..255	1	8	19834
Lunar Y Position	65	count	0..255	1	8	19835
Lunar Z Position	66	count	0..255	1	8	19836

Total Meta Bits/File:	256
Total Data Bits/Record:	55720
Total Records/File:	13091
Total Data Bits/File:	729430520
Total Bits/File:	729430776

Instrument Quicklook Data Set (INSTR_QLKD)

The instrument quicklook data (INSTR_QLKD) consists of level 0 data downlinked by a spacecraft from a CERES instrument during one TDRSS contact. The data packets are formatted like any other CERES data packet (see INSTR_PDS discussion for the format of a CERES data packet), but the packets are contained in a single file that holds up to three groups of time-ordered packets, where each group has a separate APID. This data structure principally contains solar and deep-space calibration data and instrument diagnostic data. During normal operations, it is expected that three quicklook data files will be needed for each instrument every two weeks to support calibration activities. For monthly storage sizing purposes, however, a estimate of one quicklook data file per instrument per day was used. This larger estimate is used to factor in instrument anomalies or instrument diagnostic modes that do not occur during normal operations.

Level: 0
Type: Archival
Frequency: 1/day

Portion of Globe Covered
File: Satellite swath
Record: N/A

Time Interval Covered
File: Variable
Record: Single 6.6-sec scans

Portion of Atmosphere Covered
File: N/A

Table A-3. Instrument Quicklook Data Set (INSTR_QLKD)

Description	Parameter Number	Units	Range	Elements/ Record	Bits/ Elem	Elem Num
INSTR_QLKD						
INSTR_QLKD File Header		N/A		1	256	
INSTR_QLKD_Data_Packets is Array[500] of:						
INSTR_QLKD_Data_Packet						
INSTR_Data_Packet						
INSTR_Packet_Hdr						
INSTR_Packet_Header_Data						
Version Number	1	N/A	0..7	1	3	1
Packet Type	2	N/A	0..1	1	1	2
Secondary Header Flag	3	N/A	0..1	1	1	3
Application Identifier	4	N/A	0..2047	1	11	4
Segment Flags	5	N/A	0..3	1	2	5
Source Sequence Count	6	N/A	0..16383	1	14	6
Packet Length	7	N/A	0..65535	1	16	7
Packet Time Code	8	day	Mission Life	1	64	8
EOS_Supplem_Secondary_Hdr is selection of						
EOS_Supplem_Flags						
EOS Quicklook Flag	9	N/A	0..1	1	1	9
EOS User Flag	10	N/A	0..127	1	7	10
INSTR_Data						
INSTR_Digital_Status_Block is selection of						
Instrument Digital Status - see DRL64, Rev B. (TRW) for details	11	-	-	1	2288	11
Instrument Digital Status Fixed Pattern	12	count	N/A	1	2288	12
INSTR_Measurement_Data is selection of						
INSTR_Science_Data is Array[660] of:						
INSTR_Science_Record						
Elevation Position Count	13	count	0..65535	660	16	13
Azimuth Position Count	14	count	0..65535	660	16	673
Total Detector Output	15	count	0..4095	660	12	1333
SW Detector Output	16	count	0..4095	660	12	1993
Window Detector Output	17	count	0..4095	660	12	2653
Instrument Analog Data - see DRL64, Rev. B (TRW) for details	18	-	-	660	12	3313
INSTR_Memory_Data is Array[660] of:						
INSTR_Memory_Record						
Elevation Position Count	19	count	0..65535	660	16	3973
Azimuth Position Count	20	count	0..65535	660	16	4633
DAP Memory Dump Data	21	N/A	0..65535	660	16	5293
ICP Memory Dump Data	22	N/A	0..65535	660	16	5953
Fill Data	23	N/A	0..15	660	4	6613
Instrument Analog Data - see DRL64, Rev. B (TRW) for details	24	-	-	660	12	7273
INSTR_Gimbal_Operation_Data is Array[660] of:						
INSTR_Gimbal_Record						
Elevation Position Count	25	count	0..65535	660	16	7933
Azimuth Position Count	26	count	0..65535	660	16	8593
Elevation Error	27	count	0..55535	660	16	9253
Azimuth Error	28	count	0..65535	660	16	9913
Fill Data	29	N/A	0..15	660	4	10573
Instrument Analog Data - see DRL64, Rev. B (TRW) for details	30	-	-	660	12	11233
INSTR_Processor_Operation_Data is Array[660] of:						
INSTR_Processor_Op_Record						
Elevation Position Count	31	count	0..65535	660	16	11893
Azimuth Position Count	32	count	0..65535	660	16	12553
DAP Timing	33	N/A	0..65535	660	16	13213
ICP Timing	34	N/A	0..65535	660	16	13873

Table A-3. Concluded

Description	Parameter Number	Units	Range	Elements/ Record	Bits/ Elem	Elem Num
Fill Data	35	N/A	0..15	660	4	14533
Instrument Analog Data - see DRL64, Rev. B (TRW) for details	36	-	-	660	12	15193
INSTR_Diagnostic_Pattern_Data is Array[660] of:						
INSTR_Fixed_Record						
Fixed Pattern in Elevation Field	37	N/A	0..65535	660	16	15853
Fixed Pattern for Azimuth Field	38	N/A	0..65535	660	16	16513
Fixed Pattern for Total Channel Field	39	N/A	0..4095	660	12	17173
Fixed Pattern for Window Channel Field	40	N/A	0..4095	660	12	17833
Fixed Pattern for Shortwave Channel Field	41	N/A	0..4095	660	12	18493
Fixed Pattern for Analog Field	42	N/A	0..4095	660	12	19153
INSTR-EOS_Ancillary_Data is selection of						
INSTR_Ancillary_Data						
Ancillary Time Stamp	43	count	$0..1.84x10^{19}$	1	64	19813
GPS/UTC Time Conversion	44	count	$0..4.29x10^{9}$	1	32	19814
Solar Array Current	45	count	0..255	1	8	19815
Mag Coil Current X	46	count	0..255	1	8	19816
Mag Coil Current Y	47	count	0..255	1	8	19817
Mag Coil Current Z	48	count	0..255	1	8	19818
Satellite Position (X) Count	49	count	$0..4.29x10^{9}$	1	32	19819
Satellite Position (Y) Count	50	count	$0..4.29x10^{9}$	1	32	19820
Satellite Position (Z) Count	51	count	$0..4.29x10^{9}$	1	32	19821
Satellite Velocity (X) Count	52	count	$0..4.29x10^{9}$	1	32	19822
Satellite Velocity (Y) Count	53	count	$0..4.29x10^{9}$	1	32	19823
Satellite Velocity (Z) Count	54	count	$0..4.29x10^{9}$	1	32	19824
Satellite Attitude (Roll) Count	55	count	0..65535	1	16	19825
Satellite Attitude (Pitch) Count	56	count	0..65535	1	16	19826
Satellite Attitude (Yaw) Count	57	count	0..65535	1	16	19827
Satellite Attitude Rate (Roll) Count	58	count	0..65535	1	16	19828
Satellite Attitude Rate (Pitch) Count	59	count	0..65535	1	16	19829
Satellite Attitude Rate (Yaw) Count	60	count	0..65535	1	16	19830
Solar X Position	61	count	0..255	1	8	19831
Solar Y Position	62	count	0..255	1	8	19832
Solar Z Position	63	count	0..255	1	8	19833
Lunar X Position	64	count	0..255	1	8	19834
Lunar Y Position	65	count	0..255	1	8	19835
Lunar Z Position	66	count	0..255	1	8	19836

Total Meta Bits/File:	256
Total Data Bits/Record:	55720
Total Records/File:	500
Total Data Bits/File:	27860000
Total Bits/File:	27860256

Satellite Ephemeris/Ancillary Data (EPH_ANC)

The EPH_ANC (satellite ephemeris and ancillary) data stream contains information about spacecraft position and velocity, spacecraft attitude errors and attitude error rates, sun and moon positions, and additional spacecraft information needed to process CERES instrument data, such as spacecraft direction or spacecraft mode. This additional spacecraft data is mission-dependent.

The position and attitude data are used to Earth-locate each CERES footprint and calculate viewing geometry. The sun position data are important to identify the proper angular distribution model based on the geometry of the CERES footprint relative to the sun.

Level: 0
Type: Archival
Frequency: 1/day

Time Interval Covered
File: 1 day
Record: 1 minute

Portion of Globe Covered
File: N/A
Record: N/A

Portion of Atmosphere Covered
File: N/A

Table A-4. Satellite Ephemeris/Ancillary Data (EPH_ANC)

Description	Parameter Number	Units	Range	Elements/ Record	Bits/ Elem	Elem Num
EPH_ANC						
EPH_ANC File Header		N/A		1	2048	
EPH_ANC_Record is Array[1440] of:						
EPH_ANC_Data						
Orbital_Ephemeris						
Ephemeris Record Time	1	TBD	TBD	1	32	1
Satellite Altitude	2	km	0..1200	1	16	2
Earth-Sun distance	3	AU	0.98..1.02	1	16	3
Number of orbits	4	N/A	TBD	1	16	4
Satellite X Position	5	km	TBD	1	32	5
Satellite Y Position	6	km	TBD	1	32	6
Satellite Z Position	7	km	TBD	1	32	7
Satellite X Velocity	8	km sec^{-1}	TBD	1	32	8
Satellite Y Velocity	9	km sec^{-1}	TBD	1	32	9
Satellite Z Velocity	10	km sec^{-1}	TBD	1	32	10
Satellite Roll Attitude	11	deg	TBD	1	16	11
Satellite Pitch Attitude	12	deg	TBD	1	16	12
Satellite Yaw Attitude	13	deg	TBD	1	16	13
Satellite Roll Attitude Rate	14	deg sec^{-1}	TBD	1	16	14
Satellite Pitch Attitude Rate	15	deg sec^{-1}	TBD	1	16	15
Satellite Yaw Attitude Rate	16	deg sec^{-1}	TBD	1	16	16
Solar X Position	17	count	0..255	1	8	17
Solar Y Position	18	count	0..255	1	8	18
Solar Z Position	19	count	0..255	1	8	19
Lunar X Position	20	count	0..255	1	8	20
Lunar Y Position	21	count	0..255	1	8	21
Lunar Z Position	22	count	0..255	1	8	22
SC_ANCILLARY						
Satellite Direction	23	N/A	TBD	1	16	23
Satellite Mode	24	N/A	TBD	1	16	24
Satellite Command	25	N/A	TBD	1	16	25
Solar Array Current	26	count	0..255	1	8	26

Total Meta Bits/File:	2048
Total Data Bits/Record:	472
Total Records/File:	1440
Total Data Bits/File:	679680
Total Bits/File:	681728

Appendix B

Output Data Products

Geolocate and Calibrate Earth Radiances (Subsystem 1.0)

This appendix describes the data products which are produced by the algorithms in this subsystem. Table B-1 below summarizes these products, listing the CERES and EOSDIS product codes or abbreviations, a short product name, the product type, the production frequency, and volume estimates for each individual product as well as a complete data month of production. The product types are defined as follows:

Archival products:	Assumed to be permanently stored by EOSDIS
Internal products:	Temporary storage by EOSDIS (days to years)

The following pages describe each product. An introductory page provides an overall description of the product and specifies the temporal and spatial coverage. The table which follows the introductory page briefly describes every parameter which is contained in the product. Each product may be thought of as metadata followed by data records. The metadata (or header data) is not well-defined yet and is included mainly as a placeholder. The description of parameters which are present in each data record includes parameter number (a unique number for each distinct parameter), units, dynamic range, the number of elements per record, an estimate of the number of bits required to represent each parameter, and an element number (a unique number for each instance of every parameter). A summary at the bottom of each table shows the current estimated sizes of metadata, each data record, and the total data product. A more detailed description of each data product will be contained in a user's guide to be published before the first CERES launch.

Table B-1. Output Products Summary

Product code		Name	Category	Frequency	Size, MB	Monthly size, MB
CERES	EOSDIS					
BDS	CER01	Bidirectional scan	archival	1/day	313.6	9722
IES	CER09	Instrument earth scans	internal	1/hour	14.5	10788

Bidirectional Scan (BDS)

The BDS data product is an archival product containing level 1B CERES scanner data obtained for a 24-hour period. All science scan modes are included in the BDS, including the fixed and rotating azimuth scan modes that perform normal earth, internal calibration, and short scan elevation profiles. The BDS product includes samples taken at all scan elevation positions (including space looks and internal calibration views).

The BDS includes the raw count data stream and the converted engineering representative data. These data are divided into the following seven groups that are carried forward from the level-0 product:

1. Time
2. Instrument status
3. Radiometric channel counts
4. Instrument telescope pointing (elevation and azimuth)
5. Temperatures
6. Voltages and currents
7. Satellite ephemeris and ancillary data

In addition, we add the following filtered radiance data from the three radiometric channels and their associated field of view location geometry:

8. Filtered radiances, including quality flags
9. Earth location geometry, including quality flags

In the BDS data product, the filtered radiances and the Earth location geometry are considered a multiband, single data element footprint. Quality flags are used to indicate the reliability of the radiance and Earth location measurements. This product is also used to diagnose instrument performance conditions.

Level: 1B
Type: archival
Frequency: 1/day

Time Interval Covered
File: 24 hours
Record: Single 6.6-sec scans

Portion of Globe Covered
File: Satellite swath
Record: N/A

Portion of Atmosphere Covered
File: Satellite altitude

Table B-2. Bidirectional Scan (BDS)

Description	Parameter Number	Units	Range	Elements/ Record	Bits/ Elem	Elem Num
BDS						
BDS File Header		N/A		1	256	
BDS_Data is Array[13091] of:						
BDS_Record						
Julian Day at Scan Start	1	day	2449353..2458500	1	32	1
Julian Time at Scan Start	2	day	0..1	1	32	2
BDS Instrument Status	3	N/A	0..65535	1	16	3
BDS_Scan_Information						
BDS_Radiometric_Data is Array[660] of:						
BDS_Pixel_Radiometric						
BDS_Filtered_Radiances						
CERES total filtered radiance, upwards	4	$W\text{-}m^{-2}\ sr^{-1}$	0..700	660	16	4
CERES shortwave filtered radiance, upwards	5	$W\text{-}m^{-2}\ sr^{-1}$	-10..510	660	16	664
CERES window filtered radiance, upwards	6	$W\text{-}m^{-2}\ sr^{-1}$	0..50	660	16	1324
BDS Quality Flags	7	N/A	0..65535	660	16	1984
BDS_Detector_Output_(Raw)						
Total Detector Output	8	count	0..4095	660	12	2644
SW Detector Output	9	count	0..4095	660	12	3304
Window Detector Output	10	count	0..4095	660	12	3964
BDS_Location_Data is Array[660] of:						
BDS_Pixel_Location						
BDS_Raw_Location						
Azimuth Position Count	11	count	0..65535	660	16	4624
Elevation Position Count	12	count	0..65535	660	16	5284
BDS_TOA_Location						
Colatitude of CERES FOV at TOA	13	deg	0..180	660	16	5944
Longitude of CERES FOV at TOA	14	deg	0..360	660	16	6604
CERES viewing zenith at TOA	15	deg	0..90	660	16	7264
CERES solar zenith at TOA	16	deg	0..180	660	16	7924
CERES relative azimuth at TOA	17	deg	0..360	660	16	8584
BDS_Housekeeping_Data						
BDS_Temperature_Measurements						
BDS_Raw_Temperature_Count						
12_Raw_Temp_Samples is Array[12] of:						
12_Raw_Temp_Samples_per_Scan						
Total Heater DAC Value	18	N/A	0..4095	12	12	9244
SW Heater DAC Value	19	N/A	0..4095	12	12	9256
Window Heater DAC Value	20	N/A	0..4095	12	12	9268
BB Heater DAC Value	21	N/A	0..4095	12	12	9280
Total Control Temp Count	22	count	0..4095	12	12	9292
Total Measured Temp Count	23	count	0..4095	12	12	9304
SW Control Temp Count	24	count	0..4095	12	12	9316
SW Measured Temp Count	25	count	0..4095	12	12	9328
Window Control Temp Count	26	count	0..4095	12	12	9340
Window Measured Temp Count	27	count	0..4095	12	12	9352
Total Blackbody Temp Count	28	count	0..4095	12	12	9364
LW Blackbody Temp Count	29	count	0..4095	12	12	9376
3_Raw_Temp_Samples is Array[3] of:						
3_Raw_Temp_Samples_per_Scan						
Elevation Spindle Temp (Motor) Count	30	count	0..4095	3	12	9388
Elevation Spindle Temp (Cable Wrap) Count	31	count	0..4095	3	12	9391
Elevation Bearing Temp (Motor) Count	32	count	0..4095	3	12	9394
Elevation Bearing Temp (Cable Wrap) Count	33	count	0..4095	3	12	9397
SWICS Photodiode Temp Count	34	count	0..4095	3	12	9400

Table B-2. Continued

Description	Parameter Number	Units	Range	Elements/ Record	Bits/ Elem	Elem Num
Sensor Module Temp Count	35	count	0..4095	3	12	9403
Sensor Electronics Temp Count	36	count	0..4095	3	12	9406
Main Cover Motor Temp Count	37	count	0..4095	3	12	9409
MAM Total Baffle Temp #1 Count	38	count	0..4095	3	12	9412
MAM Total Baffle Temp #2 Count	39	count	0..4095	3	12	9415
MAM SW Assembly Temp Count	40	count	0..4095	3	12	9418
MAM Total Assembly Temp Count	41	count	0..4095	3	16	9421
DAA Radiator Temp Count	42	count	0..4095	3	12	9424
DAA CPU Elect Temp Count	43	count	0..4095	3	12	9427
DAA Prom Elect Temp Count	44	count	0..4095	3	12	9430
DAA RAM Elect Temp Count	45	count	0..4095	3	12	9433
DAA ADC Elect Temp Count	46	count	0..4095	3	12	9436
ECA Radiator Temp Count	47	count	0..4095	3	12	9439
ECA Elect Temp Count	48	count	0..4095	3	12	9442
ACA Elect Temp Count	49	count	0..4095	3	12	9445
Azimuth Lower Bearing Temp Count	50	count	0..4095	3	12	9448
Azimuth High Bearing Temp Count	51	count	0..4095	3	12	9451
ICA Radiator Temp Count	52	count	0..4095	3	12	9454
ICA CPU Elect Temp Count	53	count	0..4095	3	12	9457
ICA Prom Elect Temp Count	54	count	0..4095	3	12	9460
ICA RAM Elect Temp Count	55	count	0..4095	3	12	9463
ICA ADC Elect Temp Cnt	56	count	0..4095	3	12	9466
PCA Radiator Temp Count	57	count	0..4095	3	12	9469
PCA Electronics Temp Count	58	count	0..4095	3	12	9472
PCA Q1 Transistor Case Temp Count	59	count	0..4095	3	12	9475
Pedestal Temp #1 (Brake Hsg) Count	60	count	0..4095	3	12	9478
Pedestal Temp #2 (@ Isolator) Count	61	count	0..4095	3	12	9481
BDS_Converted_Temperature						
12_Temp_Samples is Array[12] of:						
12_Temp_Samples_per_Scan						
Total Control Temp	62	°C	36..40	12	16	9484
Total Measured Temp	63	°C	36..40	12	16	9496
SW Control Temp	64	°C	36..40	12	16	9508
SW Measured Temp	65	°C	36..40	12	16	9520
Window Control Temp	66	°C	36..40	12	16	9532
Window Measured Temp	67	°C	36..40	12	16	9544
Total Blackbody Temp	68	°C	-15..60	12	16	9556
LW Blackbody Temp	69	°C	-15..60	12	16	9568
3_Temp_Samples is Array[3] of:						
3_Temp_Samples_per_Scan						
Elevation Spindle Temp (Motor)	70	°C	-30..70	3	16	9580
Elevation Spindle Temp (Cable Wrap)	71	°C	-30..70	3	16	9583
Elevation Bearing Temp (Motor)	72	°C	-30..70	3	16	9586
Elevation Bearing Temp (Cable Wrap)	73	°C	-30..70	3	16	9589
Sensor Module Temp	74	°C	-30..70	3	16	9592
Sensor Elect Temp	75	°C	-30..70	3	16	9595
Main Cover Motor Temp	76	°C	-30..70	3	16	9598
SWICS Photodiode Temp	77	°C	-30..70	3	16	9601
MAM Total Baffle Temp #1	78	°C	-30..70	3	16	9604
MAM Total Baffle Temp #2	79	°C	-30..70	3	16	9607
MAM SW Assembly Temp	80	°C	-30..70	3	16	9610
MAM Total Assembly Temp	81	°C	-30..70	3	16	9613
DAA Radiator Temp	82	°C	-30..70	3	16	9616

Table B-2. Continued

Description	Parameter Number	Units	Range	Elements/ Record	Bits/ Elem	Elem Num
DAA CPU Elect Temp	83	°C	-30..70	3	16	9619
DAA Prom Elect Temp	84	°C	-30..70	3	16	9622
DAA RAM Elect Temp	85	°C	-30..70	3	16	9625
DAA ADC Elect Temp	86	°C	-30..70	3	16	9628
ECA Radiator Temp	87	°C	-30..70	3	16	9631
ECA Elect Temp	88	°C	-30..70	3	16	9634
ACA Elect Temp	89	°C	-30..70	3	16	9637
Azimuth Lower Bearing Temp	90	°C	-30..70	3	16	9640
Azimuth Upper Bearing Temp	91	°C	-30..70	3	16	9643
ICA Radiator Temp	92	°C	-30..70	3	16	9646
ICA CPU Elect Temp	93	°C	-30..70	3	16	9649
ICA Prom Elect Temp	94	°C	-30..70	3	16	9652
ICA RAM Elect Temp	95	°C	-30..70	3	16	9655
ICA ADC Elect Temp	96	°C	-30..70	3	16	9658
PCA Radiator Temp	97	°C	-30..70	3	16	9661
PCA Electronics Temp	98	°C	-30..70	3	16	9664
PCA Q1 Transistor Case Temp	99	°C	-30..70	3	16	9667
Pedestal Temp #1 (Brake Hsg)	100	°C	-30..70	3	16	9670
Pedestal Temp #2 (@ Isolator)	101	°C	-30..70	3	16	9673
BDS_Voltage_Measurements						
BDS_Raw_Voltage_Count						
3_Raw_Volt_Samples is Array[3] of:						
3_Raw_Volt_Samples_per_Scan						
Sensor +120V Bias Count	102	count	0..4095	3	12	9676
Sensor -120V Bias Count	103	count	0..4095	3	12	9679
SWICS Photodiode Output Count	104	count	0..4095	3	12	9682
SWICS Lamp Current Count	105	count	0..4095	3	12	9685
ICA +5V Digital Count	106	count	0..4095	3	12	9688
ICA +15V (to ECA/ACA) Count	107	count	0..4095	3	12	9691
ICA -15V (to ECA/ACA) Count	108	count	0..4095	3	12	9694
ICA +18V Count	109	count	0..4095	3	12	9697
ICA -18V Count	110	count	0..4095	3	12	9700
ICA +15V (Internal) Count	111	count	0..4095	3	12	9703
ICA -15V (Internal) Count	112	count	0..4095	3	12	9706
DAA Ground #1 Count	113	count	0..4095	3	12	9709
DAA Ground #2 Count	114	count	0..4095	3	12	9712
DAA -10V Reference Count	115	count	0..4095	3	12	9715
DAA +130V Count	116	count	0..4095	3	12	9718
DAA -130V Count	117	count	0..4095	3	12	9721
DAA +12V Count	118	count	0..4095	3	12	9724
DAA -12V Count	119	count	0..4095	3	12	9727
DAA +15V Count	120	count	0..4095	3	12	9730
DAA -15V Count	121	count	0..4095	3	12	9733
DAA +18V Count	122	count	0..4095	3	12	9736
DAA -18V Count	123	count	0..4095	3	12	9739
12_Raw_Volt_Samples is Array[12] of:						
12_Raw_Volt_Samples_per_Scan						
Elevation Torque Output Count	124	count	0..4095	12	12	9742
Azimuth Torque Output Count	125	count	0..4095	12	12	9754
BDS_Converted_Voltage						
3_Volt_Samples is Array[3] of:						
3_Volt_Samples_per_Scan						
Sensor +120V Bias	126	volt	115..125	3	16	9766

Table B-2. Continued

Description	Parameter Number	Units	Range	Elements/ Record	Bits/ Elem	Elem Num
Sensor -120V Bias	127	volt	-125..-115	3	16	9769
SWICS Photodiode Output	128	volt	0..8	3	16	9772
SWICS Lamp Current	129	milliamp	0..100	3	16	9775
ICA +5V Digital	130	volt	0..8	3	16	9778
ICA +15V (to ECA/ACA)	131	volt	0..20	3	16	9781
ICA -15V (to ECA/ACA)	132	volt	-20..0	3	16	9784
ICA +18V	133	volt	0..20	3	16	9787
ICA -18V	134	volt	-20..0	3	16	9790
ICA +15V (Internal)	135	volt	0..30	3	16	9793
ICA -15V (Internal)	136	volt	-30..0	3	16	9796
DAA Ground #1	137	volt	0..10	3	16	9799
DAA Ground #2	138	volt	0..10	3	16	9802
DAA -10V Reference	139	volt	-20..0	3	16	9805
DAA +130V	140	volt	90..170	3	16	9808
DAA -130V	141	volt	-224..-36	3	16	9811
DAA +12V	142	volt	0..20	3	16	9814
DAA -12V	143	volt	-20..0	3	16	9817
DAA +15V	144	volt	0..20	3	16	9820
DAA -15V	145	volt	-20..0	3	16	9823
DAA +18V	146	volt	0..20	3	16	9826
DAA -18V	147	volt	-20..0	3	16	9829
12_Volt_Samples is Array[12] of:						
12_Volt_Samples_per_Scan						
Elevation Torque Output	148	volt	-20..20	12	16	9832
Azimuth Torque Output	149	volt	-20..20	12	16	9844
BDS_Position_Measurements						
BDS_Raw_Position_Count						
3_Pos_Samples is Array[3] of:						
3_Pos_Samples_per_Scan						
ACA Encoder Clear Track A Count	150	count	0..4095	3	12	9856
ACA Encoder Clear Track B Count	151	count	0..4095	3	12	9859
ECA Encoder Clear Track A Count	152	count	0..4095	3	12	9862
ECA Encoder Clear Track B Count	153	count	0..4095	3	12	9865
Main Cover Pos #1 Count	154	count	0..4095	3	12	9868
Main Cover Pos #2 Count	155	count	0..4095	3	12	9871
MAM Cover Pos Count	156	count	0..4095	3	12	9874
Azimuth Caging (Brake) Pos Count	157	count	0..4095	3	12	9877
60_Pos_Samples is Array[60] of:						
60_Pos_Samples_per_Scan						
SPS 1 Narrow Field Output Count	158	count	0..4095	60	12	9880
SPS 1 Wide Field Output Count	159	count	0..4095	60	12	9940
SPS 2 Narrow Field Output Count	160	count	0..4095	60	12	10000
SPS 2 Wide Field Output Count	161	count	0..4095	60	12	10060
660_Raw_Pos_Samples is Array[660] of:						
660_Raw_Pos_Samples_per_Scan						
Elevation Position Count	162	count	0..65535	660	16	10120
Azimuth Position Count	163	count	0..65535	660	16	10780
BDS_Converted_Position						
3_Conv_Pos_Samples is Array[3] of:						
3_Conv_Pos_Samples_per_Scan						
ACA Encoder Clear Track A	164	deg	0..360	3	16	11440
ACA Encoder Clear Track B	165	deg	0..360	3	16	11443
ECA Encoder Clear Track A	166	deg	0..360	3	16	11446

Table B-2. Continued

Description	Parameter Number	Units	Range	Elements/ Record	Bits/ Elem	Elem Num
ECA Encoder Clear Track B	167	deg	0..360	3	16	11449
Main Cover Pos #1	168	inch	TBD	3	16	11452
Main Cover Pos #2	169	inch	TBD	3	16	11455
MAM Cover Pos	170	deg	TBD	3	16	11458
Azimuth Caging (Brake) Pos	171	N/A	TBD	3	16	11461
60_Conv_Pos_Samples is Array[60] of:						
60_Conv_Pos_Samples_per_Scan						
SPS 1 Narrow Field Output	172	N/A	TBD	60	16	11464
SPS 1 Wide Field Output	173	N/A	TBD	60	16	11524
SPS 2 Narrow Field Output	174	N/A	TBD	60	16	11584
SPS 2 Wide Field Output	175	N/A	TBD	60	16	11644
660_Conv_Pos_Samples is Array[660] of:						
660_Conv_Pos_Samples_per_Scan						
Elevation Scan Position	176	deg	0..260	660	16	11704
Azimuth Scan Position	177	deg	0..360	660	16	12364
BDS_Raw_Digital_Status_Measurement						
BDS_Internal_Cal_Status						
BB Temp Setpoint	178	N/A	0..4095	1	12	13024
BB Temp Control	179	N/A	0..1	1	1	13025
SWICS Intensity Command	180	N/A	0..3	1	2	13026
BDS_Sensor_Operation						
BDS_Detector_Controls						
Total Temp Set Point	181	N/A	0..4095	1	12	13027
Total Detector Temperature Control Status	182	N/A	0..3	1	2	13028
SW Temp Set Point	183	N/A	0..4095	1	12	13029
SW Detector Temperature Control Status	184	N/A	0..3	1	2	13030
Window Temp Set Point	185	N/A	0..4095	1	12	13031
Window Detector Temperature Control Status	186	N/A	0..3	1	2	13032
Total_Detector_Bridge_Bal						
Total Bridge Bal Coarse DAC Value	187	N/A	0..4095	1	12	13033
Total Bridge Bal Fine DAC Value	188	N/A	0..4095	1	12	13034
Total Detector Bridge Bal Control Status	189	N/A	0..7	1	3	13035
Total Detector Bridge Bal DAC Update Status	190	N/A	0..1	1	1	13036
Total Detector Bridge Bal Reset Calculation Counter	191	N/A	0..31	1	5	13037
SW_Detector_Bridge_Bal						
SW Bridge Bal Coarse DAC Value	192	N/A	0..4095	1	12	13038
SW Bridge Bal Fine DAC Value	193	N/A	0..4095	1	12	13039
SW Detector Bridge Bal Control Status	194	N/A	0..7	1	3	13040
SW Detector Bridge Bal DAC Update Status	195	N/A	0..1	1	1	13041
SW Detector Bridge Bal Reset Calculation Counter	196	N/A	0..31	1	5	13042
Wn_Detector_Bridge_Bal						
Window Bridge Balance Coarse DAC Value	197	N/A	0..4095	1	12	13043
Window Bridge Bal Fine DAC Value	198	N/A	0..4095	1	12	13044
Window Detector Bridge Bal Control Status	199	N/A	0..7	1	3	13045
Window Detector Bridge Bal DAC Update Status	200	N/A	0..1	1	1	13046
Window Detector Bridge Bal Reset Calculation Counter	201	N/A	0..31	1	5	13047
BDS_Bridge_Balance_Status						
Bridge Bal Window Low	202	N/A	0..4095	1	12	13048
Bridge Bal Window High	203	N/A	0..4095	1	12	13049
Bridge Bal Set Point	204	N/A	0..4095	1	12	13050
Bridge Bal Spacelook Start	205	N/A	0..4095	1	12	13051
Bridge Bal Spacelook End	206	N/A	0..4095	1	12	13052
Bridge Bal DAC Update	207	N/A	0..4095	1	12	13053

Table B-2. Continued

Description	Parameter Number	Units	Range	Elements/ Record	Bits/ Elem	Elem Num
BDS_Space_Look_Status						
Total Spacelook Average	208	N/A	0..4095	1	12	13054
SW Spacelook Average	209	N/A	0..4095	1	12	13055
Window Spacelook Average	210	N/A	0..4095	1	12	13056
BDS_Cover_Status						
Main_Cover_Status						
Main Cover Command	211	N/A	0..15	1	4	13057
Main Cover Motion Status	212	N/A	0..15	1	4	13058
Main Cover Position Status	213	N/A	0..15	1	4	13059
Main Cover Active Position Sensor	214	N/A	0..3	1	2	13060
Main Cover Commanded Position	215	N/A	0..4095	1	12	13061
Main Cover Step Count	216	N/A	0..65535	1	16	13062
Main Cover Closed Position Definition	217	N/A	0..4095	1	12	13063
Main Cover Open Position Definition	218	N/A	0..4095	1	12	13064
Main Cover Closed Margin Definition	219	N/A	0..4095	1	12	13065
Main Cover Open Margin Definition	220	N/A	0..4095	1	12	13066
MAM_Cover_Status						
MAM Cover Command	221	N/A	0..15	1	4	13067
MAM Cover Motion Status	222	N/A	0..15	1	4	13068
MAM Cover Position Status	223	N/A	0..15	1	4	13069
MAM Cover Active Position Sensor	224	N/A	0..3	1	2	13070
MAM Cover Commanded Position	225	N/A	0..4095	1	12	13071
MAM Cover Step Count	226	N/A	0..65535	1	16	13072
MAM Cover Closed Position Definition	227	N/A	0..4095	1	12	13073
MAM Cover Open Position Definition	228	N/A	0..4095	1	12	13074
MAM Cover Closed Margin Definition	229	N/A	0..4095	1	12	13075
MAM Cover Open Margin Definition	230	N/A	0..4095	1	12	13076
BDS_Gimbal_Operation						
BDS_Elevation_Status						
Elevation Status	231	N/A	0..3	1	2	13077
Elevation scan mode	232	N/A	0..31	1	5	13078
On-Deck Elevation Scan Mode	233	N/A	0..31	1	5	13079
Elevation Encoder LED Level	234	N/A	0..1	1	1	13080
Elevation Offset Correction	235	N/A	0..65535	1	16	13081
BDS_Azimuth_Status						
Azimuth Mode	236	N/A	0..31	1	5	13082
Azimuth Motion Status	237	N/A	0..31	1	5	13083
Azimuth Direction Status	238	N/A	0..1	1	1	13084
Azimuth Position Status	239	N/A	0..15	1	4	13085
Azimuth Motor Drive Status	240	N/A	0..1	1	1	13086
Azimuth Encoder LED Level	241	N/A	0..1	1	1	13087
Azimuth Offset Correction	242	N/A	0..65535	1	16	13088
BDS_Azimuth_Definition_Status						
Crosstrack Position Definition	243	N/A	0..65535	1	16	13089
Cal Position Definition	244	N/A	0..65535	1	16	13090
Azimuth Position A Definition	245	N/A	0..65535	1	16	13091
Azimuth Position A Definition	246	N/A	0..65535	1	16	13092
Azimuth Caged Position Definition	247	N/A	0..65535	1	16	13093
Spare Azimuth Position Definition #1	248	N/A	0..65535	1	16	13094
Spare Azimuth Position Definition #2	249	N/A	0..65535	1	16	13095
Spare Azimuth Position Definition #3	250	N/A	0..65535	1	16	13096
Normal Azimuth Scan Rate Definition	251	N/A	0..65535	1	16	13097
Unsync Azimuth Scan Rate Definition	252	N/A	0..65535	1	16	13098

Table B-2. Continued

Description	Parameter Number	Units	Range	Elements/ Record	Bits/ Elem	Elem Num
Sync Azimuth Scan Rate Definition	253	N/A	0..65535	1	16	13099
Brake Command Status	254	N/A	0..15	1	4	13100
Brake Motion Status	255	N/A	0..15	1	4	13101
Brake Position Status	256	N/A	0..15	1	4	13102
Brake Commanded Position	257	N/A	0..4095	1	12	13103
Brake Step Count	258	N/A	0..65535	1	16	13104
Brake Released Position Definition	259	N/A	0..4095	1	12	13105
Brake Applied Position Definition	260	N/A	0..4095	1	12	13106
Brake Caged Position Definition	261	N/A	0..4095	1	12	13107
Brake Released Margin	262	N/A	0..4095	1	12	13108
Brake Applied Margin	263	N/A	0..4095	1	12	13109
Brake Caged Margin	264	N/A	0..4095	1	12	13110
BDS_Processor_Status						
BDS_DAP_Status						
DAP Processor Boot Status	265	N/A	0..1	1	1	13111
DAP Processor Watchdog Enable	266	N/A	0..1	1	1	13112
DAP Processor PROM Power Status	267	N/A	N/A	1	16	13113
DAP Processor Scan Period Count	268	N/A	0..65535	1	16	13114
DAP Code Checksum	269	N/A	0000..FFFF(Hex)	1	16	13115
DAP Memory Dump Start Address Offset	270	N/A	0000..FFFF(Hex)	1	16	13116
DAP Memory Dump Start Address Segment	271	N/A	0000..FFFF(Hex)	1	16	13117
DAP Memory Dump End Address Offset	272	N/A	0000..FFFF(Hex)	1	16	13118
DAP Memory Dump End Address Segment	273	N/A	0000..FFFF(Hex)	1	16	13119
DAP Memory Dump Packet Address Offset	274	N/A	0000..FFFF(Hex)	1	16	13120
DAP Memory Dump Packet Address Segment	275	N/A	0000..FFFF(Hex)	1	16	13121
DAP Minimum Execution Time	276	N/A	0..65535	1	16	13122
DAP Minimum Execution Sample	277	N/A	0..1023	1	10	13123
DAP Maximum Execution Time	278	N/A	0..65535	1	16	13124
DAP Maximum Execution Sample	279	N/A	0..1023	1	10	13125
DAP Execution Time	280	N/A	0..65535	1	16	13126
BDS_ICP_Status						
ICP Processor Boot Status	281	N/A	0..1	1	1	13127
ICP Processor Watchdog Enable Status	282	N/A	0..1	1	1	13128
ICP Processor PROM Power Status	283	N/A	0..1	1	1	13129
ICP Processor Scan Period Count	284	N/A	0..65535	1	16	13130
ICP Code Checksum	285	N/A	0000..FFFF(Hex)	1	16	13131
ICP Memory Dump Start Address Offset	286	N/A	0000..FFFF(Hex)	1	16	13132
ICP Memory Dump Start Address Segment	287	N/A	0000..FFFF(Hex)	1	16	13133
ICP Memory Dump End Address Offset	288	N/A	0000..FFFF(Hex)	1	16	13134
ICP Memory Dump End Address Segment	289	N/A	0000..FFFF(Hex)	1	16	13135
ICP Memory Dump Packet Address Offset	290	N/A	0000..FFFF(Hex)	1	16	13136
ICP Memory Dump Packet Address Segment	291	N/A	0000..FFFF(Hex)	1	16	13137
ICP Minimum Execution Time	292	N/A	0..65535	1	16	13138
ICP Minimum Execution Sample	293	N/A	0..1023	1	10	13139
ICP Maximum Execution Time	294	N/A	0..65535	1	16	13140
ICP Maximum Execution Sample	295	N/A	0..1023	1	10	13141
ICP Execution Time	296	N/A	0..65535	1	16	13142
BDS_General_Instrument_Status						
Packet Data Indicator (Data format indicator)	297	N/A	0..15	1	4	13143
Packet Data Version	298	N/A	0..31	1	5	13144
Packet Timecode Indicator	299	N/A	0..1	1	1	13145
Packet Counter	300	N/A	0..65535	1	16	13146
Instrument ID Number	301	N/A	0..63	1	6	13147

Table B-2. Continued

Description	Parameter Number	Units	Range	Elements/ Record	Bits/ Elem	Elem Num
Instrument Mode (Sequence #)	302	N/A	0..31	1	5	13148
Instrument Previous Mode (Sequence #)	303	N/A	0..31	1	5	13149
Mode(Sequence) Changed by	304	N/A	0..7	1	3	13150
Instrument Command Counter	305	N/A	0..65535	1	16	13151
Instrument Error Counter	306	N/A	0..65535	1	16	13152
Sequence Command Index	307	N/A	0..31	1	5	13153
Sequence Execution Status	308	N/A	0..7	1	3	13154
Sequence Time to Next Command	309	N/A	0..255	1	8	13155
S/C Safe Hold A Input Status	310	N/A	0..1	1	1	13156
S/C Safe Hold B Input Status	311	N/A	0..1	1	1	13157
S/C Safe Hold A Response Status	312	N/A	0..1	1	1	13158
S/C Safe Hold B Response Status	313	N/A	0..1	1	1	13159
BDS_Solar_Sensor_Status						
Solar Presence Status	314	N/A	0..16383	1	14	13160
SPS1 Noise Threshold	315	N/A	0..4095	1	12	13161
SPS1 Ratio Threshold	316	N/A	0..127	1	7	13162
SPS1 Count Threshold	317	N/A	0..63	1	6	13163
SPS2 Noise Threshold	318	N/A	0..4095	1	12	13164
SPS2 Ratio Threshold	319	N/A	0..127	1	7	13165
SPS2 Count Threshold	320	N/A	0..63	1	6	13166
8_Dig_Samples is Array[8] of:						
Command_and_Error_Stacks						
Instrument Command Echo Stack	321	N/A	$0..2.81 \times 10^{14}$	8	48	13167
Instrument Error Stack	322	N/A	0..65535	8	16	13175
BDS_Satellite_Data						
BDS_Raw_Sat_Ephem_and_Att						
BDS_Satellite_Position						
Satellite Position (X) Count	323	count	$0..4.29 \times 10^{9}$	1	32	13183
Satellite Position (Y) Count	324	count	$0..4.29 \times 10^{9}$	1	32	13184
Satellite Position (Z) Count	325	count	$0..4.29 \times 10^{9}$	1	32	13185
BDS_Satellite_Velocity						
Satellite Velocity (X) Count	326	count	$0..4.29 \times 10^{9}$	1	32	13186
Satellite Velocity (Y) Count	327	count	$0..4.29 \times 10^{9}$	1	32	13187
Satellite Velocity (Z) Count	328	count	$0..4.29 \times 10^{9}$	1	32	13188
BDS_Satellite_Attitude						
Satellite Attitude (Roll) Count	329	count	0..65535	1	16	13189
Satellite Attitude (Pitch) Count	330	count	0..65535	1	16	13190
Satellite Attitude (Yaw) Count	331	count	0..65535	1	16	13191
BDS_Satellite_Attitude_Rate						
Satellite Attitude Rate (Roll) Count	332	count	0..65535	1	16	13192
Satellite Attitude Rate (Pitch) Count	333	count	0..65535	1	16	13193
Satellite Attitude Rate (Yaw) Count	334	count	0..65535	1	16	13194
Miscellaneous_Measures						
Earth-Sun distance	335	AU	0.98 .. 1.02	1	16	13195
Number of orbits	336	N/A	TBD	1	16	13196
Colatitude of Sun at observation	337	deg	0..180	1	16	13197
Longitude of Sun at observation	338	deg	0..360	1	16	13198
BDS_Satellite_Positions						
Satellite_Pos_Record_Start						
Satellite Position (X) at record start	339	km	-8000..8000	1	32	13199
Satellite Position (Y) at record start	340	km	-8000..8000	1	32	13200
Satellite Position (Z) at record start	341	km	-8000..8000	1	32	13201
Satellite_Pos_Record_End						

Table B-2. Concluded

Description	Parameter Number	Units	Range	Elements/ Record	Bits/ Elem	Elem Num
Satellite Position (X) at record end	342	km	-8000..8000	1	32	13202
Satellite Position (Y) at record end	343	km	-8000..8000	1	32	13203
Satellite Position (Z) at record end	344	km	-8000..8000	1	32	13204
Satellite_Vel_Record_Start						
Satellite Velocity (X) at record start	345	km sec^{-1}	-10..10	1	32	13205
Satellite Velocity (Y) at record start	346	km sec^{-1}	-10..10	1	32	13206
Satellite Velocity (Z) at record start	347	km sec^{-1}	-10..10	1	32	13207
Satellite_Vel_Record_End						
Satellite Velocity (X) at record end	348	km sec^{-1}	-10..10	1	32	13208
Satellite Velocity (Y) at record end	349	km sec^{-1}	-10..10	1	32	13209
Satellite Velocity (Z) at record end	350	km sec^{-1}	-10..10	1	32	13210
Satellite_Geolocations						
Colatitude of satellite at record start	351	deg	0..180	1	16	13211
Longitude of satellite at record start	352	deg	0..360	1	16	13212
Colatitude of satellite at record end	353	deg	0..180	1	16	13213
Longitude of Satellite at record end	354	deg	0..360	1	16	13214

Total Meta Bits/File:	256
Total Data Bits/Record:	200796
Total Records/File:	13091
Total Data Bits/File:	2628620436
Total Bits/File:	2628620692

Instrument Earth Scans (IES)

The IES data product contains the equivalent of one hour of data from a single CERES scanner. The data records are ordered along the orbital ground track, with each footprint position related to the spacecraft's suborbital point at the start of the hour. The spatial ordering of records within this product will ease the comparison of CERES data with cloud imager data in subsystem 4. The footprint record is the basic data structure for this data product. This record contains the following kinds of information:

1. Time of observation
2. Geolocation data (at both the top of atmosphere (TOA) and at Earth's surface)
3. Filtered radiances (at satellite altitude), with associated quality measures
4. Spacecraft orbital data
5. Footprint viewing geometric data

The IES data product contains only measurements that view the Earth. For the TRMM mission, this means that approximately 225 Earth-viewing footprints (records) are stored on the IES from each 3.3 second half-scan. Because the Earth scan pattern of the CERES instrument in the biaxial scan mode is irregular, the exact number of pixels in each IES data product varies. This variation is caused by the lack of predictability of the azimuth position at both the start and end of the hour. If the azimuth angle near the start (or end) of an hour is near the crosstrack position, then the number of footprints in the IES product is near the estimated value given below. If the azimuth angle is near the alongtrack position, some of the footprints are instead spatially located within the previous (or next) hour's IES. Thus, we have used an estimate of the number of 3.3 second half-scans per hour (approximately 1091) times the number of Earth-viewing measurements in a half-scan (TRMM estimate is 225, EOS estimate is 195) to arrive at our IES product sizing. For TRMM, this is estimated as 245 475 measurements per IES data product and for EOS the estimate is 212 745 measurements. The larger of these two measures is used to determine product sizing.

Level: 1B
Type: Internal
Frequency: 1/hour

Time Interval Covered
File: 1 hour
Record: 100 Hz

Portion of Globe Covered
File: Satellite swath
Record: One CERES footprint

Portion of Atmosphere Covered
File: Satellite altitude

Table B-3. Instrument Earth Scans (IES)

Description	Parameter Number	Units	Range	Elements/ Record	Bits/ Elem	Elem Num
IES						
IES File Header		N/A		1	256	
IES_Start_Info						
Julian Day at Hour Start		day	2449353..2458500	1	32	
Julian Time at Hour Start		day	0..1	1	32	
Colatitude of satellite at IES start		deg	0..180	1	16	
Longitude of satellite at IES start		deg	0..360	1	16	
Number of footprints in IES product		N/A	1..245475	1	32	
Number of orbits		N/A	TBD	1	16	
IES_Footprints is Array[245475] of:						
IES_Footprint_Records						
FOV_Centroid_Info						
TOA_CoLat_&_Long						
Colatitude of CERES FOV at TOA	1	deg	0..180	1	16	1
Longitude of CERES FOV at TOA	2	deg	0..360	1	16	2
Surface_CoLat_&_Long						
Colatitude of CERES FOV at surface	3	deg	0..180	1	16	3
Longitude of CERES FOV at surface	4	deg	0..360	1	16	4
Zenith_Angles						
CERES viewing zenith at TOA	5	deg	0..90	1	16	5
CERES solar zenith at TOA	6	deg	0..180	1	16	6
CERES relative azimuth at TOA	7	deg	0..360	1	16	7
CERES viewing azimuth at TOA wrt North	8	deg	0..360	1	16	8
Miscellaneous_Angles						
Cross-track angle of CERES FOV at TOA	9	deg	-90..90	1	16	9
Along-track angle of CERES FOV at TOA	10	deg	0..360	1	16	10
Clock_&_Cone_Angles						
Cone angle of CERES FOV at satellite	11	deg	0..180	1	16	11
Clock angle of CERES FOV at satellite wrt inertial velocity	12	deg	0..180	1	16	12
Rate of change of cone angle	13	deg sec^{-1}	-100..100	1	16	13
Rate of change of clock angle	14	deg sec^{-1}	-10..10	1	16	14
SC_Velocity						
X component of satellite inertial velocity	15	km sec^{-1}	-10..10	1	16	15
Y component of satellite inertial velocity	16	km sec^{-1}	-10..10	1	16	16
Z component of satellite inertial velocity	17	km sec^{-1}	-10..10	1	16	17
Filtered_Radiances						
CERES total filtered radiance, upwards	18	$W\text{-}m^{-2}\ sr^{-1}$	0..700	1	16	18
CERES shortwave filtered radiance, upwards	19	$W\text{-}m^{-2}\ sr^{-1}$	-10..510	1	16	19
CERES window filtered radiance, upwards	20	$W\text{-}m^{-2}\ sr^{-1}$	0..50	1	16	20
Satellite_&_Sun_Info						
Colatitude of satellite at observation	21	deg	0..180	1	16	21
Longitude of satellite at observation	22	deg	0..360	1	16	22
Radius of satellite from center of Earth at observation	23	km	6000..8000	1	32	23
Colatitude of Sun at observation	24	deg	0..180	1	16	24
Longitude of Sun at observation	25	deg	0..360	1	16	25
Earth-Sun distance	26	AU	0.98 .. 1.02	1	16	26
Observation_References						
Scan sample number	27	N/A	1..660	1	16	27
IES quality flags	28	N/A	0..255	1	16	28
Time of observation	29	day	0..1	1	32	29

Total Meta Bits/File:	400
Total Data Bits/Record:	496
Total Records/File:	245475
Total Data Bits/File:	121755600
Total Bits/File:	121756000

Clouds and the Earth's Radiant Energy System (CERES)

Algorithm Theoretical Basis Document

ERBE-Like Inversion to Instantaneous TOA and Surface Fluxes

(Subsystem 2.0)

Richard Green[1]
John Robbins[2]

[1]Atmospheric Sciences Division, NASA Langley Research Center, Hampton, Virginia 23681-0001
[2]Science Applications International Corporation (SAIC), Hampton, Virginia 23666

Abstract

This Inversion Subsystem converts filtered radiometric measurements in engineering units to instantaneous flux estimates at the top of the atmosphere (TOA). The basis for this procedure is the ERBE Data Management System, which produced TOA fluxes from the ERBE scanning radiometers aboard the ERBS, NOAA-9, and NOAA-10 satellites over a 5-year period from November 1984 to February 1990 (Barkstrom 1984; Barkstrom and Smith 1986). The ERBE Inversion Subsystem is a mature set of algorithms that has been well documented and tested. The strategy for the ERBE-like products is to process the CERES data through the same processing system as ERBE with only minimal changes necessary to adapt to the CERES instrument characteristics. This system will be coded and operational at launch. An overview of the ERBE Inversion Subsystem is given by Smith et al. (1986).

2.0. ERBE-Like Inversion to Instantaneous TOA and Surface Fluxes

2.1. Introduction

The ERBE-like Inversion Subsystem consists of a number of algorithms which are described in the following sections. The Spectral Correction Algorithm corrects the filtered radiances to unfiltered radiances. The observed scene type is then identified with the Maximum Likelihood Estimation (MLE) technique. Once the scene type is known, the Radiance-to-Flux Conversion is accomplished with the Angular Distribution Models (ADM). Finally, the Regional Averaging Algorithm produces regional fluxes from the instantaneous fluxes. At many points during the processing Quality Checks are performed to eliminate erroneous results.

2.2. Algorithm Description

2.2.1. Spectral Correction

The Spectral Correction Algorithm corrects the radiometric measurements for the imperfect spectral response of the optical path in the instrument. Radiation from the scene is collected and focused by primary and secondary mirrors, passes through the filter (for the shortwave and window channels), impinges on the detector, and causes a signal which is sampled and processed by the electronics, resulting in a filtered measurement (see subsystem 1). To correct this filtered signal, we need to know the spectral response of the individual channels and the spectral nature of the observed scene. The objective is to determine the reflected (or shortwave) radiation below 5 μm, the emitted (or longwave) radiation above 5 μm and the window radiation from 8 to 12 μm.

We model the "filtered" scanner measured radiance as

$$I_F^j = \int_0^\infty S_\lambda^j I_\lambda d\lambda + \varepsilon^j \qquad j = SW, TOT, WN$$

where λ is wavelength in μm; I_λ is the spectral radiance incident on the instrument in W-m^{-2}sr^{-1}μm^{-1}; S_λ is the normalized spectral response of the instrument (fig. 1-2) such that $0 \le S_\lambda \le 1$; ε is the instrument error in W-m^{-2}sr^{-1} with mean 0 and variance σ_ε^2 which results from count conversion error, instrument noise, and any instrument error except spectral dependence effects; and j denotes the

shortwave, total, or window scanner channel. We desire to estimate the "unfiltered" scanner radiances which are defined as

$$I^i = \int_0^\infty C_\lambda^i I_\lambda d\lambda \qquad i = SW, LW, WN$$

where

$$C_\lambda^{SW} = \begin{cases} 1 & (0 \le \lambda < 5\mu m) \\ 0 & (\text{Otherwise}) \end{cases}$$

$$C_\lambda^{LW} = \begin{cases} 0 & (5 \le \lambda \le 50\mu m) \\ 1 & (\text{Otherwise}) \end{cases}$$

$$C_\lambda^{WN} = \begin{cases} 1 & (8\mu m \le \lambda \le 12\mu m) \\ 0 & (\text{Otherwise}) \end{cases}$$

Let us consider I_λ and ε as random variables so that both the filtered and unfiltered radiances are random variables. We desire to estimate the unfiltered radiances from the filtered radiances given the statistics of I_λ and ε. For simplicity, define the random vector of filtered radiances Y and the random vector of unfiltered radiances X as

$$Y = \begin{bmatrix} I_F^{SW} \\ I_F^{TOT} \\ I_F^{WN} \end{bmatrix} \qquad X = \begin{bmatrix} I^{SW} \\ I^{LW} \\ I^{WN} \end{bmatrix}$$

We will assume a linear estimator $\hat{X} = BY$ and choose to minimize the diagonal terms of the matrix $E[(\hat{X} - X)(\hat{X} - X)^T]$ where $E[x]$ is the statistical expectation operator. This estimator is called the minimum mean square error estimator. From the Gauss-Markoff theorem (Liebelt 1967) we have

$$\hat{X} = E[XY^T]\left(E[YY^T]\right)^{-1} Y$$

We will define the quantities $E[XY^T]$ and $E[YY^T]$ empirically from data. The general elements are

$$E[X^i Y^j] = \int_0^\infty \int_0^\infty C_\lambda^i S_{\lambda'}^j E[I_\lambda I_{\lambda'}] d\lambda d\lambda' \equiv \overline{X^i Y^j} \qquad \begin{matrix} i = SW, LW, WN \\ j = SW, TOT, WN \end{matrix}$$

$$E[Y^r Y^s] = \int_0^\infty \int_0^\infty S_\lambda^r S_{\lambda'}^s E[I_\lambda I_{\lambda'}] d\lambda d\lambda' \equiv \overline{Y^r Y^s} + \sigma_{rs}^2 \qquad r, s = SW, TOT, WN$$

We have modeled I_λ as a random variable (or random function) over the ensemble of all possible scenes. Let us assume knowledge of a finite number (say N) of these possible scenes and approximate the expected value with a simple weighted average or

$$E[I_\lambda I_{\lambda'}] \approx \sum_{k=1}^{N} p^k I_\lambda^k I_{\lambda'}^k \equiv \overline{I_\lambda I_{\lambda'}}$$

where p^k is the probability of I_λ^k and $\sum_k p^k = 1$. Thus, we have

$$E[X^i Y^j] \approx \int_0^\infty \int_0^\infty C_\lambda^i S_{\lambda'}^j \overline{I_\lambda I_{\lambda'}} d\lambda d\lambda' \equiv \overline{X^i Y^j} \qquad i = SW, LW, WN \quad j = SW, TOT, WN$$

$$E[Y^r Y^s] \approx \int_0^\infty \int_0^\infty S_\lambda^r S_{\lambda'}^s \overline{I_\lambda I_{\lambda'}} d\lambda d\lambda' \equiv \overline{Y^r Y^s} + \sigma_{rs}^2 \qquad r, s = SW, TOT, WN$$

The spectral correction coefficients are mean values and thus introduce error into the process. This error is minimized by determining different coefficients for ocean, land, desert, snow, and cloud over three latitude ranges. In addition, the spectra shift with viewing zenith, solar zenith, and relative azimuth angles so that the coefficients are also functions of these angles.

The scene must be identified before the radiances can be unfiltered. However, the scene identification algorithm requires unfiltered radiances to determine the scene. This problem is overcome by first unfiltering the radiances based on the surface type and a global a priori cloud cover. This global unfiltering is within 5% of the true value. After the scene is identified, the unfiltered radiances are recomputed using the correct scene.

The spectral correction equations have been developed in general where all 3 channels affect each of the 3 unfiltered radiances. The CERES processing will use this approach (see section 4.5.3.1.). For ERBE-like processing, the shortwave and longwave radiances will be defined by the shortwave and total channels with no effect from the window channel. This unfiltering more closely resembles the ERBE spectral correction algorithm which relied almost entirely on the total and shortwave channels with only minimal effect from the nonflat longwave channel. For ERBE-like processing, the unfiltered window radiance will depend on the window channel alone with no effect from the shortwave and total channels.

The Spectral Correction Algorithm has been used very successfully on the ERBE. The best references are Avis et al. (1984) and Smith et al. (1986).

2.2.2. Scene Identification

The unfiltered radiances are a direct measurement of radiance, while the desired product is radiative flux at the top of the atmosphere (TOA). Derivation of radiative flux using the scanner radiance observations then requires the use of angular distribution models (ADM) to correct for the anisotropy of the radiation field. Two of the major causes of variability in the ADM's are change in geographic surface type (ocean, land, etc.) and change in cloud conditions (variable cloud cover, for example). The surface types can be handled using a static geographic map. Cloud conditions, however, require dynamic identification of the scene being viewed to achieve accurate flux estimates. Four basic cloud categories are defined which encompass all cloud conditions. These four types are clear (0%–5% cloud cover), partly cloudy (5%–50% cloud cover), mostly cloudy (50%–95% cloud cover), and overcast (95%–100% cloud cover). Surface type and cloud condition are combined to give the 12 ERBE scene types given in Table 2-1.

Table 2-1. ERBE Scene Types

Index	Scene types
1	Clear ocean
2	Clear land
3	Clear snow
4	Clear desert
5	Clear land-ocean mix (coastal)
6	Partly cloudy over ocean
7	Partly cloudy over land or desert
8	Partly cloudy over land-ocean mix
9	Mostly cloudy over ocean
10	Mostly cloudy over land or desert
11	Mostly cloudy over land-ocean mix
12	Overcast

The scene identification procedure first classifies the underlying surface by its geographic type: land, ocean, snow, desert, or land-ocean mix for 2.5° × 2.5° regions. The cloud class for a given measurement pair (shortwave and longwave radiances) is selected by comparing the measurement pair to a priori statistics developed from a classification of Nimbus-7 ERB scanning radiometer data. The cloud class chosen is the class which most probably produced the measurements. This classification method is known as the Maximum Likelihood Estimation (MLE) and is fully documented by Wielicki and Green (1989).

2.2.3. Radiance-to-Flux Conversion

We define the outgoing radiance I at the TOA as

$$I = \pi^{-1} FR$$

where F is the flux in W-m^{-2} and R is the Angular Distribution Model (ADM). To convert satellite radiance to flux at the TOA, we solve for F or

$$\hat{F} = \frac{\pi I}{R}$$

where I is the unfiltered measured radiance and R is a numerical model of the anisotropy evaluated at the viewing and solar geometry. A complete set of ADM's for the 12 ERBE scene types has been developed from Nimbus-7 data for both shortwave and longwave radiance and are given by Suttles et al. (1988, 1989).

2.2.4. Spatial Averaging

For each scanner measurement of radiance, the instantaneous flux is computed. These flux values are then averaged to produce estimates of the instantaneous regional fluxes. In the ERBE data analysis, all measurements whose center points lie within a 2.5° × 2.5° region are averaged with equal weight to produce the estimate of regional average flux, as has been done previously in analyses of the Earth radiation budget. In forming the estimate of the regional average flux, one encounters errors due to the spatial sampling or coverage problem. This spatial sampling problem has been studied by Smith and Bess (1978) and Smith et al. (1983).

2.3. Implementation Issues

2.3.1. Quality Checks

Restrictions are imposed on the inversion process to eliminate sensitive areas of high errors. Measurements with viewing zenith angles greater than 70° are not processed. Also, measurements in areas where the ADM anisotropy exceeds 2.0 (or twice Lambertian) are not inverted.

A number of quality control checks are performed. Each measurement is associated with a flag which is set to "good" or "bad." If the measurement is flagged "bad" for any reason by any subsystem, it is not processed. If the measurement is flagged "good," it is processed and then tested. The TOA flux estimates are replaced by default values if the estimate of albedo is outside the range 0.02–1.00 or the estimate of longwave flux is outside the range 50–400 W-m^{-2}. The MLE selects the most probable scene type. When it is 8 standard deviations away from its a priori expectation, the scene identification is considered unreliable and the measurement is not inverted to the TOA.

2.4. References

Avis, L. M. 1984: *A Robust Pseudo-Inverse Spectral Filter Applied to the Earth Radiation Budget Experiment (ERBE) Scanning Channels.* NASA TM-85781.

Barkstrom, B. R. 1984: The Earth Radiation Budget Experiment (ERBE). *Bull. Am. Meteorol. Soc.*, vol. 65, pp. 1170–1185.

Barkstrom, B. R. and Smith, G. L. 1986: The Earth Radiation Budget Experiment—Science and Implementation. *Rev. Geophys.*, vol. 24, pp. 379–390.

Liebelt, Paul B. 1967: *An Introduction to Optimal Estimation*. Addison-Wesley.

Smith, G. L.; and Bess, T. D. 1978: Systems Considerations for an Earth Radiation Budget Scanning Radiometer. Presented at the Fourth Symposium on Meteorological Observations and Instrumentations, Am. Meteorol. Soc.

Smith, G. L.; Bess, T. D.; and Minnis, P. 1983: Sampling Errors in Regional Radiation Results Based on Satellite Radiation Measurements. Presented at the Ninth Conference on Aerospace and Aeronautical Meteorology, Am. Meteorol. Soc.

Smith, G. L.; Green, R. N.; Avis, L. M.; Suttles, J. T.; Wielicki, B. A.; Raschke, E.; and Davies, R. 1986: Inversion Methods for Satellite Studies of the Earth Radiation Budget—Development of Algorithms for the ERBE Mission. *Rev. Geophys.*, vol. 24, pp. 407–421.

Suttles, J. T.; Green, R. N.; Minnis, P.; Smith, G. L.; Staylor, W. F.; Wielicki, B. A.; Walker, I. J.; Young, D. F.; Taylor, V. R.; and Stowe, L. L. 1988a: *Angular Radiation Models for Earth-Atmosphere System. Volume I—Shortwave Radiation.* NASA RP-1184.

Suttles, J. T.; Green, R. N.; Smith, G. L.; Wielicki, B. A.; Walker, I. J.; Taylor, V. R.; and Stowe, L. L. 1988b: *Angular Radiation Models for Earth-Atmosphere System. II—Longwave Radiation.* NASA RP-1184.

Wielicki, Bruce A.; and Green, Richard N. 1989: Cloud Identification for ERBE Radiative Flux Retrieval. *J. Appl. Meteorol.*, vol. 28, pp. 1133–1146.

Appendix A

Input Data Products

ERBE-Like Inversion to Instantaneous TOA and Surface Fluxes (Subsystem 2.0)

This appendix describes the data products which are used by the algorithms in this subsystem. Table A-1 below summarizes these products, listing the CERES and EOSDIS product codes or abbreviations, a short product name, the product type, the production frequency, and volume estimates for each individual product as well as a complete data month of production. The product types are defined as follows:

Archival products:	Assumed to be permanently stored by EOSDIS
Internal products:	Temporary storage by EOSDIS (days to years)
Ancillary products:	Non-CERES data needed to interpret measurements

The following pages describe each product. An introductory page provides an overall description of the product and specifies the temporal and spatial coverage. The table which follows the introductory page briefly describes every parameter which is contained in the product. Each product may be thought of as metadata followed by data records. The metadata (or header data) is not well-defined yet and is included mainly as a placeholder. The description of parameters which are present in each data record includes parameter number (a unique number for each distinct parameter), units, dynamic range, the number of elements per record, an estimate of the number of bits required to represent each parameter, and an element number (a unique number for each instance of every parameter). A summary at the bottom of each table shows the current estimated sizes for metadata, each data record, and the total data product. A more detailed description of each data product will be contained in a user's guide to be published before the first CERES launch.

Table A-1. Input Products Summary

Product Code		Name	Type	Frequency	Size, MB	Monthly size, MB
CERES	EOSDIS					
BDS	CER01	Bidirectional scan	archival	1/day	313.6	9722
ASTR	CER34	Atmospheric structures	archival	1/hour	10.5	7797

Bidirectional Scan (BDS)

The BDS data product is an archival product containing level 1B CERES scanner data obtained for a 24 hour period. All science scan modes are included in the BDS, including the fixed and rotating azimuth scan modes that perform normal earth, internal calibration, and short scan elevation profiles. The BDS product includes samples taken at all scan elevation positions (including space looks and internal calibration views).

The BDS includes the raw count data stream and the converted engineering representative data. These data are divided into the following seven groups that are carried forward from the level-0 product:

1. Time
2. Instrument status
3. Radiometric channel counts
4. Instrument telescope pointing (elevation and azimuth)
5. Temperatures
6. Voltages and currents
7. Satellite ephemeris and ancillary data

In addition, we add the following filtered radiance data from the three radiometric channels and their associated field of view location geometry:

8. Filtered Radiances, including quality flags
9. Earth location Geometry, including quality flags

In the BDS data product, the filtered radiances and the Earth location geometry are considered a multiband, single data element footprint. Quality flags are used to indicate the reliability of the radiance and Earth location measurements. This product is also used to diagnose instrument performance conditions.

Level: 1B
Type: Archival
Frequency: 1/Day

Time Interval Covered
File: 24 hours
Record: Single 6.6 second scans

Portion of Globe Covered
File: Satellite swath
Record: N/A

Portion of Atmosphere Covered
File: Satellite altitude

Table A-2. Bidirectional Scan (BDS)

Description	Parameter Number	Units	Range	Elements/ Record	Bits/ Elem	Elem Num
BDS						
BDS File Header		N/A		1	256	
BDS_Data is Array[13091] of:						
BDS_Record						
Julian Day at Scan Start	1	day	2449353..2458500	1	32	1
Julian Time at Scan Start	2	day	0..1	1	32	2
BDS Instrument Status	3	N/A	0..65535	1	16	3
BDS_Scan_Information						
BDS_Radiometric_Data is Array[660] of:						
BDS_Pixel_Radiometric						
BDS_Filtered_Radiances						
CERES total filtered radiance, upwards	4	$W\text{-}m^{-2}\ sr^{-1}$	0..700	660	16	4
CERES shortwave filtered radiance, upwards	5	$W\text{-}m^{-2}\ sr^{-1}$	-10..510	660	16	664
CERES window filtered radiance, upwards	6	$W\text{-}m^{-2}\ sr^{-1}$	0..50	660	16	1324
BDS Quality Flags	7	N/A	0..65535	660	16	1984
BDS_Detector_Output_(Raw)						
Total Detector Output	8	count	0..4095	660	12	2644
SW Detector Output	9	count	0..4095	660	12	3304
Window Detector Output	10	count	0..4095	660	12	3964
BDS_Location_Data is Array[660] of:						
BDS_Pixel_Location						
BDS_Raw_Location						
Azimuth Position Count	11	count	0..65535	660	16	4624
Elevation Position Count	12	count	0..65535	660	16	5284
BDS_TOA_Location						
Colatitude of CERES FOV at TOA	13	deg	0..180	660	16	5944
Longitude of CERES FOV at TOA	14	deg	0..360	660	16	6604
CERES viewing zenith at TOA	15	deg	0..90	660	16	7264
CERES solar zenith at TOA	16	deg	0..180	660	16	7924
CERES relative azimuth at TOA	17	deg	0..360	660	16	8584
BDS_Housekeeping_Data						
BDS_Temperature_Measurements						
BDS_Raw_Temperature_Count						
12_Raw_Temp_Samples is Array[12] of:						
12_Raw_Temp_Samples_per_Scan						
Total Heater DAC Value	18	N/A	0..4095	12	12	9244
SW Heater DAC Value	19	N/A	0..4095	12	12	9256
Window Heater DAC Value	20	N/A	0..4095	12	12	9268
BB Heater DAC Value	21	N/A	0..4095	12	12	9280
Total Control Temp Count	22	count	0..4095	12	12	9292
Total Measured Temp Count	23	count	0..4095	12	12	9304
SW Control Temp Count	24	count	0..4095	12	12	9316
SW Measured Temp Count	25	count	0..4095	12	12	9328
Window Control Temp Count	26	count	0..4095	12	12	9340
Window Measured Temp Count	27	count	0..4095	12	12	9352
Total Blackbody Temp Count	28	count	0..4095	12	12	9364
LW Blackbody Temp Count	29	count	0..4095	12	12	9376
3_Raw_Temp_Samples is Array[3] of:						
3_Raw_Temp_Samples_per_Scan						
Elevation Spindle Temp (Motor) Count	30	count	0..4095	3	12	9388
Elevation Spindle Temp (Cable Wrap) Count	31	count	0..4095	3	12	9391
Elevation Bearing Temp (Motor) Count	32	count	0..4095	3	12	9394
Elevation Bearing Temp (Cable Wrap) Count	33	count	0..4095	3	12	9397
SWICS Photodiode Temp Count	34	count	0..4095	3	12	9400

Table A-2. Continued

Description	Parameter Number	Units	Range	Elements/ Record	Bits/ Elem	Elem Num
Sensor Module Temp Count	35	count	0..4095	3	12	9403
Sensor Electronics Temp Count	36	count	0..4095	3	12	9406
Main Cover Motor Temp Count	37	count	0..4095	3	12	9409
MAM Total Baffle Temp #1 Count	38	count	0..4095	3	12	9412
MAM Total Baffle Temp #2 Count	39	count	0..4095	3	12	9415
MAM SW Assembly Temp Count	40	count	0..4095	3	12	9418
MAM Total Assembly Temp Count	41	count	0..4095	3	16	9421
DAA Radiator Temp Count	42	count	0..4095	3	12	9424
DAA CPU Elect Temp Count	43	count	0..4095	3	12	9427
DAA Prom Elect Temp Count	44	count	0..4095	3	12	9430
DAA RAM Elect Temp Count	45	count	0..4095	3	12	9433
DAA ADC Elect Temp Count	46	count	0..4095	3	12	9436
ECA Radiator Temp Count	47	count	0..4095	3	12	9439
ECA Elect Temp Count	48	count	0..4095	3	12	9442
ACA Elect Temp Count	49	count	0..4095	3	12	9445
Azimuth Lower Bearing Temp Count	50	count	0..4095	3	12	9448
Azimuth High Bearing Temp Count	51	count	0..4095	3	12	9451
ICA Radiator Temp Count	52	count	0..4095	3	12	9454
ICA CPU Elect Temp Count	53	count	0..4095	3	12	9457
ICA Prom Elect Temp Count	54	count	0..4095	3	12	9460
ICA RAM Elect Temp Count	55	count	0..4095	3	12	9463
ICA ADC Elect Temp Cnt	56	count	0..4095	3	12	9466
PCA Radiator Temp Count	57	count	0..4095	3	12	9469
PCA Electronics Temp Count	58	count	0..4095	3	12	9472
PCA Q1 Transistor Case Temp Count	59	count	0..4095	3	12	9475
Pedestal Temp #1 (Brake Hsg) Count	60	count	0..4095	3	12	9478
Pedestal Temp #2 (@ Isolator) Count	61	count	0..4095	3	12	9481
BDS_Converted_Temperature						
12_Temp_Samples is Array[12] of:						
12_Temp_Samples_per_Scan						
Total Control Temp	62	°C	36..40	12	16	9484
Total Measured Temp	63	°C	36..40	12	16	9496
SW Control Temp	64	°C	36..40	12	16	9508
SW Measured Temp	65	°C	36..40	12	16	9520
Window Control Temp	66	°C	36..40	12	16	9532
Window Measured Temp	67	°C	36..40	12	16	9544
Total Blackbody Temp	68	°C	-15..60	12	16	9556
LW Blackbody Temp	69	°C	-15..60	12	16	9568
3_Temp_Samples is Array[3] of:						
3_Temp_Samples_per_Scan						
Elevation Spindle Temp (Motor)	70	°C	-30..70	3	16	9580
Elevation Spindle Temp (Cable Wrap)	71	°C	-30..70	3	16	9583
Elevation Bearing Temp (Motor)	72	°C	-30..70	3	16	9586
Elevation Bearing Temp (Cable Wrap)	73	°C	-30..70	3	16	9589
Sensor Module Temp	74	°C	-30..70	3	16	9592
Sensor Elect Temp	75	°C	-30..70	3	16	9595
Main Cover Motor Temp	76	°C	-30..70	3	16	9598
SWICS Photodiode Temp	77	°C	-30..70	3	16	9601
MAM Total Baffle Temp #1	78	°C	-30..70	3	16	9604
MAM Total Baffle Temp #2	79	°C	-30..70	3	16	9607
MAM SW Assembly Temp	80	°C	-30..70	3	16	9610
MAM Total Assembly Temp	81	°C	-30..70	3	16	9613
DAA Radiator Temp	82	°C	-30..70	3	16	9616

Table A-2. Continued

Description	Parameter Number	Units	Range	Elements/ Record	Bits/ Elem	Elem Num
DAA CPU Elect Temp	83	°C	-30..70	3	16	9619
DAA Prom Elect Temp	84	°C	-30..70	3	16	9622
DAA RAM Elect Temp	85	°C	-30..70	3	16	9625
DAA ADC Elect Temp	86	°C	-30..70	3	16	9628
ECA Radiator Temp	87	°C	-30..70	3	16	9631
ECA Elect Temp	88	°C	-30..70	3	16	9634
ACA Elect Temp	89	°C	-30..70	3	16	9637
Azimuth Lower Bearing Temp	90	°C	-30..70	3	16	9640
Azimuth Upper Bearing Temp	91	°C	-30..70	3	16	9643
ICA Radiator Temp	92	°C	-30..70	3	16	9646
ICA CPU Elect Temp	93	°C	-30..70	3	16	9649
ICA Prom Elect Temp	94	°C	-30..70	3	16	9652
ICA RAM Elect Temp	95	°C	-30..70	3	16	9655
ICA ADC Elect Temp	96	°C	-30..70	3	16	9658
PCA Radiator Temp	97	°C	-30..70	3	16	9661
PCA Electronics Temp	98	°C	-30..70	3	16	9664
PCA Q1 Transistor Case Temp	99	°C	-30..70	3	16	9667
Pedestal Temp #1 (Brake Hsg)	100	°C	-30..70	3	16	9670
Pedestal Temp #2 (@ Isolator)	101	°C	-30..70	3	16	9673
BDS_Voltage_Measurements						
BDS_Raw_Voltage_Count						
3_Raw_Volt_Samples is Array[3] of:						
3_Raw_Volt_Samples_per_Scan						
Sensor +120V Bias Count	102	count	0..4095	3	12	9676
Sensor -120V Bias Count	103	count	0..4095	3	12	9679
SWICS Photodiode Output Count	104	count	0..4095	3	12	9682
SWICS Lamp Current Count	105	count	0..4095	3	12	9685
ICA +5V Digital Count	106	count	0..4095	3	12	9688
ICA +15V (to ECA/ACA) Count	107	count	0..4095	3	12	9691
ICA -15V (to ECA/ACA) Count	108	count	0..4095	3	12	9694
ICA +18V Count	109	count	0..4095	3	12	9697
ICA -18V Count	110	count	0..4095	3	12	9700
ICA +15V (Internal) Count	111	count	0..4095	3	12	9703
ICA -15V (Internal) Count	112	count	0..4095	3	12	9706
DAA Ground #1 Count	113	count	0..4095	3	12	9709
DAA Ground #2 Count	114	count	0..4095	3	12	9712
DAA -10V Reference Count	115	count	0..4095	3	12	9715
DAA +130V Count	116	count	0..4095	3	12	9718
DAA -130V Count	117	count	0..4095	3	12	9721
DAA +12V Count	118	count	0..4095	3	12	9724
DAA -12V Count	119	count	0..4095	3	12	9727
DAA +15V Count	120	count	0..4095	3	12	9730
DAA -15V Count	121	count	0..4095	3	12	9733
DAA +18V Count	122	count	0..4095	3	12	9736
DAA -18V Count	123	count	0..4095	3	12	9739
12_Raw_Volt_Samples is Array[12] of:						
12_Raw_Volt_Samples_per_Scan						
Elevation Torque Output Count	124	count	0..4095	12	12	9742
Azimuth Torque Output Count	125	count	0..4095	12	12	9754
BDS_Converted_Voltage						
3_Volt_Samples is Array[3] of:						
3_Volt_Samples_per_Scan						
Sensor +120V Bias	126	volt	115..125	3	16	9766

Table A-2. Continued

Description	Parameter Number	Units	Range	Elements/ Record	Bits/ Elem	Elem Num
Sensor -120V Bias	127	volt	-125..-115	3	16	9769
SWICS Photodiode Output	128	volt	0..8	3	16	9772
SWICS Lamp Current	129	milliamp	0..100	3	16	9775
ICA +5V Digital	130	volt	0..8	3	16	9778
ICA +15V (to ECA/ACA)	131	volt	0..20	3	16	9781
ICA -15V (to ECA/ACA)	132	volt	-20..0	3	16	9784
ICA +18V	133	volt	0..20	3	16	9787
ICA -18V	134	volt	-20..0	3	16	9790
ICA +15V (Internal)	135	volt	0..30	3	16	9793
ICA -15V (Internal)	136	volt	-30..0	3	16	9796
DAA Ground #1	137	volt	0..10	3	16	9799
DAA Ground #2	138	volt	0..10	3	16	9802
DAA -10V Reference	139	volt	-20..0	3	16	9805
DAA +130V	140	volt	90..170	3	16	9808
DAA -130V	141	volt	-224..-36	3	16	9811
DAA +12V	142	volt	0..20	3	16	9814
DAA -12V	143	volt	-20..0	3	16	9817
DAA +15V	144	volt	0..20	3	16	9820
DAA -15V	145	volt	-20..0	3	16	9823
DAA +18V	146	volt	0..20	3	16	9826
DAA -18V	147	volt	-20..0	3	16	9829
12_Volt_Samples is Array[12] of:						
12_Volt_Samples_per_Scan						
Elevation Torque Output	148	volt	-20..20	12	16	9832
Azimuth Torque Output	149	volt	-20..20	12	16	9844
BDS_Position_Measurements						
BDS_Raw_Position_Count						
3_Pos_Samples is Array[3] of:						
3_Pos_Samples_per_Scan						
ACA Encoder Clear Track A Count	150	count	0..4095	3	12	9856
ACA Encoder Clear Track B Count	151	count	0..4095	3	12	9859
ECA Encoder Clear Track A Count	152	count	0..4095	3	12	9862
ECA Encoder Clear Track B Count	153	count	0..4095	3	12	9865
Main Cover Pos #1 Count	154	count	0..4095	3	12	9868
Main Cover Pos #2 Count	155	count	0..4095	3	12	9871
MAM Cover Pos Count	156	count	0..4095	3	12	9874
Azimuth Caging (Brake) Pos Count	157	count	0..4095	3	12	9877
60_Pos_Samples is Array[60] of:						
60_Pos_Samples_per_Scan						
SPS 1 Narrow Field Output Count	158	count	0..4095	60	12	9880
SPS 1 Wide Field Output Count	159	count	0..4095	60	12	9940
SPS 2 Narrow Field Output Count	160	count	0..4095	60	12	10000
SPS 2 Wide Field Output Count	161	count	0..4095	60	12	10060
660_Raw_Pos_Samples is Array[660] of:						
660_Raw_Pos_Samples_per_Scan						
Elevation Position Count	162	count	0..65535	660	16	10120
Azimuth Position Count	163	count	0..65535	660	16	10780
BDS_Converted_Position						
3_Conv_Pos_Samples is Array[3] of:						
3_Conv_Pos_Samples_per_Scan						
ACA Encoder Clear Track A	164	deg	0..360	3	16	11440
ACA Encoder Clear Track B	165	deg	0..360	3	16	11443
ECA Encoder Clear Track A	166	deg	0..360	3	16	11446

Table A-2. Continued

Description	Parameter Number	Units	Range	Elements/ Record	Bits/ Elem	Elem Num
ECA Encoder Clear Track B	167	deg	0..360	3	16	11449
Main Cover Pos #1	168	inch	TBD	3	16	11452
Main Cover Pos #2	169	inch	TBD	3	16	11455
MAM Cover Pos	170	deg	TBD	3	16	11458
Azimuth Caging (Brake) Pos	171	N/A	TBD	3	16	11461
60_Conv_Pos_Samples is Array[60] of:						
60_Conv_Pos_Samples_per_Scan						
SPS 1 Narrow Field Output	172	N/A	TBD	60	16	11464
SPS 1 Wide Field Output	173	N/A	TBD	60	16	11524
SPS 2 Narrow Field Output	174	N/A	TBD	60	16	11584
SPS 2 Wide Field Output	175	N/A	TBD	60	16	11644
660_Conv_Pos_Samples is Array[660] of:						
660_Conv_Pos_Samples_per_Scan						
Elevation Scan Position	176	deg	0..260	660	16	11704
Azimuth Scan Position	177	deg	0..360	660	16	12364
BDS_Raw_Digital_Status_Measurement						
BDS_Internal_Cal_Status						
BB Temp Setpoint	178	N/A	0..4095	1	12	13024
BB Temp Control	179	N/A	0..1	1	1	13025
SWICS Intensity Command	180	N/A	0..3	1	2	13026
BDS_Sensor_Operation						
BDS_Detector_Controls						
Total Temp Set Point	181	N/A	0..4095	1	12	13027
Total Detector Temperature Control Status	182	N/A	0..3	1	2	13028
SW Temp Set Point	183	N/A	0..4095	1	12	13029
SW Detector Temperature Control Status	184	N/A	0..3	1	2	13030
Window Temp Set Point	185	N/A	0..4095	1	12	13031
Window Detector Temperature Control Status	186	N/A	0..3	1	2	13032
Total_Detector_Bridge_Bal						
Total Bridge Bal Coarse DAC Value	187	N/A	0..4095	1	12	13033
Total Bridge Bal Fine DAC Value	188	N/A	0..4095	1	12	13034
Total Detector Bridge Bal Control Status	189	N/A	0..7	1	3	13035
Total Detector Bridge Bal DAC Update Status	190	N/A	0..1	1	1	13036
Total Detector Bridge Bal Reset Calculation Counter	191	N/A	0..31	1	5	13037
SW_Detector_Bridge_Bal						
SW Bridge Bal Coarse DAC Value	192	N/A	0..4095	1	12	13038
SW Bridge Bal Fine DAC Value	193	N/A	0..4095	1	12	13039
SW Detector Bridge Bal Control Status	194	N/A	0..7	1	3	13040
SW Detector Bridge Bal DAC Update Status	195	N/A	0..1	1	1	13041
SW Detector Bridge Bal Reset Calculation Counter	196	N/A	0..31	1	5	13042
Wn_Detector_Bridge_Bal						
Window Bridge Balance Coarse DAC Value	197	N/A	0..4095	1	12	13043
Window Bridge Bal Fine DAC Value	198	N/A	0..4095	1	12	13044
Window Detector Bridge Bal Control Status	199	N/A	0..7	1	3	13045
Window Detector Bridge Bal DAC Update Status	200	N/A	0..1	1	1	13046
Window Detector Bridge Bal Reset Calculation Counter	201	N/A	0..31	1	5	13047
BDS_Bridge_Balance_Status						
Bridge Bal Window Low	202	N/A	0..4095	1	12	13048
Bridge Bal Window High	203	N/A	0..4095	1	12	13049
Bridge Bal Set Point	204	N/A	0..4095	1	12	13050
Bridge Bal Spacelook Start	205	N/A	0..4095	1	12	13051
Bridge Bal Spacelook End	206	N/A	0..4095	1	12	13052
Bridge Bal DAC Update	207	N/A	0..4095	1	12	13053

Table A-2. Continued

Description	Parameter Number	Units	Range	Elements/ Record	Bits/ Elem	Elem Num
BDS_Space_Look_Status						
Total Spacelook Average	208	N/A	0..4095	1	12	13054
SW Spacelook Average	209	N/A	0..4095	1	12	13055
Window Spacelook Average	210	N/A	0..4095	1	12	13056
BDS_Cover_Status						
Main_Cover_Status						
Main Cover Command	211	N/A	0..15	1	4	13057
Main Cover Motion Status	212	N/A	0..15	1	4	13058
Main Cover Position Status	213	N/A	0..15	1	4	13059
Main Cover Active Position Sensor	214	N/A	0..3	1	2	13060
Main Cover Commanded Position	215	N/A	0..4095	1	12	13061
Main Cover Step Count	216	N/A	0..65535	1	16	13062
Main Cover Closed Position Definition	217	N/A	0..4095	1	12	13063
Main Cover Open Position Definition	218	N/A	0..4095	1	12	13064
Main Cover Closed Margin Definition	219	N/A	0..4095	1	12	13065
Main Cover Open Margin Definition	220	N/A	0..4095	1	12	13066
MAM_Cover_Status						
MAM Cover Command	221	N/A	0..15	1	4	13067
MAM Cover Motion Status	222	N/A	0..15	1	4	13068
MAM Cover Position Status	223	N/A	0..15	1	4	13069
MAM Cover Active Position Sensor	224	N/A	0..3	1	2	13070
MAM Cover Commanded Position	225	N/A	0..4095	1	12	13071
MAM Cover Step Count	226	N/A	0..65535	1	16	13072
MAM Cover Closed Position Definition	227	N/A	0..4095	1	12	13073
MAM Cover Open Position Definition	228	N/A	0..4095	1	12	13074
MAM Cover Closed Margin Definition	229	N/A	0..4095	1	12	13075
MAM Cover Open Margin Definition	230	N/A	0..4095	1	12	13076
BDS_Gimbal_Operation						
BDS_Elevation_Status						
Elevation Status	231	N/A	0..3	1	2	13077
Elevation scan mode	232	N/A	0..31	1	5	13078
On-Deck Elevation Scan Mode	233	N/A	0..31	1	5	13079
Elevation Encoder LED Level	234	N/A	0..1	1	1	13080
Elevation Offset Correction	235	N/A	0..65535	1	16	13081
BDS_Azimuth_Status						
Azimuth Mode	236	N/A	0..31	1	5	13082
Azimuth Motion Status	237	N/A	0..31	1	5	13083
Azimuth Direction Status	238	N/A	0..1	1	1	13084
Azimuth Position Status	239	N/A	0..15	1	4	13085
Azimuth Motor Drive Status	240	N/A	0..1	1	1	13086
Azimuth Encoder LED Level	241	N/A	0..1	1	1	13087
Azimuth Offset Correction	242	N/A	0..65535	1	16	13088
BDS_Azimuth_Definition_Status						
Crosstrack Position Definition	243	N/A	0..65535	1	16	13089
Cal Position Definition	244	N/A	0..65535	1	16	13090
Azimuth Position A Definition	245	N/A	0..65535	1	16	13091
Azimuth Position A Definition	246	N/A	0..65535	1	16	13092
Azimuth Caged Position Definition	247	N/A	0..65535	1	16	13093
Spare Azimuth Position Definition #1	248	N/A	0..65535	1	16	13094
Spare Azimuth Position Definition #2	249	N/A	0..65535	1	16	13095
Spare Azimuth Position Definition #3	250	N/A	0..65535	1	16	13096
Normal Azimuth Scan Rate Definition	251	N/A	0..65535	1	16	13097
Unsync Azimuth Scan Rate Definition	252	N/A	0..65535	1	16	13098

Table A-2. Continued

Description	Parameter Number	Units	Range	Elements/ Record	Bits/ Elem	Elem Num
Sync Azimuth Scan Rate Definition	253	N/A	0..65535	1	16	13099
Brake Command Status	254	N/A	0..15	1	4	13100
Brake Motion Status	255	N/A	0..15	1	4	13101
Brake Position Status	256	N/A	0..15	1	4	13102
Brake Commanded Position	257	N/A	0..4095	1	12	13103
Brake Step Count	258	N/A	0..65535	1	16	13104
Brake Released Position Definition	259	N/A	0..4095	1	12	13105
Brake Applied Position Definition	260	N/A	0..4095	1	12	13106
Brake Caged Position Definition	261	N/A	0..4095	1	12	13107
Brake Released Margin	262	N/A	0..4095	1	12	13108
Brake Applied Margin	263	N/A	0..4095	1	12	13109
Brake Caged Margin	264	N/A	0..4095	1	12	13110
BDS_Processor_Status						
BDS_DAP_Status						
DAP Processor Boot Status	265	N/A	0..1	1	1	13111
DAP Processor Watchdog Enable	266	N/A	0..1	1	1	13112
DAP Processor PROM Power Status	267	N/A	N/A	1	16	13113
DAP Processor Scan Period Count	268	N/A	0..65535	1	16	13114
DAP Code Checksum	269	N/A	0000..FFFF(Hex)	1	16	13115
DAP Memory Dump Start Address Offset	270	N/A	0000..FFFF(Hex)	1	16	13116
DAP Memory Dump Start Address Segment	271	N/A	0000..FFFF(Hex)	1	16	13117
DAP Memory Dump End Address Offset	272	N/A	0000..FFFF(Hex)	1	16	13118
DAP Memory Dump End Address Segment	273	N/A	0000..FFFF(Hex)	1	16	13119
DAP Memory Dump Packet Address Offset	274	N/A	0000..FFFF(Hex)	1	16	13120
DAP Memory Dump Packet Address Segment	275	N/A	0000..FFFF(Hex)	1	16	13121
DAP Minimum Execution Time	276	N/A	0..65535	1	16	13122
DAP Minimum Execution Sample	277	N/A	0..1023	1	10	13123
DAP Maximum Execution Time	278	N/A	0..65535	1	16	13124
DAP Maximum Execution Sample	279	N/A	0..1023	1	10	13125
DAP Execution Time	280	N/A	0..65535	1	16	13126
BDS_ICP_Status						
ICP Processor Boot Status	281	N/A	0..1	1	1	13127
ICP Processor Watchdog Enable Status	282	N/A	0..1	1	1	13128
ICP Processor PROM Power Status	283	N/A	0..1	1	1	13129
ICP Processor Scan Period Count	284	N/A	0..65535	1	16	13130
ICP Code Checksum	285	N/A	0000..FFFF(Hex)	1	16	13131
ICP Memory Dump Start Address Offset	286	N/A	0000..FFFF(Hex)	1	16	13132
ICP Memory Dump Start Address Segment	287	N/A	0000..FFFF(Hex)	1	16	13133
ICP Memory Dump End Address Offset	288	N/A	0000..FFFF(Hex)	1	16	13134
ICP Memory Dump End Address Segment	289	N/A	0000..FFFF(Hex)	1	16	13135
ICP Memory Dump Packet Address Offset	290	N/A	0000..FFFF(Hex)	1	16	13136
ICP Memory Dump Packet Address Segment	291	N/A	0000..FFFF(Hex)	1	16	13137
ICP Minimum Execution Time	292	N/A	0..65535	1	16	13138
ICP Minimum Execution Sample	293	N/A	0..1023	1	10	13139
ICP Maximum Execution Time	294	N/A	0..65535	1	16	13140
ICP Maximum Execution Sample	295	N/A	0..1023	1	10	13141
ICP Execution Time	296	N/A	0..65535	1	16	13142
BDS_General_Instrument_Status						
Packet Data Indicator (Data format indicator)	297	N/A	0..15	1	4	13143
Packet Data Version	298	N/A	0..31	1	5	13144
Packet Timecode Indicator	299	N/A	0..1	1	1	13145
Packet Counter	300	N/A	0..65535	1	16	13146
Instrument ID Number	301	N/A	0..63	1	6	13147

Table A-2. Continued

Description	Parameter Number	Units	Range	Elements/ Record	Bits/ Elem	Elem Num
Instrument Mode (Sequence #)	302	N/A	0..31	1	5	13148
Instrument Previous Mode (Sequence #)	303	N/A	0..31	1	5	13149
Mode(Sequence) Changed by	304	N/A	0..7	1	3	13150
Instrument Command Counter	305	N/A	0..65535	1	16	13151
Instrument Error Counter	306	N/A	0..65535	1	16	13152
Sequence Command Index	307	N/A	0..31	1	5	13153
Sequence Execution Status	308	N/A	0..7	1	3	13154
Sequence Time to Next Command	309	N/A	0..255	1	8	13155
S/C Safe Hold A Input Status	310	N/A	0..1	1	1	13156
S/C Safe Hold B Input Status	311	N/A	0..1	1	1	13157
S/C Safe Hold A Response Status	312	N/A	0..1	1	1	13158
S/C Safe Hold B Response Status	313	N/A	0..1	1	1	13159
BDS_Solar_Sensor_Status						
Solar Presence Status	314	N/A	0..16383	1	14	13160
SPS1 Noise Threshold	315	N/A	0..4095	1	12	13161
SPS1 Ratio Threshold	316	N/A	0..127	1	7	13162
SPS1 Count Threshold	317	N/A	0..63	1	6	13163
SPS2 Noise Threshold	318	N/A	0..4095	1	12	13164
SPS2 Ratio Threshold	319	N/A	0..127	1	7	13165
SPS2 Count Threshold	320	N/A	0..63	1	6	13166
8_Dig_Samples is Array[8] of:						
Command_and_Error_Stacks						
Instrument Command Echo Stack	321	N/A	$0..2.81x10^{14}$	8	48	13167
Instrument Error Stack	322	N/A	0..65535	8	16	13175
BDS_Satellite_Data						
BDS_Raw_Sat_Ephem_and_Att						
BDS_Satellite_Position						
Satellite Position (X) Count	323	count	$0..4.29x10^{9}$	1	32	13183
Satellite Position (Y) Count	324	count	$0..4.29x10^{9}$	1	32	13184
Satellite Position (Z) Count	325	count	$0..4.29x10^{9}$	1	32	13185
BDS_Satellite_Velocity						
Satellite Velocity (X) Count	326	count	$0..4.29x10^{9}$	1	32	13186
Satellite Velocity (Y) Count	327	count	$0..4.29x10^{9}$	1	32	13187
Satellite Velocity (Z) Count	328	count	$0..4.29x10^{9}$	1	32	13188
BDS_Satellite_Attitude						
Satellite Attitude (Roll) Count	329	count	0..65535	1	16	13189
Satellite Attitude (Pitch) Count	330	count	0..65535	1	16	13190
Satellite Attitude (Yaw) Count	331	count	0..65535	1	16	13191
BDS_Satellite_Attitude_Rate						
Satellite Attitude Rate (Roll) Count	332	count	0..65535	1	16	13192
Satellite Attitude Rate (Pitch) Count	333	count	0..65535	1	16	13193
Satellite Attitude Rate (Yaw) Count	334	count	0..65535	1	16	13194
Miscellaneous_Measures						
Earth-Sun distance	335	AU	0.98 .. 1.02	1	16	13195
Number of orbits	336	N/A	TBD	1	16	13196
Colatitude of Sun at observation	337	deg	0..180	1	16	13197
Longitude of Sun at observation	338	deg	0..360	1	16	13198
BDS_Satellite_Positions						
Satellite_Pos_Record_Start						
Satellite Position (X) at record start	339	km	-8000..8000	1	32	13199
Satellite Position (Y) at record start	340	km	-8000..8000	1	32	13200
Satellite Position (Z) at record start	341	km	-8000..8000	1	32	13201
Satellite_Pos_Record_End						

Table A-2. Concluded

Description	Parameter Number	Units	Range	Elements/ Record	Bits/ Elem	Elem Num
Satellite Position (X) at record end	342	km	-8000..8000	1	32	13202
Satellite Position (Y) at record end	343	km	-8000..8000	1	32	13203
Satellite Position (Z) at record end	344	km	-8000..8000	1	32	13204
Satellite_Vel_Record_Start						
Satellite Velocity (X) at record start	345	km sec^{-1}	-10..10	1	32	13205
Satellite Velocity (Y) at record start	346	km sec^{-1}	-10..10	1	32	13206
Satellite Velocity (Z) at record start	347	km sec^{-1}	-10..10	1	32	13207
Satellite_Vel_Record_End						
Satellite Velocity (X) at record end	348	km sec^{-1}	-10..10	1	32	13208
Satellite Velocity (Y) at record end	349	km sec^{-1}	-10..10	1	32	13209
Satellite Velocity (Z) at record end	350	km sec^{-1}	-10..10	1	32	13210
Satellite_Geolocations						
Colatitude of satellite at record start	351	deg	0..180	1	16	13211
Longitude of satellite at record start	352	deg	0..360	1	16	13212
Colatitude of satellite at record end	353	deg	0..180	1	16	13213
Longitude of Satellite at record end	354	deg	0..360	1	16	13214

Total Meta Bits/File:	256
Total Data Bits/Record:	200796
Total Records/File:	13091
Total Data Bits/File:	2628620436
Total Bits/File:	2628620692

Atmospheric Structures (ASTR)

The CERES archival product, atmospheric structures (ASTR), is produced by the CERES Regrid Humidity and Temperature Subsystem. Each ASTR file contains meteorological data for one hour, and is used by several of the CERES subsystems. Data on the ASTR are derived from several data sources external to the CERES system, such as NMC, MODIS, SAGE, and various other meteorological satellites. These data arrive anywhere from four times daily to once a month. These data are also horizontally and vertically organized differently from what the CERES system requires. The Regrid Humidity and Temperature Subsystem interpolates these data temporally, horizontally, and vertically to conform with CERES processing requirements.

The ASTR contains

- Surface temperature and pressure
- Vertical profiles for up to 38 internal atmospheric levels of temperature, humidity, pressure, and geopotential height
- Column precipitable water
- Vertical ozone profiles for 26 (of the 38) internal atmospheric levels
- Column ozone
- Total column aerosol
- Stratospheric aerosol

The 38 internal atmospheric levels, in hPa, as requested by the CERES Clouds and SARB working groups are:

Surface	925	775	550	275	125	5
Surface - 10	900	750	500	250	100	1
Surface - 20	875	725	450	225	70	
1000	850	700	400	200	50	
975	825	650	350	175	30	
950	800	600	300	150	10	

Level: 3
Type: Archival
Frequency: 1/hour

Time Interval Covered
File: 1 hour
Record: 1 hour

Portion of Globe Covered
File: Global
Record: 1.25-deg equal area region

Portion of Atmosphere Covered
File: Surface and internal

Table A-3. Atmospheric Structures (ASTR)

Description	Parameter Number	Units	Range	Elements/ Record	Bits/Elem ElemNum	
Meta Data						
Header				1	320	
Regional Data						
Region Number	1	N/A	1..26542	1	16	1
Surface Data						
Surface Temperature	2	K	175..375	1	16	2
Surface Pressure	3	hPa	1100..400	1	16	3
Flag, Source Surface Data	4	N/A	TBD	1	16	4
Temperature and Humidity Profiles						
Geopotential Height Profiles	5	km	0..50	38	16	5
Pressure Profiles	6	hPa	1100..0	38	16	43
Temperature Profiles	7	K	175..375	38	16	81
Humidity Profiles	8	N/A	0..100	38	16	119
Flag, Source Temp. and Humidity Profiles	9	N/A	TBD	1	16	157
Column Precipitable Water						
Precipitable Water	10	cm	0.001..8.000	1	16	158
Precipitable Water, std	11	cm	TBD	1	16	159
Flag, Source Column Precipitable Water	12	N/A	TBD	1	16	160
Ozone Profile Data						
Ozone Profiles	13	$g\ kg^{-1}$	0.00002..0.02	26	16	161
Flag, Source Ozone Profile Data	14	N/A	TBD	1	16	187
Column Ozone						
Column Ozone	15	du	200..500	1	16	188
Flag, Source Column Ozone	16	N/A	TBD	1	16	189
Total Column Aerosol						
Aerosol Mass Loading, Total Column	17	$g\ m^{-2}$	TBD	1	16	190
Flag, Source Aerosol Mass Loading, Total Column	18	N/A	TBD	1	16	191
Optical Depth, Total Column	19	N/A	0.0..2.0	1	16	192
Flag, Source Optical Depth, Total Column	20	N/A	TBD	1	16	193
Asymmetry Factor, Total Column	21	N/A	0.0..1.0	1	16	194
Flag, Source Asymmetry Factor, Total Column	22	N/A	TBD	1	16	195
Single Scattering Albedo, Total Column	23	N/A	0.0..1.0	1	16	196
Flag, Source Single Scattering Albedo, Total Column	24	N/A	TBD	1	16	197
Effective Particle Size, Total Column	25	µm	0.0..20.0	1	16	198
Flag, Source Effective Particle Size, Total Column	26	N/A	TBD	1	16	199
Mean Aerosol Layer Temperature, Total Column	27	K	150..280	1	16	200
Flag, Source Mean Aerosol Layer Temperature, Total Column	28	N/A	TBD	1	16	201
Stratospheric Aerosol						
Optical Depth, Stratosphere	29	N/A	0.0..0.5	1	16	202
Asymmetry Factor, Stratosphere	30	N/A	0.0..1.0	1	16	203
Single Scattering Albedo, Stratosphere	31	N/A	0.0..1.0	1	16	204
Effective Particle Size, Stratosphere	32	µm	0.0..10.0	1	16	205
Mean Aerosol Layer Temperature, Stratosphere	33	K	150..280	1	16	206
Flag, Source Stratospheric Aerosol	34	N/A	TBD	1	16	207

Total Meta Bits/File:	320
Total Data Bits/Record:	3312
Total Records/File:	26542
Total Data Bits/File:	87907104
Total Bits/File:	87907424

Appendix B

Output Data Products

ERBE-Like Inversion to Instantaneous TOA and Surface Fluxes (Subsystem 2.0)

This appendix describes the data products which are produced by the algorithms in this subsystem. Table B-1 below summarizes these products, listing the CERES and EOSDIS product codes or abbreviations, a short product name, the product type, the production frequency, and volume estimates for each individual product as well as a complete data month of production. The product types are defined as follows:

Archival products:	Assumed to be permanently stored by EOSDIS
Internal products:	Temporary storage by EOSDIS (days to years)

The following pages describe each product. An introductory page provides an overall description of the product and specifies the temporal and spatial coverage. The table which follows the introductory page briefly describes every parameter which is contained in the product. Each product may be thought of as metadata followed by data records. The metadata (or header data) is not well-defined yet and is included mainly as a placeholder. The description of parameters which are present in each data record includes parameter number (a unique number for each distinct parameter), units, dynamic range, the number of elements per record, an estimate of the number of bits required to represent each parameter, and an element number (a unique number for each instance of every parameter). A summary at the bottom of each table shows the current estimated sizes for metadata, each data record, and the total data product. A more detailed description of each data product will be contained in a User's Guide to be published before the first CERES launch.

Table B-1. Output Products Summary

Product Code		Name	Type	Frequency	Size, MB	Monthly size, MB
CERES	EOSDIS					
EDDB	None	ERBE-like daily data base	internal	1/month	113.5	114
ES-8	CER02	ERBE-like science product 8	archival	1/day	217.8	6752

ERBE-Like Daily Data Base Product (EDDB)

Subsystem 2 includes ERBE-like Inversion and the ERBE-like daily database processor. ERBE-like inversion passes averaged regional data to the daily database processor using the ERBE-like EID-6 file, and the daily database processor updates the 36 latitudinal band files in the EDDB data store. The daily database processor also maintains a housekeeping file with information about the status of the regional data. The housekeeping and regional data are stored in the EDDB for processing by the ERBE-like monthly time and space averaging process. The following table describes the parameters associated with a single 2.5-deg region. Instances of this record are accumulated by the daily processor for the regions that are received in the EID-6 records from ERBE-like inversion. After accumulating a month of data, the regional data for each latitudinal band are sorted by the daily processor and stored in a second set of 36 files for processing by the ERBE-like Monthly Time and Space Averaging Subsystem. The housekeeping file, also described in the following table, is a random access file. The housekeeping random access records store either arrays of integers (32-bit elements), or double precision floating point arrays (64-bit elements). Each parameter of the housekeeping file corresponds to one or more random access records.

Level: 2
Type: Internal
Frequency: 1/month

Time Interval Covered
File: Month
Record: Month

Portion of Globe Covered
File: Regional
Record: Regional

Portion of Atmosphere Covered
File: Surface and TOA

Table B-2. ERBE-Like Daily Database Product (EDDB)

Description	Parameter Number	Units	Range	Elements/ Record	Bits/ Elem	Elem Num
EDDB						
EDDB File Header		N/A				
Regional_Data is Array[36] of:						
Regional_Files is Array[2] of:						
Latitudinal_Bands						
Regional						
Regional_Descriptive						
2.5 degree one-dimensional region number	1	N/A	1..10368	72	32	1
The hour day number index is one of 24 hours for each of 31 days	2	N/A	1..744	72	32	3
Average whole Julian date for one record	3	day	2.4 .. 2.5*1E06	72	32	5
Average fractional Julian date	4	day	0..1	72	32	7
Regional_Average_Estimates						
Estimate of the average shortwave flux at the TOA	5	$W\text{-}m^{-2}$	0..1400	72	32	9
Estimate of the average longwave flux at the TOA	6	$W\text{-}m^{-2}$	0..400	72	32	11
Regional_Estimate_Statistics						
Regional_SW_Stats						
Number of individual shortwave estimates	7	N/A	0..200	72	32	13
Standard deviation of individual shortwave estimates	8	$W\text{-}m^{-2}$	0..999	72	32	15
Minimum value of individual shortwave flux at TOA	9	$W\text{-}m^{-2}$	0..1400	72	32	17
Maximum individual estimate of shortwave flux at TOA	10	$W\text{-}m^{-2}$	0..1400	72	32	19
Regional_LW_Stats						
Number of individual longwave estimates	11	N/A	0..200	72	32	21
Standard deviation of individual longwave estimates	12	$W\text{-}m^{-2}$	0..400	72	32	23
Minimum of individual longwave flux at TOA	13	$W\text{-}m^{-2}$	0..400	72	32	25
Maximum individual longwave flux at TOA	14	$W\text{-}m^{-2}$	0..400	72	32	27
Regional_Regions						
Geographic scene type of this 2.5 degree region	15	N/A	1..5	72	32	29
Regional_Fractional_Components						
Fraction of clear sky areas in this 2.5 degree region	16	N/A	0..1	72	32	31
Fraction of partly cloudy areas in this 2.5 degree region	17	N/A	0..1	72	32	33
Fraction of mostly cloudy areas in this 2.5 degree region	18	N/A	0..1	72	32	35
Fraction of overcast areas in this 2.5 degree region	19	N/A	0..1	72	32	37
Regional_Albedos						
Albedo of clear sky areas in 2.5 degree region	20	N/A	0..1	72	32	39
Albedo of partly cloudy areas in 2.5 degree region	21	N/A	0..1	72	32	41
Albedo of mostly cloudy areas in 2.5 degree region	22	N/A	0..1	72	32	43
Albedo of overcast areas in 2.5 degree region	23	N/A	0..1	72	32	45
Regional_Statistics						
Angular_Averages_Scaled						
Average of individual cosines of solar zenith angle at target point for SW	24	N/A	0..1	72	32	47
Average of individual spacecraft zenith angles from target point	25	deg	0..90	72	32	49
Average of individual relative azimuth at target point	26	deg	0..180	72	32	51
Standard deviation of individual SW albedos for clear sky areas	27	N/A	0..1	72	32	53
Average of individual LW estimates of flux at TOA clear sky	28	$W\text{-}m^{-2}$	0..400	72	32	55
Standard deviation of LW estimates of flux at TOA clear sky	29	$W\text{-}m^{-2}$	0..400	72	32	57
Number of individual longwave estimates for clear sky areas	30	N/A	0..200	72	32	59
Regional_Spares is Array[2] of:						
Spares	31	N/A	N/A	144	32	61

Table B-2. Concluded

Description	Parameter Number	Units	Range	Elements/ Record	Bits/ Elem	Elem Num
Housekeeping						
Records_for_Records_Per_Region is Array[72] of:						
Direct_Access_Records is Array[144] of:						
144 integer array storing the number of records per region.	32	N/A	TBD	10368	32	1
ERBE-like_Product_Key_Record						
Product used for validation of the Housekeeping file.	33	N/A	N/A	1	64	10369
Housekeeping_Ibuf_Array is Array[9] of:						
9 integer array containing file information.	34	N/A	N/A	9	32	10370
Scale_Factors_Record is Array[45] of:						
Scale factors for various data elements.	35	N/A	N/A	45	64	10379
Days_with_Data_Information_Record is Array[34] of:						
Array of integer flags denoting days with inversion processing.	36	N/A	N/A	34	32	10424
File_Sorted_Record is Array[36] of:						
Array of flags indicating sort status of regional data.	37	N/A	N/A	36	32	10458
Julian_Start_Inversion_Header_Record is Array[33] of:						
Start dates and times for each of 31 days, prior and succeeding days.	38	N/A	N/A	33	64	10494
Julian_End_Inversion_Header_Record is Array[33] of:						
End dates and times for 31 days, prior and succeeding days.	39	N/A	N/A	33	64	10560
ERBE-like_Product_key_Record_for_Files is Array[33] of:						
Product keys for 31 days, prior and succeeding days.	40	N/A	N/A	33	64	10593

Total Meta Bits/EDDB Product	**343584**
Total Data Bits/Day	**30720000**
Total Data Bits/Month	**952320000**
Total Bits/EDDB Product	**952663584**

ERBE-Like Science Product 8 (ES-8)

The ES-8 data product contains a 24-hour, single-satellite, instantaneous view of scanner fluxes at the top-of-atmosphere reduced from spacecraft altitude unfiltered radiances using the ERBE scanner inversion algorithms and the ERBE shortwave (SW) and longwave (LW) ADM's. The ES-8 also includes the SW, LW, and window (WN) channel radiometric data; SW, LW, and WN unfiltered radiance values; the ERBE scene identification results on a pixel basis; and surface parameters*, including SW and LW fluxes and precipitable water. This data is organized according to the CERES 3.3-sec scan into 6.6-sec records. These records contain only Earth-viewing measurements, approximately 450 for TRMM and 390 for EOS. As long as there is one valid scanner measurement within a record, the ES-8 record will be generated.

The ES-8 is output by the CERES ERBE-like process. The TOA and surface fluxes for each CERES pixel will be archived on the ES-8, as well as flags describing instrument status, the radiometric data, and FOV location.

Specifically, the ES-8 contains the following kinds of information:

1. Scan-Level Data
   a. Julian date and time
   b. Earth-Sun distance
   c. Satellite position and velocity and sun position
2. Pixel-Level Data
   a. Satellite instrument field of view data
   b. Radiometric Data
   c. Satellite and sun geometry data
   d. Unfiltered Radiances
   e. TOA Fluxes and surface fluxes
   f. ERBE Scene Identification

(1) clear ocean	(5) clear coastal	(9) mostly-cloudy ocean
(2) clear land	(6) partly-cloudy ocean	(10) mostly-cloudy land-desert
(3) clear snow	(7) partly-cloudy land-desert	(11) mostly-cloudy coastal
(4) clear desert	(8) partly-cloudy coastal	(12) overcast

The ES-8 will be produced starting at launch and will be externally archived for use by the global scientific community.

Level: 2
Type: Archival
Frequency: 1/day

Portion of Globe Covered
File: Satellite swath
Record: N/A

Time Interval Covered
File: 24 hours
Record: 6.6 seconds

Portion of Atmosphere Covered
File: Satellite altitude, TOA, and surface

*Surface parameters have been transferred from the ES-8 to the SSF data product.

Table B-3. ERBE-Like Science Product 8 (ES-8)

Description	Parameter Number	Units	Range	Elements/ Record	Bits/ Elem	Elem Num
ES-8				1	64	
ES-8 File Header		N/A				
Scale_Factors is Array[10056] of:				10056	32	
Offsets is Array[10056] of:				10056	32	
ES-8_Data_Record						
Scan_Level_Data						
Julian_Date						
Julian day	1	day	2449353 .. 2458500	1	32	1
Julian time	2	day	0.0 .. 1.0	1	32	2
Earth-Sun_Distance						
Earth-Sun distance	3	AU	0.98 .. 1.02	1	16	3
Satellite_State_Vector						
Satellite_Position_Vector						
X component of satellite position	4	km	-8000 .. 8000	2	32	4
Y component of satellite position	5	km	-8000 .. 8000	2	32	6
Z component of satellite position	6	km	-8000 .. 8000	2	32	8
Satellite_Velocity_Vector						
X component of satellite inertial velocity	7	km/sec	-10 .. 10	2	32	10
Y component of satellite inertial velocity	8	km/sec	-10 .. 10	2	32	12
Z component of satellite inertial velocity	9	km/sec	-10 .. 10	2	32	14
Satellite_Nadir						
Colatitude of satellite at observation	10	deg	0 .. 180	2	16	16
Longitude of satellite at observation	11	deg	0 .. 360	2	16	18
Sun_Position						
Colatitude of Sun at observation	12	deg	0 .. 180	1	16	20
Longitude of Sun at observation	13	deg	0 .. 360	1	16	21
Orbit_Number						
Satellite orbit number	14	N/A	0 .. 54000	1	16	22
Pixel_Level_Data						
FOV_Location_at_TOA						
Colatitude of CERES FOV at TOA	15	deg	0 .. 180	450	16	23
Longitude of CERES FOV at TOA	16	deg	0 .. 360	450	16	473
Radiometric_Data						
CERES total filtered radiance, upwards	17	$W\text{-}m^{-2}sr^{-1}$	0 .. 700	450	16	923
CERES shortwave filtered radiance, upwards	18	$W\text{-}m^{-2}sr^{-1}$	-10 .. 510	450	16	1373
CERES window filtered radiance, upwards	19	$W\text{-}m^{-2}sr^{-1}$	0 .. 50	450	16	1823
FOV_Geometry_at_TOA						
CERES viewing zenith at TOA	20	deg	0 .. 90	450	16	2273
CERES solar zenith at TOA	21	deg	0 .. 180	450	16	2723
CERES relative azimuth at TOA	22	deg	0 .. 360	450	16	3173
Unfiltered_Measurements						
CERES shortwave radiance, upwards	23	$W\text{-}m^{-2}$	-10 .. 510	450	16	3623
CERES longwave radiance, upwards	24	$W\text{-}m^{-2}$	0 .. 200	450	16	4073
CERES window radiance, upwards	25	$W\text{-}m^{-2}$	0 .. 50	450	16	4523
TOA_Estimates						
CERES shortwave flux at TOA, upwards	26	$W\text{-}m^{-2}$	0 .. 1200	450	16	4973
CERES longwave flux at TOA, upwards	27	$W\text{-}m^{-2}$	50 .. 400	450	16	5423
ERBE scene type for inversion process	28	N/A	0 .. 12.4	450	16	5873
Surface_Parameters						
Surface_Flux						
CERES shortwave flux at surface, downwards	29	$W\text{-}m^{-2}$	0 .. 1200	450	16	6323

Table B-3. Concluded

Description	Parameter Number	Units	Range	Elements/ Record	Bits/ Elem	Elem Num
CERES longwave flux at surface, downwards	30	$W\text{-}m^{-2}$	50 .. 400	450	16	7223
CERES net shortwave flux at surface	31	$W\text{-}m^{-2}$	0 .. 1200	450	16	6773
CERES net longwave flux at surface	32	$W\text{-}m^{-2}$	50 .. 400	450	16	7673
Precipitable water	33	cm	0.001 .. 8.0	450	16	8123
Flag_Words_Data						
Scanner operations flag word	34	N/A	N/A	2	16	8573
Quality flag for total radiance value	35	N/A	N/A	33	16	8575
Quality flag for shortwave radiance value	36	N/A	N/A	33	16	8608
Quality flag for window radiance value	37	N/A	N/A	33	16	8641
Quality flag for FOV	38	N/A	N/A	33	16	8674

Total Meta Bits/File:	643648
Total Data Bits/Record:	139520
Total Records/File:	13091
Total Data Bits/File:	1826456320
Total Bits/File:	1827099968

Clouds and the Earth's Radiant Energy System (CERES)

Algorithm Theoretical Basis Document

ERBE-Like Averaging to Monthly TOA

(Subsystem 3.0)

Edwin F. Harrison[1]
Patrick Minnis[1]
David F. Young[2]
Gary G. Gibson[2]
Olivia C. Smith[3]

[1]NASA Langley Research Center, Hampton, Virginia 23681-0001
[2]Analytical Services & Materials, Inc., Hampton, Virginia 23666
[3]Science Applications International Corporation (SAIC), Hampton, Virginia 23666

CERES Top Level Data Flow Diagram

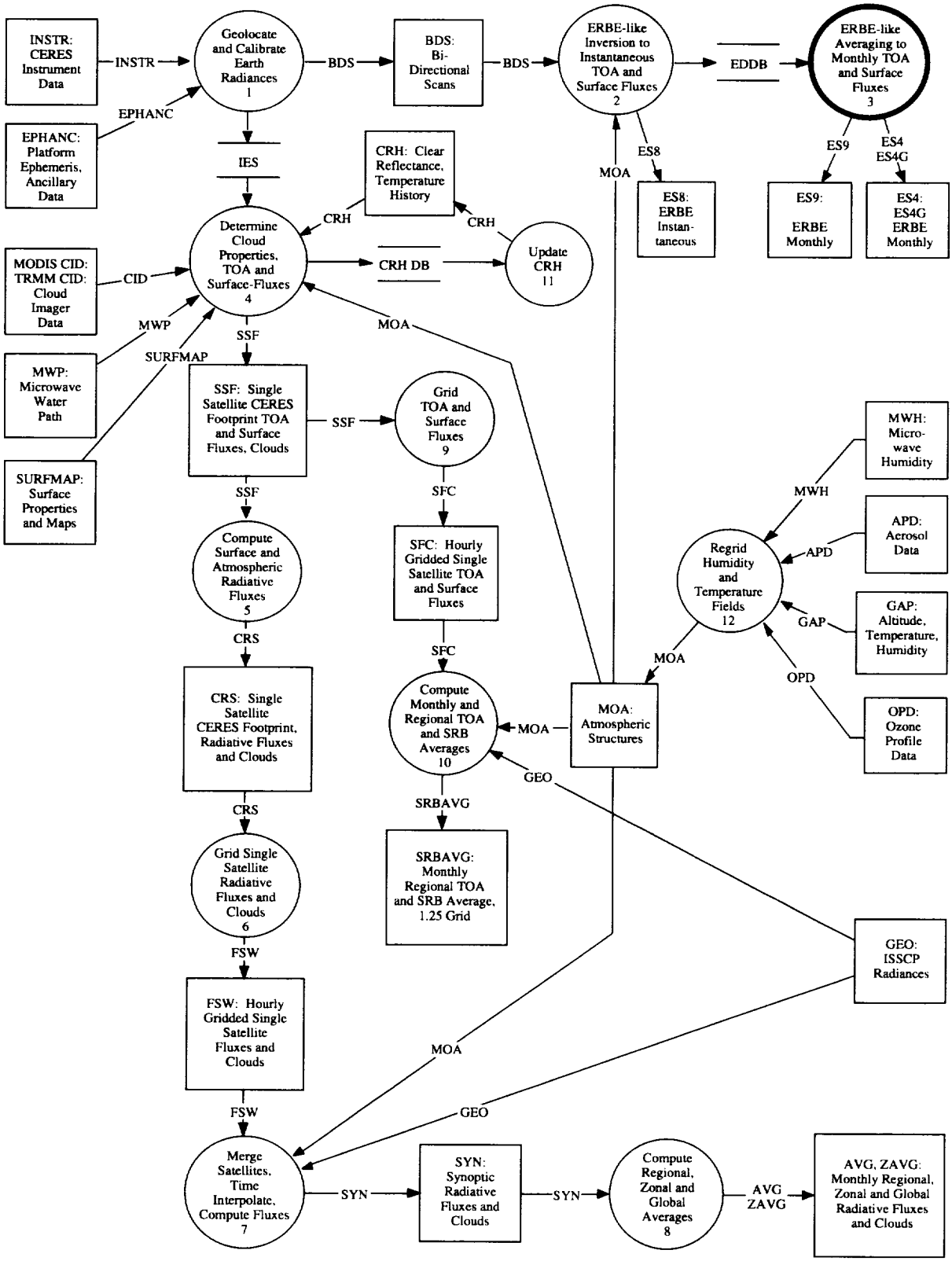

Abstract

This subsystem describes methods to temporally interpolate CERES measurements to compute ERBE-like averages of top-of-atmosphere (TOA) radiative parameters. CERES observations of shortwave (SW) and longwave (LW) flux are time-averaged using a data interpolation method similar to that employed by the Earth Radiation Budget Experiment (ERBE). The averaging process produces daily, monthly-hourly, and monthly means of TOA SW and LW flux on regional, zonal, and global spatial scales. Separate calculations are performed for clear-sky and total-sky fluxes.

3.0. ERBE-Like Averaging to Monthly TOA

3.1. Introduction

The satellites that carry the CERES instrument do not provide continuous spatial and temporal coverage of the Earth's entire surface. Historically, the sparse distribution of satellite measurements is the most critical factor in temporal averaging of radiation data from regional to global scales (Brooks et al. 1986). Because a satellite does not view all portions of the Earth at all times, temporal modeling of the diurnal variability of the Earth's radiation field is required to recover daily or monthly averaged radiative parameters. A clear understanding of the Earth's radiative behavior demands realistic models of diurnal variations that depend on the surface type and cloud cover and accurately describe the solar zenith angle dependence of albedo and longwave exitance.

A major emphasis of radiation budget research is on the monitoring and analysis of long-term variations in the Earth's climate. This can only be accomplished using stable, long-term global data sets. In order to fulfill this research need, CERES will produce an ERBE-like product to provide a data set processed in a manner consistent with the earlier experiment (see Brooks et al. 1986).

3.2. Input

The chief input to the ERBE-like monthly time-space averaging (TSA) subsystem is the stream of CERES SW and LW TOA flux observations. Included with each measurement is necessary information such as satellite viewing geometry, the latitude and longitude of the observation, and the underlying geographic scene type. In addition, cloud amount is estimated for each pixel in the ovserved area. See appendix A for tables describing the input data products. Additional input data include TOA albedo angular distribution models (ADM's) and solar declination data.

3.3. Output

The TSA process produces daily, monthly-hourly, and monthly means of TOA SW and LW flux on regional, zonal, and global spatial scales. Separate calculations are performed for clear-sky and total-sky fluxes. Daily SW clear-sky fluxes are provided only for days with clear-sky measurements; daily clear-sky LW over land regions is not provided. See appendix B for tables describing the output data products.

3.4. Summary of Processes

One month of data is sorted and averaged into the standard ERBE 2.5° latitude × 2.5° longitude grid. All data within each grid box are sorted and averaged in 1-hour increments (hour boxes).

Total-sky TOA LW flux is estimated for all hours during the month by interpolating between those hours containing observations. Linear interpolation is used over oceans, while a half-sine curve fit is applied over land and desert regions based on studies by Brooks and Minnis (1984). Monthly and monthly-hourly means are then computed using the combination of observed and interpolated values.

Clear-sky TOA LW flux is calculated in the same manner as total-sky TOA LW in oceanic regions. However, over land regions, a different technique is used to compensate for the effects of undersampling. Hours with clear-sky LW observations are averaged over the month for each local hour. A single half-sine curve is fitted to this monthly composited data, and the monthly-hourly means from this fit are averaged to produce monthly means.

Monthly mean total-sky and clear-sky TOA SW fluxes are produced in a manner similar to total-sky TOA LW flux. For all days with at least one SW observation, a value of SW flux is interpolated for all daylight hours using models of the albedo variation with solar zenith angle (Suttles et al. 1988). Monthly mean albedos are calculated by summing the modeled SW flux values and dividing that sum by the sum of solar incident flux from the same hours. Monthly mean SW flux is calculated by multiplying the monthly mean albedo by a more precise value of monthly mean solar incident flux that is produced by integrating the solar incident flux over all days of the month.

Finally, the TOA LW and SW fluxes are averaged on zonal and global scales using the appropriate area weighting functions for each latitude.

3.5. Technical Basis

The ultimate goal of radiation budget monitoring experiments such as ERBE (Barkstrom 1984; Barkstrom and Smith 1986) and CERES (Wielicki and Barkstrom 1991) is to accurately determine the components of the Earth's radiation budget on regional, zonal, and global spatial scales at various temporal resolutions. Regional and global analyses of the large sets of highly accurate satellite measurements of incoming and outgoing energy in the Earth's climate system can be achieved only by adequately sampling the radiation fields and properly averaging the data in space and time. The CERES Data Management System will produce a data product which is processed in a manner consistent with ERBE to provide a stable, long-term data set for monitoring and analyzing Earth's climate variations. The averaging processes which are used in the CERES ERBE-like processing are described below.

ERBE is the most accurate experiment to date for measuring the Earth's radiation budget (Barkstrom et al. 1990), the diurnal variability of radiation (Harrison et al. 1988; Hartmann et al. 1991; Cheruy et al. 1991), cloud-radiative forcing (Ramanathan et al. 1989a; Ramanathan et al. 1989b; Harrison et al. 1990b), and volcanic climate radiative forcing (Minnis et al. 1993). For a discussion of the ERBE errors, see Harrison et al. (1990b) and Barkstrom et al. (1990). The largest sources of uncertainty in the pre-ERBE radiation budget missions arose from errors due to calibration and stability, sampling, and data analysis methods. The ERBE instruments reflect an improved understanding of instrument operation and incorporate reliable calibration sources for better measurement accuracy.

ERBE used multiple satellites to account for widespread semiregular diurnal variations in cloudiness that can cause substantial errors in regional radiation budgets derived with single Sun-synchronous satellite measurements (Harrison et al. 1983). The multisatellite ERBE measurements, combined with models to estimate fluxes at unsampled hours, produced the best estimates to date of the diurnal variability of TOA radiation (Harrison et al. 1988; Harrison et al. 1990a; Hartmann et al. 1991).

CERES instruments will also be flown on multiple satellites to provide the diurnal sampling necessary to obtain accurate monthly flux averages using the ERBE-like interpolation techniques. The temporal coverage of the three CERES satellites (TRMM, EOS-AM, and EOS-PM) for 1 month of observations is shown in figure 3-1. The TRMM spacecraft is in a 35°-inclined, precessing orbit which covers all local times at the equator in slightly over 26 days. The EOS satellites are in Sun-synchronous

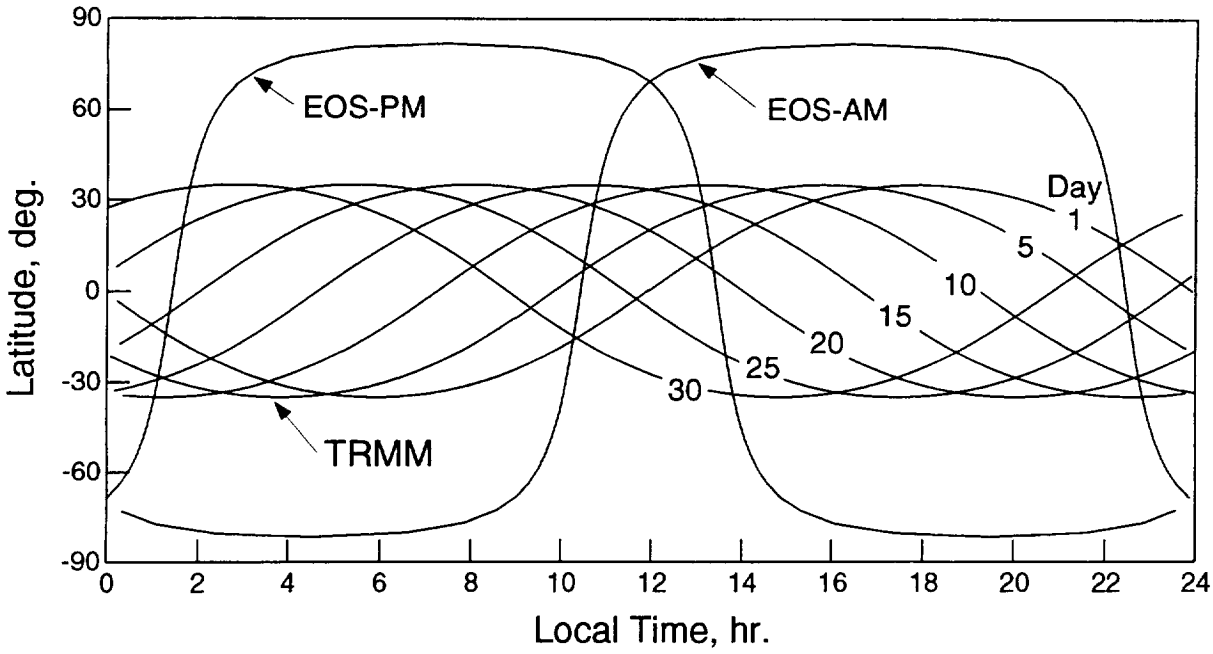

Figure 3-1. Temporal coverage of CERES satellites.

orbits, sampling at the same local times each day. From figure 3-1, it is evident that a single satellite cannot provide sufficient temporal sampling to accurately estimate SW and LW fluxes at all local hours.

For ERBE, a comprehensive set of LW and SW angular dependence models was developed (Suttles et al. 1988 and 1989) and used to convert radiances to fluxes. A method for separating and identifying clear-sky and cloud-contaminated measurements (Wielicki and Green 1989) was constructed to improve radiance interpretation for selecting the correct angular models and to better understand the effects of clouds. Geostationary satellite data were used to develop a more accurate technique for averaging the data over the diurnal cycle (Brooks and Minnis 1984).

All of these improvements in the instruments, satellite sampling, and the data processing system allowed ERBE to meet many of the goals of the scientific community. CERES will make further improvements in ERB measurements, particularly in determining more accurate and com-prehensive cloud information. However, in the interest of compiling a long-term, consistent data set for climate studies, an ERBE-like data product will be produced.

3.5.1. Temporal Interpolation and Spatial Averaging

The first step in the averaging process is to sort the data in space and time. CERES data enter this subsystem as a chronologically-ordered stream of flux measurements. Spatially, these data are averaged and processed on an ERBE 2.5° × 2.5° grid. Each region (grid box) is processed independently from all others. Within each region, a month of CERES measurements is sorted and averaged into local time intervals of one hour (referred to as hour boxes). There is a maximum of 744 hour boxes in a month (24 hours/day × 31 days).

The averaging of the LW flux is straightforward. All observations from a region that were measured within an hour box are linearly combined. Since albedo is a function of solar zenith angle, each SW measurement is first corrected to the central time, latitude, and longitude of the regional hour box into which it is collected. The temporal correction is performed using 12 ADM's. As shown in figure 3-2, there are separate ADM's for the five ERBE clear-sky geographical scene types (ocean, land, snow,

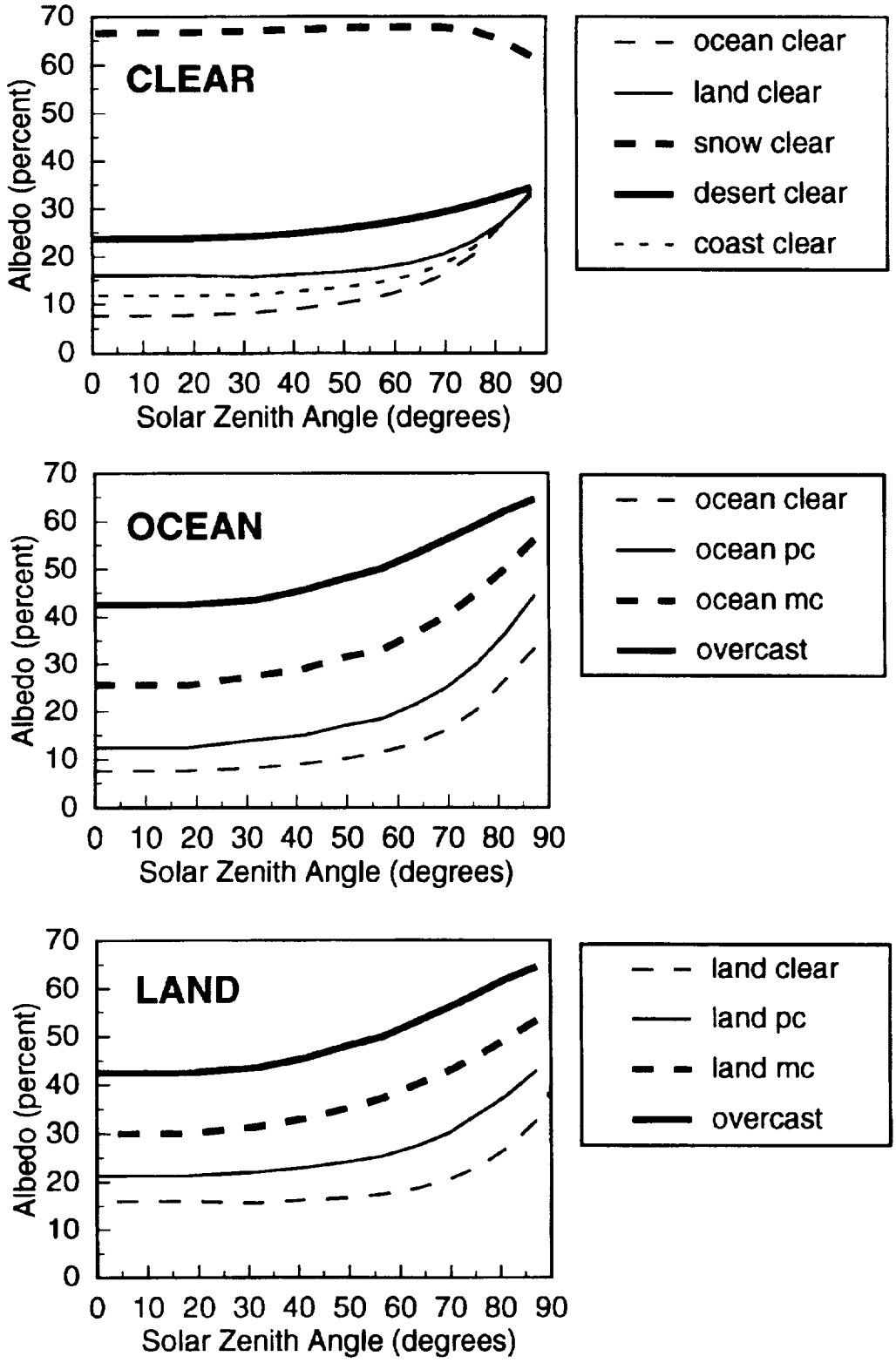

Figure 3-2. ERBE angular distribution models (ADM's).

desert, and coast). Over land and ocean surfaces, there are models for partly cloudy and mostly cloudy ERBE scene classifications. Finally, a single model is used for overcast conditions over all surfaces. The ADM's for partly and mostly cloudy coastal scenes are not shown. Within each hour box, a separate mean albedo is calculated for each cloud class, and a histogram of cloud class is also retained. The geographic scene type for each region is constant for a month.

3.5.2. Total-Sky TOA LW Flux

The ERBE TSA algorithm was designed to provide daily model fits to the TOA LW flux data as well as monthly averages of these data. To accomplish this goal, an estimate of LW flux is made for every hour box. This interpolation is performed in one of two ways, depending on the geographic scene type of the region.

Over ocean regions, there is little diurnal variability in LW flux due to solar insulation. The greatest variations in LW flux over the oceans occur due to changes in the amount and types of clouds. Therefore, no attempt is made to develop complex models for estimating the LW flux between the times of observations. Rather, it is assumed that changes in LW flux are due to changes in cloud conditions, and that this change is linear. Therefore, simple linear interpolation is used to provide a value of LW flux for each hour box not observed by CERES. At the beginning of the month, all hours preceding the first observation are filled with the value from the first observed time. The same procedure is applied at the end of the month using the last observed LW flux. This technique is also used for regions designated as either snow-covered or coastal.

Over land and desert regions, the effects of solar heating are much more pronounced than over ocean regions. During relatively cloud-free periods, there is generally a sinusoidal variation in LW flux over the daylight hours. In order to account for this variation, these regions are treated in a different manner from oceans in the TSA algorithm. For any day when an observation was made during daylight hours and during the preceding and following nights, the LW flux for the remaining hours of the day is modeled by fitting a half-sine curve to the observations. The modeling is performed by linear interpolation on days lacking the required observations or having any daylight observations of LW flux that are less than the nighttime values, or when the resultant half-sine curve has a negative amplitude.

The results of this type of interpolation are demonstrated in figure 3-3 that shows a time series of ERBE scanner data from April 1985 over a 2.5° region in eastern New Mexico. In this figure, observations are represented by circles, and the interpolated values are displayed as the solid line. The early part of the month was relatively clear, and half-sine fits were performed on days 1, 2, 4, 6, 7, and 8. However, on days 10, 11, and 12, no half-sine fit was used since low values of LW were observed in the late afternoon, which indicates that clouds must have been developing. In such cases, the half-sine fit is not realistic, and linear interpolation is used.

Once all hour boxes for the month have been filled with a value of LW flux, it is a simple matter to calculate daily, monthly-hourly, and monthly means. Two slightly different techniques are used to compute monthly means. In the first method (monthly-daily), a daily mean is computed by averaging the 24-hour box values for each day. The monthly mean TOA LW flux, $\bar{F}_{LW}$, is then computed by averaging all of the daily means:

$$\bar{F}_{LW} = \sum_{d=1}^{D} \frac{\sum_{h=1}^{24} F_{LW}(d, h)/24}{D} \tag{3.1}$$

where $F_{LW}(d, h)$ is the TOA LW flux for day d and local hour h, and D is the total number of days in the month. In the second method (monthly-hourly), hour box values for all days in which an observation

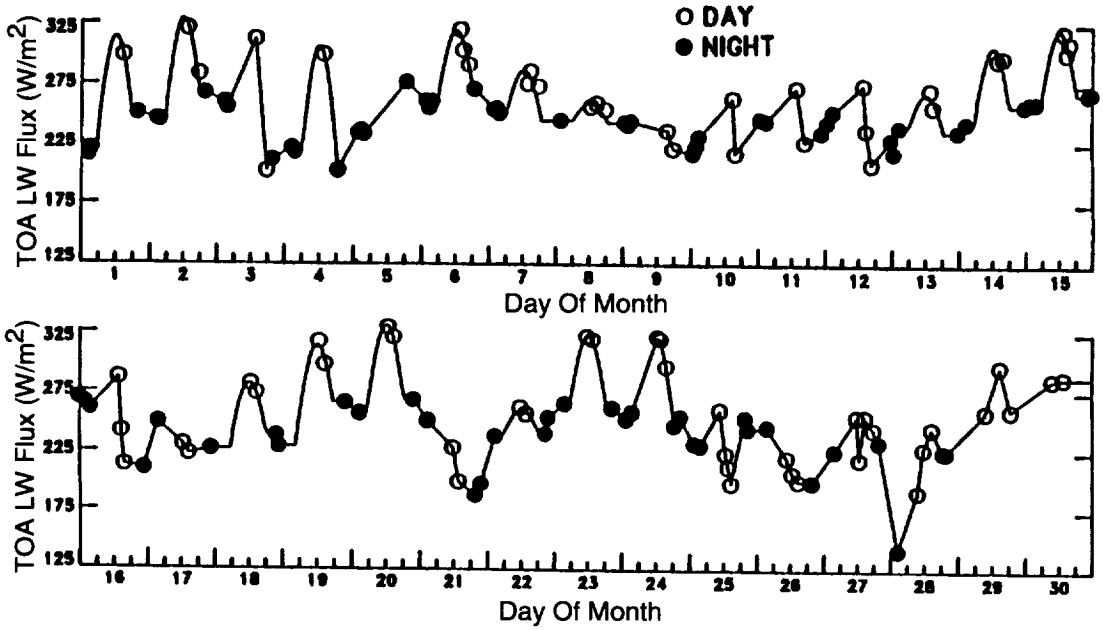

Figure 3-3. Time series of ERBS and NOAA-9 ERBE scanner TOA LW flux data and diurnal models for a 2.5° region in eastern New Mexico in April 1985.

was made are averaged at each local hour. The resulting 24 monthly-hourly means are then averaged to produce a monthly mean:

$$\bar{F}_{LW} = \sum_{h=1}^{24} \frac{\sum_{d=1}^{D_{LW}} F_{LW}(d,h)/D_{LW}}{24} \tag{3.2}$$

where D_{LW} is the total number of days in the month with at least one LW measurement. The two estimates of monthly mean LW flux will be equal unless there were days during the month when no observations were made.

3.5.3. Clear-Sky TOA LW Flux

The above algorithm works very well for total-sky LW flux for regions that are well-sampled in local time. However, problems may arise when applying this technique to clear-sky LW flux data. The ERBE cloud classification procedure is quite restrictive in terms of classifying an observation as clear (Wielicki and Green 1989). Also, there are many regions over the globe where cloudy conditions prevail throughout the month. Consequently, a region may have a very limited number of clear-sky observations during the month. In addition, satellite sampling patterns often result in a local-time bias in the occurrence of clear-sky measurements. An example of this is shown in figure 3-4 for the same 2.5° ERBE region over New Mexico discussed in the above section. For this case, with the exception of the two measurements from days 4 and 5, all of the limited number of clear-sky observations occurred during daylight hours. The lack of nighttime data means that the requirements for performing the diurnal half-sine fits are never met. The linear interpolation between the times of observation results in a monthly average that is unrealistically high because only daytime values are available. This problem is particularly serious over land and desert regions where large diurnal variations in LW flux are expected during clear-sky conditions. Since clear ocean areas generally have a much smaller LW flux diurnal

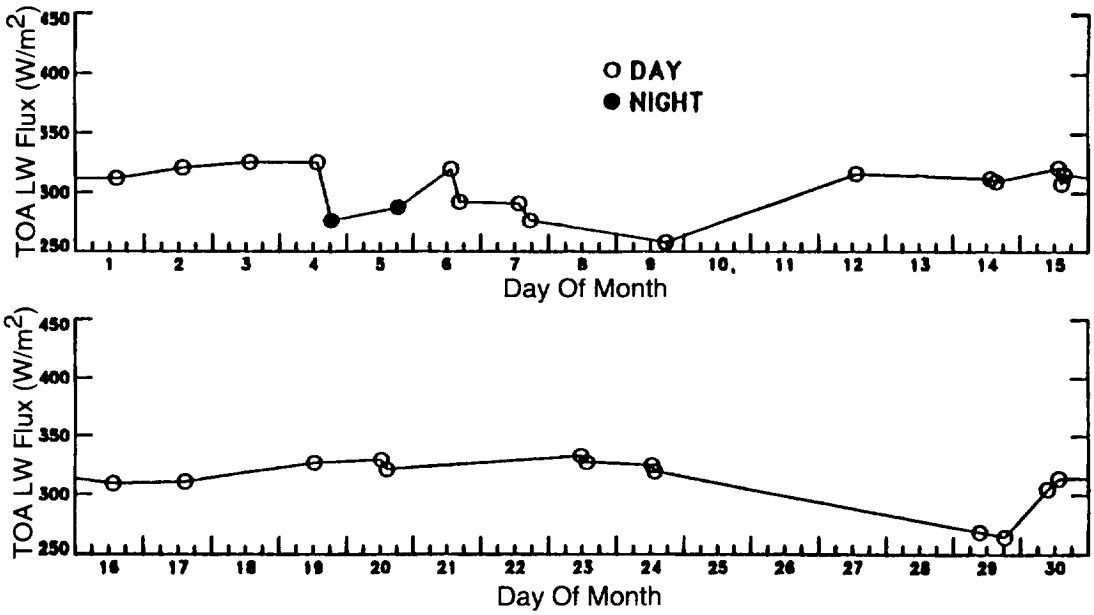

Figure 3-4. Time series of ERBS and NOAA-9 ERBE scanner clear-sky TOA LW flux data and diurnal models for a 2.5° region in eastern New Mexico in April 1985.

change, the day-night sampling bias does not severely affect the ocean monthly means. Therefore, in ocean regions, the clear-sky LW flux is averaged in a manner identical to the total-sky data.

Because of these problems associated with obtaining accurate averages of clear-sky LW flux over land and deserts, an improved TSA algorithm has been developed that involves calculating a single diurnal fit to the monthly ensemble of all clear-sky LW flux data. In the clear-sky case, it is reasonable to process all of the measurements together because the scene is essentially unchanged throughout the month and, consequently, the variance of measurements at the same local hour is expected to be small. Some exceptions occur due to scene variability of the measurement footprints within the region, changing atmospheric conditions such as water vapor content, wind, and surface temperature during the month, cloud contamination of presumably clear-sky scenes, and possible errors due to measurements taken at high viewing zenith angles. The underlying assumption is that this variability is small relative to the overall diurnal variation and can be effectively averaged out for a region having several clear-sky observations over the course of a month.

The clear-sky LW flux averaging technique is demonstrated in figure 3-5. The data shown in figure 3-4 have been sorted and averaged for the entire month in terms of local hour. The daytime points (open symbols) are then modeled using a least-squares half-sine fit weighted by the number of measurements at each local hour during the month. The nighttime data (filled symbols) are simply averaged and the constant value is used for all nighttime hours. The monthly mean is then calculated by averaging the fit over 24 hours if the fit meets five basic criteria:

(a) There must be at least one daylight measurement located more than one hour from the terminator

(b) There must be at least one nighttime measurement

(c) The least squares half-sine fit to the daylight data produces a positive amplitude

(d) The peak value of the fit must not exceed 400 $W\text{-}m^{-2}$

(e) The length of day 15 of the month must be greater than 2 hours

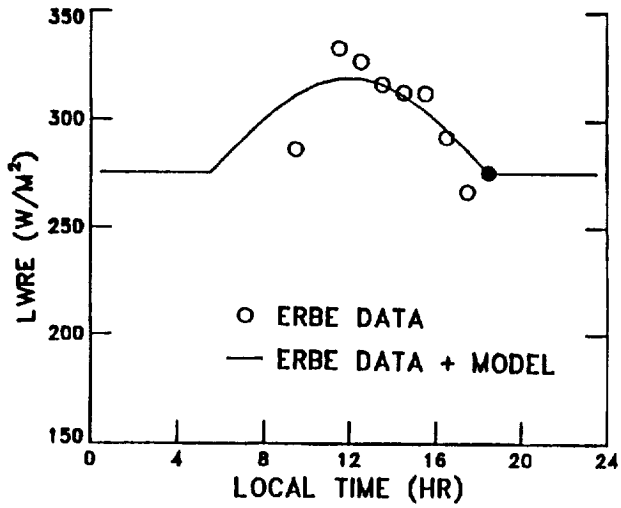

Figure 3-5. ERBE time averaged monthly-hourly clear-sky TOA LW flux results for the region shown in figure 3-4.

If these criteria are not met, no monthly mean TOA LW clear-sky flux is calculated for the region. Since the modeling process is performed on data accumulated throughout the month, daily means are not calculated for land and desert regions.

This technique produces realistic values of monthly mean clear-sky LW flux, even in regions with sparse data sampling. However, in many regions no estimate can be made due to the total lack of nighttime, clear-sky data due to persistent overcast conditions or the overly restrictive ERBE clear classification scheme. To compensate for missing nighttime data, the clear-sky averaging algorithm attempts to correct for the misclassification of nighttime clear pixels as partly cloudy. For each nighttime hour box over land regions, a new clear-sky amount is estimated by assuming that 10% of the pixels classified as partly cloudy are actually clear. If the new clear-sky amount exceeds 5% and is greater than the original clear-sky percentage, then the clear-sky longwave flux is recalculated using the mean and standard deviation of the total longwave flux.

3.5.4. Total-Sky and Clear-Sky TOA SW Flux

The procedure for producing diurnal, monthly-hourly, and monthly means of SW flux is quite different from that for LW flux. Since TOA SW flux is obviously only pertinent to daylight hours, the difficulty of interpolating across day-night boundaries that causes problems in modeling sparsely sampled LW data is not encountered. Furthermore, as shown in figure 3-2, there exist well-developed models of the variation of albedo with solar zenith angle for various clear and cloudy backgrounds (Suttles et al. 1988). These angular distribution models (ADM's) are used to interpolate observations to other times of the day. In addition, the clear-sky SW flux (or albedo) can be modeled in the same manner as the total-sky since the lack of nighttime clear data is not a factor.

As explained in the section on spatial averaging, for each hour box with an observation, a separate albedo is calculated for each of the four ERBE cloud classifications: clear, partly cloudy, mostly cloudy, and overcast. In addition, a frequency histogram of the relative quantity of each type is stored. Because the diurnal variability of SW radiation is pronounced even within a single hour, measured values are first adjusted to the nearest local solar half hour. For a given surface type and cloud cover category (i.e., scene type for selecting an ADM), the normalized ADM function, $\delta_i(\mu_o)$, at time t is defined as the ratio of the albedo at time t and the albedo at overhead sun:

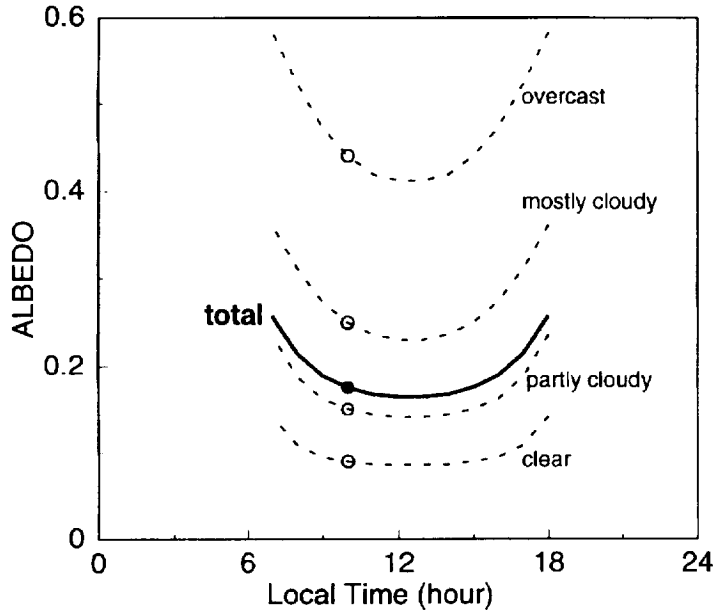

Figure 3-6. An example of time interpolation of albedo for days with only 1 hour of observation.

$$\delta_i(\mu_o(t)) = \frac{\alpha_{\mathrm{mod}_i}(\mu_o(t))}{\alpha_{\mathrm{mod}_i}(\mu_o = 1)} \tag{3.3}$$

where μ_o is the cosine of the solar zenith angle and α_{mod_i} is the ADM albedo for scene type i (from fig. 3-2). The albedo at any time t' (e.g., at the local solar half hour) can be expressed as the product of the observed albedo and the ratio of the normalized ADM functions from t' and the time of observation, t_{obs}:

$$\alpha_i(t') = \alpha_i(\mu_o(t_{obs}))\frac{\delta_i(\mu_o(t'))}{\delta_i(\mu_o(t_{obs}))} \tag{3.4}$$

For days with only one SW flux measurement, each of the four cloud type albedos from the hour of observation is modeled to all daylight hours using equation (3.4) and the appropriate ADM's. This modeling is illustrated in figure 3-6. The albedos for the four cloud types are then recombined by weighting each cloud type albedo with the appropriate areal coverage fraction to obtain the mean albedo at each hour for the entire region (solid line in fig. 3-6). This process assumes that the relative abundance of the cloud classifications remains constant throughout the day.

For days with more than one measurement, this technique is modified as illustrated in figure 3-7. This figure presents albedos for all hours for each of the two measurements individually, and then shows how the two are combined to determine the best estimates of albedo. All daylight hours preceding the first measurement of the day and following the last measurement assume constant cloud class from the nearest measurement. These hours are modeled using equation (3.4) in the single measurement case. For hours between two measurements, it is assumed that the cloud histograms are varying linearly over that span. The four cloud type albedos are modeled from each surrounding measurement using equation (3.4) and the appropriate ADM's. Total albedo for each hour between the two measurements is then produced by inversely weighting the two estimates by the time from the hour of interest.

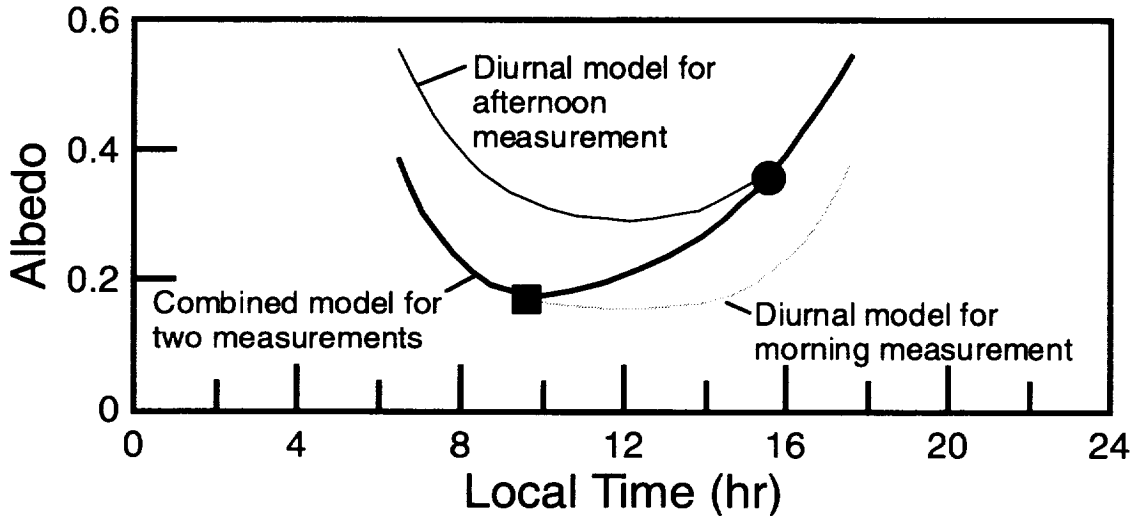

Figure 3-7. An example of time interpolation of albedo with 2 hours of observation during a day.

Monthly means are calculated once all hours are filled with albedo values for days with at least one measurement. The SW flux at each hour h of a given day d is:

$$F_{SW}(d,h) = E_o(d)\mu_o(d,h)\alpha(d,h) \tag{3.5}$$

where E_o is the mean daily distance-corrected solar constant. The SW flux is summed over all hours for days with measure nd divided by a summation of solar incident flux over the same hours to produce a monthly mean albedo:

$$\bar{\alpha} = \sum_{d=1}^{D_{SW}} \left(\sum_{h=1}^{24} F_{SW}(d,h)/24 \right) / D_{SW}/S_o \tag{3.6}$$

where $F_{SW}(d,h)$ is the TOA SW flux for day d and local hour h, D_{SW} is the total number of days in the month with at least one SW measurement, and S_o is the summed solar incident SW flux. Monthly mean SW flux, $\bar{F}_{SW}$ is then calculated by multiplying monthly mean albedo by the incident solar flux integrated and averaged over all hours of the month:

$$\bar{F}_{SW} = \alpha S_o' \tag{3.7}$$

where S_o' is the integrated solar incident SW flux.

Mean clear-sky SW flux is produced in a similar manner. In fact, the process is simpler because only the clear albedo from each hour box needs to be interpolated to non-measured hours. Again, only days with at least one measurement are filled using the clear-sky ADM's, and values from these days are combined to produce daily, monthly-hourly, and monthly means.

3.5.5. Zonal and Global Means

Zonal and global means of TOA LW and SW flux are calculated in the same manner as used with ERBE data. Since this product is produced on the ERBE 2.5° equal-angle grid, the regional means must be weighted by area when computing global means. The 2.5° regional data will also be nested into 5° and 10° grids as was done with ERBE.

3.6. Uncertainty Estimates

Although a complete, rigorous error analysis for all of the ERBE products is not yet available, several studies of the ERBE error sources have resulted in reliable estimates of the uncertainties in monthly mean TOA LW and SW radiation. Bias errors for monthly mean regional total-sky fluxes are less than 1 $W\text{-}m^{-2}$. The rms uncertainties in total-sky LW and SW fluxes are estimated to be 3 $W\text{-}m^{-2}$ and 5 $W\text{-}m^{-2}$, respectively. In terms of SW albedo, the error is approximately ±0.014. The rms errors in clear-sky LW and SW fluxes are estimated to be 2 $W\text{-}m^{-2}$. The clear-sky LW fluxes, however, may be overestimated by about 4 $W\text{-}m^{-2}$. The clear-sky reflected flux is overestimated by approximately 1 $W\text{-}m^{-2}$. For an overview of the uncertainties in the ERBE monthly mean flux values, see Harrison et al. (1990b).

3.7. Strategic Concerns

Estimates of surface fluxes can be produced using TOA-to-surface parameterization schemes and included as part of the archived output from the ERBE-like processing of subsystem 3. These surface fluxes were originally planned for inclusion with the ERBE-like products. However, it has been decided that they will not be included in subsystem 3 for Release 1, in order for this subsystem to produce only truly ERBE-like results. However, surface fluxes will be produced in subsystem 10.

The basic algorithmic development for this subsystem has already been accomplished because of the similarities with the existing ERBE TSA code. New concerns arise only in the possible inclusion of the TOA-surface flux parameterization schemes. All information necessary to use these models is available from the data stream or from the ancillary atmospheric data, with the exception of the cloud base temperature which will be needed to calculate surface total-sky LW flux if surface fluxes are included in future releases. This parameter may be available if ISCCP C1 data are the source for the GEO ancillary data set. Otherwise, another source must be identified.

The ERBE TSA currently extrapolates total-sky LW as a constant from the first observation back to the beginning of the month and from the last observation forward to the end of the month. The simple solution to the problems caused by this is to always average using only those days that contain at least one measurement.

Currently, the 2.5° regional data will also be nested into 5° and 10° grids as was done with ERBE. The need for these two additional product spatial resolutions should be evaluated. Eliminating these products would reduce the data volume considerably, and the nesting could easily be performed by research analysts using the basic 2.5° data.

3.8. References

Barkstrom, B. R. 1984: The Earth Radiation Budget Experiment (ERBE). *Am. Meteorol. Soc.*, vol. 65, pp. 1170–1185.

Barkstrom, B. R.; and Smith G. L. 1986: The Earth Radiation Budget Experiment—Science and Implementation. *Rev. Geophys.*, vol. 24, pp. 379–390.

Barkstrom, Bruce R.; Harrison, Edwin F.; and Lee, Robert B., III 1990: Earth Radiation Budget Experiment—Preliminary Seasonal Results. *EOS*, vol. 71, p. 279, 299, 304 and 305.

Brooks, D. R.; and Minnis, P. 1984: Simulation of the Earth's Monthly Average Regional Radiation Balance Derived From Satellite Measurements. *J. Climat. & Appl. Meteorol.*, vol. 23, pp. 392–403.

Brooks, D. R.; Harrison, E. F.; Minnis, P.; Suttles, J. T.; and Kandel, R. S. 1986: Development of Algorithms for Understanding the Temporal and Spatial Variability of the Earth's Radiation Balance. *Rev. Geophys.*, vol. 24, pp. 422–438.

Cheruy, F.; Kandel, R. S.; and Duvel, J. P. 1991: Outgoing Longwave Radiation and Its Diurnal Variation From Combined ERBE and Meteosat Observations. I—Estimating OLR From Meteosat Data. II—Using Meteosat Data to Determine the Longwave Diurnal Cycle. *J. Geophys. Res.*, vol. 96, p. 22, 611–622 and 630.

Harrison, Edwin F.; Brooks, David R.; Minnis, Patrick; Wielicki, Bruce A.; and Staylor, W. Frank 1988: First Estimates of the Diurnal Variation of Longwave Radiation From the Multiple-Satellite Earth Radiation Budget Experiment (ERBE). *Bull. Am. Meteorol. Soc.*, vol. 69, pp. 1144–1151.

Harrison, Edwin F.; Minnis, Patrick; and Gibson, Gary G. 1983: Orbital and Cloud Cover Sampling Analyses for Multisatellite Earth Radiation Budget Experiment. *J. Spacecr. & Rockets*, vol. 20, no. 5, pp. 491–495.

Harrison, E. F.; Minnis, P.; Barkstrom, B. R.; Wielicki, B. A.; Gibson, G. G.; Denn, F. M.; and Young, D. F. 1990a: Seasonal Variation of the Diurnal Cycles of Earth's Radiation Budget Determined From ERBE. *Am. Meteorol. Soc.*, pp. 87–91.

Harrison, E. F.; Minnis, P.; Barkstrom, B. R.; Ramanathan, V.; and Cess, R. D. 1990b: Seasonal Variation of Cloud Radiative Forcing Derived From the Earth Radiation Budget Experiment. *J. Geophys. Res.*, vol. 95, pp. 18687–18703.

Hartmann, Dennis L.; Kowalewsky, Karen J.; and Michelsen, Marc L. 1991: Diurnal Variations of Outgoing Longwave Radiation and Albedo From ERBE Scanner Data. *J. Climat.*, vol. 4, pp. 598–617.

Minnis, P.; Harrison, E. F.; Stowe, L. L.; Gibson, G. G.; Denn, F. M.; Doelling, D. R.; and Smith, W. L. 1993: Radiative Climate Forcing by the Mount Pinatubo Eruption. *Science,* vol. 259, no. 5100, pp. 1411–1414.

Ramanathan, V.; Barkstrom, Bruce R.; and Harrison, Edwin F. 1989a: Climate and the Earth's Radiation Budget. *Phys. Today*, vol. 42, pp. 22–32.

Ramanathan, V.; Cess, R. D.; Harrison, E. F.; Minnis, P.; and Barkstrom, B. R. 1989b: Cloud-Radiative Forcing and Climate—Results From the Earth Radiation Budget Experiment. *Science*, vol. 243, pp. 57–63.

Suttles, J. T.; Green, R. N.; Smith, G. L.; Wielicki, B. A.; Walker, I. J.; Taylor, V. R.; and Stowe, L. L. 1989: *Angular Radiation Models for Earth-Atmosphere System. II—Longwave Radiation.* NASA RP-1184.

Suttles, J. T.; Green, R. N.; Minnis, P.; Smith, G. L.; Staylor, W. F.; Wielicki, B. A.; Walker, I. J.; Young, D. F.; Taylor, V. R.; and Stowe, L. L. 1988: *Angular Radiation Models for Earth-Atmosphere System. Volume I: Shortwave Radiation.* NASA RP-1184.

Wielicki, Bruce A.; and Barkstrom, Bruce R. 1991: Clouds and the Earth's Radiant Energy System (CERES)—An Earth Observing System Experiment. *Am. Meteorol. Soc.*, pp. 11–16.

Wielicki, Bruce A.; and Green, Richard N. 1989: Cloud Identification for ERBE Radiative Flux Retrieval. *J. Appl. Meteorol.*, vol. 28, pp. 1133–1146.

Appendix A

Input Data Products

ERBE-Like Averaging to Monthly TOA and Surface Fluxes (Subsystem 3.0)

This appendix describes the data products which are used by the algorithms in this subsystem. Table A-1 below summarizes these products, listing the CERES and EOSDIS product codes or abbreviations, a short product name, the product type, the production frequency, and volume estimates for each individual product as well as a complete data month of production. The product types are defined as follows:

Archival products:	Assumed to be permanently stored by EOSDIS
Internal products:	Temporary storage by EOSDIS (days to years)
Ancillary products:	Non-CERES data needed to interpret measurements

The following pages describe each product. An introductory page provides an overall description of the product and specifies the temporal and spatial coverage. The table which follows the introductory page briefly describes every parameter which is contained in the product. Each product may be thought of as metadata followed by data records. The metadata (or header data) is not well-defined yet and is included mainly as a placeholder. The description of parameters which are present in each data record includes parameter number (a unique number for each distinct parameter), units, dynamic range, the number of elements per record, an estimate of the number of bits required to represent each parameter, and an element number (a unique number for each instance of every parameter). A summary at the bottom of each table shows the current estimated sizes of metadata, each data record, and the total data product. A more detailed description of each data product will be contained in a user's guide to be published before the first CERES launch.

Table A-1. Input Products Summary

Product code		Name	Type	Frequency	Size, MB	Monthly size, MB
CERES	EOSDIS					
EDDB	None	ERBE-like daily database	Internal	1/month	113.5	114

ERBE-Like Daily Database Product (EDDB)

Subsystem 2 includes ERBE-like Inversion and the ERBE-like daily database processor. ERBE-like inversion passes averaged regional data to the daily database processor using the ERBE-like EID-6 file, and the daily database processor updates the 36 latitudinal band files in the EDDB data store. The daily database processor also maintains a housekeeping file with information about the status of the regional data. The housekeeping and regional data are stored in the EDDB for processing by the ERBE-like monthly time and space averaging process. The following table describes the parameters associated with a single 2.5-deg region. Instances of this record are accumulated by the daily processor for the regions that are received in the EID-6 records from ERBE-like inversion. After accumulating a month of data, the regional data for each latitudinal band are sorted by the daily processor and stored in a second set of 36 files for processing by the ERBE-like Monthly Time and Space Averaging Subsystem. The housekeeping file, also described in the following table, is a random access file. The housekeeping random access records store either arrays of integers (32-bit elements), or double precision floating point arrays (64-bit elements). Each parameter of the housekeeping file corresponds to one or more random access records.

Level: 2
Type: Internal
Frequency: 1/month

Time Interval Covered
File: Month
Record: Month

Portion of Globe Covered
File: Regional
Record: Regional

Portion of Atmosphere Covered
File: Surface and TOA

Table A-2. ERBE-Like Daily Database Product (EDDB)

Description	Parameter Number	Units	Range	Elements/ Record	Bits/ Elem	Elem Num
EDDB						
EDDB File Header		N/A				
Regional_Data is Array[36] of:						
Regional_Files is Array[2] of:						
Latitudinal_Bands						
Regional						
Regional_Descriptive						
2.5 degree one-dimensional region number	1	N/A	1..10368	72	32	1
The hour day number index is one of 24 hours for each of 31 days	2	N/A	1..744	72	32	3
Average whole Julian date for one record	3	day	2.4 .. 2.5*1E06	72	32	5
Average fractional Julian date	4	day	0..1	72	32	7
Regional_Average_Estimates						
Estimate of the average shortwave flux at the TOA	5	$W\text{-}m^{-2}$	0..1400	72	32	9
Estimate of the average longwave flux at the TOA	6	$W\text{-}m^{-2}$	0..400	72	32	11
Regional_Estimate_Statistics						
Regional_SW_Stats						
Number of individual shortwave estimates	7	N/A	0..200	72	32	13
Standard deviation of individual shortwave estimates	8	$W\text{-}m^{-2}$	0..999	72	32	15
Minimum value of individual shortwave flux at TOA	9	$W\text{-}m^{-2}$	0..1400	72	32	17
Maximum individual estimate of shortwave flux at TOA	10	$W\text{-}m^{-2}$	0..1400	72	32	19
Regional_LW_Stats						
Number of individual longwave estimates	11	N/A	0..200	72	32	21
Standard deviation of individual longwave estimates	12	$W\text{-}m^{-2}$	0..400	72	32	23
Minimum of individual longwave flux at TOA	13	$W\text{-}m^{-2}$	0..400	72	32	25
Maximum individual longwave flux at TOA	14	$W\text{-}m^{-2}$	0..400	72	32	27
Regional_Regions						
Geographic scene type of this 2.5 degree region	15	N/A	1..5	72	32	29
Regional_Fractional_Components						
Fraction of clear sky areas in this 2.5 degree region	16	N/A	0..1	72	32	31
Fraction of partly cloudy areas in this 2.5 degree region	17	N/A	0..1	72	32	33
Fraction of mostly cloudy areas in this 2.5 degree region	18	N/A	0..1	72	32	35
Fraction of overcast areas in this 2.5 degree region	19	N/A	0..1	72	32	37
Regional_Albedos						
Albedo of clear sky areas in 2.5 degree region	20	N/A	0..1	72	32	39
Albedo of partly cloudy areas in 2.5 degree region	21	N/A	0..1	72	32	41
Albedo of mostly cloudy areas in 2.5 degree region	22	N/A	0..1	72	32	43
Albedo of overcast areas in 2.5 degree region	23	N/A	0..1	72	32	45
Regional_Statistics						
Angular_Averages_Scaled						
Average of individual cosines of solar zenith angle at target point for SW	24	N/A	0..1	72	32	47
Average of individual spacecraft zenith angles from target point	25	deg	0..90	72	32	49
Average of individual relative azimuth at target point	26	deg	0..180	72	32	51
Standard deviation of individual SW albedos for clear sky areas	27	N/A	0..1	72	32	53
Average of individual LW estimates of flux at TOA clear sky	28	$W\text{-}m^{-2}$	0..400	72	32	55
Standard deviation of LW estimates of flux at TOA clear sky	29	$W\text{-}m^{-2}$	0..400	72	32	57
Number of individual longwave estimates for clear sky areas	30	N/A	0..200	72	32	59
Regional_Spares is Array[2] of:						
Spares	31	N/A	N/A	144	32	61

Table A-2. Concluded

Description	Parameter Number	Units	Range	Elements/ Record	Bits/ Elem	Elem Num
Housekeeping						
Records_for_Records_Per_Region is Array[72] of:						
Direct_Access_Records is Array[144] of:						
144 integer array storing the number of records per region.	32	N/A	TBD	10368	32	1
ERBE-like_Product_Key_Record						
Product used for validation of the Housekeeping file.	33	N/A	N/A	1	64	10369
Housekeeping_Ibuf_Array is Array[9] of:						
9 integer array containing file information.	34	N/A	N/A	9	32	10370
Scale_Factors_Record is Array[45] of:						
Scale factors for various data elements.	35	N/A	N/A	45	64	10379
Days_with_Data_Information_Record is Array[34] of:						
Array of integer flags denoting days with inversion processing.	36	N/A	N/A	34	32	10424
File_Sorted_Record is Array[36] of:						
Array of flags indicating sort status of regional data.	37	N/A	N/A	36	32	10458
Julian_Start_Inversion_Header_Record is Array[33] of:						
Start dates and times for each of 31 days, prior and succeeding days.	38	N/A	N/A	33	64	10494
Julian_End_Inversion_Header_Record is Array[33] of:						
End dates and times for 31 days, prior and succeeding days.	39	N/A	N/A	33	64	10560
ERBE-like_Product_key_Record_for_Files is Array[33] of:						
Product keys for 31 days, prior and succeeding days.	40	N/A	N/A	33	64	10593

Total Meta Bits/EDDB Product	**343584**
Total Data Bits/Day	**30720000**
Total Data Bits/Month	**952320000**
Total Bits/EDDB Product	**952663584**

Appendix B

Output Data Products

ERBE-Like Averaging to Monthly TOA and Surface Fluxes (Subsystem 3.0)

This appendix describes the data products which are produced by the algorithms in this subsystem. Table B-1 below summarizes these products, listing the CERES and EOSDIS product codes or abbreviations, a short product name, the product type, the production frequency, and volume estimates for each individual product as well as a complete data month of production. The product types are defined as follows:

Archival products: Assumed to be permanently stored by EOSDIS
Internal products: Temporary storage by EOSDIS (days to years)

The following pages describe each product. An introductory page provides an overall description of the product and specifies the temporal and spatial coverage. The table which follows the introductory page briefly describes every parameter which is contained in the product. Each product may be thought of as metadata followed by data records. The metadata (or header data) is not well-defined yet and is included mainly as a placeholder. The description of parameters which are present in each data record includes parameter number (a unique number for each distinct parameter), units, dynamic range, the number of elements per record, an estimate of the number of bits required to represent each parameter, and an element number (a unique number for each instance of every parameter). A summary at the bottom of each table shows the current estimated sizes for metadata, each data record, and the total data product. A more detailed description of each data product will be contained in a user's guide to be published before the first CERES launch.

Table B-1. Output Products Summary

Product code		Name	Type	Frequency	Size, MB	Monthly size, MB
CERES	EOSDIS					
ES-4	CER03	Geographical averages	archival	1/month	27.6	28
ES-4G	CER03	Gridded averages	archival	1/month	24.5	25
ES-9	CER03	Regional averages	archival	1/month	104.2	104

ERBE-Like Science Product 4 (ES-4)

The ES-4 data is a regional, zonal, and global averages product. The instantaneous scanner estimates at the TOA and surface are arranged temporally to hours, days, and the month, and they are averaged spatially to regions, latitude zones, and the globe. There are seven sets of records constituting a maximum of 13737 records across all sets. Each record set corresponds to a regional, nested regional, zonal, or global average. For example, there are 10368 2.5-degree regions in the scanner field of view for the ERBE-like data. Therefore, there is a maximum of 10368 records in the 2.5 degree regional record set. The second set of records is the 2.5 degree nested to 5.0 degree regional data which constitutes 2592 records. The third set of records is the 5.0 degree nested to 10.0 degree regional data which constitutes 648 records. The fourth, fifth, and sixth sets of records are the 2.5 degree, 5.0 degree, and 10.0 degree zonally averaged data which constitute 72, 36, and 18 records, respectively. The last set is the global data which constitutes 3 records.

Level: 3
Type: Archival
Frequency: 1/month

Time Interval Covered
File: Month
Record: Month

Portion of Globe Covered
File: Regional, zonal, global
Record: Regional, zonal, global

Portion of Atmosphere Covered
File: Surface and TOA

Table B-2. ERBE-Like Science Product 4 (ES-4)

Description	Parameter Number	Units	Range	Elements/ Record	Bits/ Elem	Elem Num
ES-4						
ES-4_Header_Vector is Array[9] of:						
File header vector		N/A	N/A	9	32	
ES-4_Record_Mapping_Matrix is Array[30] of:						
10 X 3 mapping matrix for spatial boundaries		N/A	N/A	30	32	
ES-4_Record_Data_Scaling is Array[1213] of:						
Scale factor vector for repeating data records		N/A	N/A	1213	32	
ES-4ES-4_Nested_Data_Records is Array[13737] of:						
ES-4_Record						
ES-4_Record_Instance						
ES-4_32-bit_Data (TOA)						
Mth_Avg_Day						
Solar Incidence for Monthly Averages by Day	1	W h m^{-2}	0 .. 500000	1	32	1
Monthly net radiant flux by day	2	W-m^{-2}	-200 .. 200	1	32	2
Clear sky net radiant flux, monthly by day	3	W-m^{-2}	-200 .. 200	1	32	3
Clear sky solar incidence, monthly by day	4	W-m^{-2}	0 .. 500000	1	32	4
Mth_Avg_Hr						
Monthly net radiant flux by hour	5	W-m^{-2}	-200 .. 200	1	32	5
Solar incidence, monthly by hour	6	W h m^{-2}	0 .. 500000	1	32	6
Clear sky net radiant flux, monthly by hour	7	W-m^{-2}	-200 .. 200	1	32	7
Clear sky solar incidence, monthly by hour	8	W h m^{-2}	0 .. 500000	1	32	8
SolInc						
Day is Array[31] of:						
Daily solar incidence	9	W h m^{-2}	0 .. 500000	31	32	9
Hr is Array[24] of:						
Hourly solar incidence	10	W h m^{-2}	0 .. 500000	24	32	40
ClrSky is Array[24] of:						
Clear sky solar incidence	11	W h m^{-2}	0 .. 500000	24	32	64
ES-4_16-bit_Data						
ES-4_Descriptive						
Region numbered consecutively from east to west	12	N/A	1 .. 144	1	16	88
Year and month (YYMM) of data processed	13	N/A	N/A	1	16	89
Spacecraft code (TBD)	14	N/A	TBD	1	16	90
Mth_Avg_Day						
TOA						
Flux_and_Albedo						
Longwave flux	15	W-m^{-2}	50 .. 400	1	16	91
Short wave flux	16	W-m^{-2}	0 .. 1200	1	16	92
Monthly mean albedo	17	N/A	0 .. 1	1	16	93
ClrSky_Flux_and_Albedo						
Clear sky longwave flux	18	W-m^{-2}	50 .. 400	1	16	94
Clear sky short wave flux	19	W-m^{-2}	0 .. 1200	1	16	95
Monthly mean clear sky albedo	20	N/A	0 .. 1	1	16	96
Surface_Day						
SW_Flux_Sfc_Day						
Short wave surface flux downwards by day	21	W-m^{-2}	TBD	1	16	97
Short wave surface flux net by day	22	W-m^{-2}	TBD	1	16	98
LW_Flux_Sfc_Day						
Longwave surface flux downward by day	23	W-m^{-2}	50 .. 400	1	16	99
Longwave surface flux net by day	24	W-m^{-2}	50 .. 400	1	16	100
Water vapor data by day	25	cm	TBD	1	16	101

Table B-2. Continued

Description	Parameter Number	Units	Range	Elements/ Record	Bits/ Elem	Elem Num
Mth_Avg_Hr						
TOA						
Flux_and_Albedo						
Longwave flux by the hour	26	$W\text{-}m^{-2}$	50 .. 400	1	16	102
Short wave flux by the hour	27	$W\text{-}m^{-2}$	0 .. 1200	1	16	103
Monthly average albedo by the hour	28	N/A	0 .. 1	1	16	104
ClrSky_Flux_and_Albedo						
Clear sky longwave flux by the hour	29	$W\text{-}m^{-2}$	50 .. 400	1	16	105
Clear sky short wave flux by the hour	30	$W\text{-}m^{-2}$	0 .. 1200	1	16	106
Clear sky Monthly averaged albedo by the hour	31	N/A	0 .. 1	1	16	107
Surface_Hr						
SW_Flux_Sfc_Hr						
Short wave surface flux downward by the hour	32	$W\text{-}m^{-2}$	TBD	1	16	108
Short wave surface flux net by the hour	33	$W\text{-}m^{-2}$	TBD	1	16	109
LW_Flux_Sfc_Hr						
Longwave surface flux downward by the hour	34	$W\text{-}m^{-2}$	50 .. 400	1	16	110
Longwave surface flux net by the hour	35	$W\text{-}m^{-2}$	50 .. 400	1	16	111
Surface water vapor data by the hour	36	cm	TBD	1	16	112
Mth_Avg_Daily						
TOA_Daily						
Flux_and_Albedo_Daily						
LW_Flux_Vector is Array[31] of:						
Longwave flux, daily	37	$W\text{-}m^{-2}$	50 .. 400	31	16	113
SW_Flux_Vector is Array[31] of:						
Short wave flux, daily	38	$W\text{-}m^{-2}$	0 .. 1200	31	16	144
Albedo_Vector is Array[31] of:						
Monthly mean albedo, daily	39	N/A	0 .. 1	31	16	175
ClrSky_Flux_and_Albedo_Daily						
ClrSky_Flux_LW_Vector is Array[31] of:						
Clear sky longwave flux, daily	40	$W\text{-}m^{-2}$	50 .. 400	31	16	206
ClrSky_Flux_SW_Vector is Array[31] of:						
Clear sky short wave flux, daily	41	$W\text{-}m^{-2}$	0 .. 1200	31	16	237
ClrSky_Albedo_Vector is Array[31] of:						
Monthly mean clear sky albedo, daily	42	N/A	0 .. 1	31	16	268
Surface_Daily						
SW_Flux_Sfc_Daily						
SW_Flux_Vector_Daily is Array[31] of:						
Short wave surface flux downwards, daily	43	$W\text{-}m^{-2}$	TBD	31	16	299
SW_Flux_Net_Vector_Daily is Array[31] of:						
Short wave surface flux net, daily	44	$W\text{-}m^{-2}$	TBD	31	16	330
LW_Flux_Sfc_Daily						
LW_Flux_Vector_Daily is Array[31] of:						
Longwave surface flux downward, daily	45	$W\text{-}m^{-2}$	50 .. 400	31	16	361
LW_Flux_Net_Vector_Daily is Array[31] of:						
Longwave surface flux net, daily	46	$W\text{-}m^{-2}$	50 .. 400	31	16	392
H2OV_Vector_Daily is Array[31] of:						
Water vapor data, daily	47	cm	TBD	31	16	423
Mth_Avg_Hourly						
TOA_Hourly						
Flux_and_Albedo_Hourly						
LW_Flux_Vector_Hourly is Array[24] of:						
Longwave flux, hourly	48	$W\text{-}m^{-2}$	50 .. 400	24	16	454
SW_Flux_Vector_Hourly is Array[24] of:						

Table B-2. Continued

Description	Parameter Number	Units	Range	Elements/ Record	Bits/ Elem	Elem Num
Short wave flux, hourly	49	W-m^{-2}	0 .. 1200	24	16	478
Albedo_Vector_Hourly is Array[24] of:						
Monthly average albedo, hourly	50	N/A	0 .. 1	24	16	502
ClrSky_Flux_and_Albedo_Hourly						
ClrSky_Flux_LW_Vector_Hourly is Array[24] of:						
Clear sky longwave flux, hourly	51	W-m^{-2}	50 .. 400	24	16	526
ClrSky_Flux_SW_Vector_Hourly is Array[24] of:						
Clear sky short wave flux, hourly	52	W-m^{-2}	0 .. 1200	24	16	550
ClrSky_Albedo_Vector_Hourly is Array[24] of:						
Clear sky Monthly averaged albedo, hourly	53	N/A	0 .. 1	24	16	574
Surface_Hourly						
SW_Flux_Sfc_Hrly						
SW_Flux_Vector_Hrly is Array[24] of:						
Short wave surface flux downward, hourly	54	W-m^{-2}	TBD	24	16	598
SW_Flux_Net_Vector_Hrly is Array[24] of:						
Short wave surface flux net, hourly	55	W-m^{-2}	TBD	24	16	622
LW_Flux_Sfc_Hrly						
LW_Flux_Vector_Hrly is Array[24] of:						
Longwave surface flux downward, hourly	56	W-m^{-2}	50 .. 400	24	16	646
LW_Flux_Net_Vector_Hrly is Array[24] of:						
Longwave surface flux net, hourly	57	W-m^{-2}	50 .. 400	24	16	670
H2OV_Vector_Hrly is Array[24] of:						
Surface water vapor data, hourly	58	cm	TBD	24	16	694
ES-4_8-bit_Data						
Number_of_Observations						
Daily_Observations						
TOA_Observations						
LW_Vector is Array[31] of:						
Number of observations for LW, daily	59	N/A	TBD	31	8	718
SW_Vector is Array[31] of:						
Number of observations SW, daily	60	N/A	TBD	31	8	749
Surface_Observations						
Surface_LW_Vector is Array[31] of:						
Number of observations for Surface LW, Daily	61	N/A	TBD	31	8	780
Surface_SW_Vector is Array[31] of:						
Number of observations for Surface SW, daily	62	N/A	TBD	31	8	811
Surface_Net_LW_Vector is Array[31] of:						
Number of Observations for surface net LW	63	N/A	TBD	31	8	842
Surface_Net_SW_Vector is Array[31] of:						
Number of observations for surface net SW	64	N/A		31	8	873
Surface_H2OV_Vector is Array[31] of:						
Number of observations for surface water vapor, daily	65	N/A	TBD	31	8	904
ClrSky_Observations						
ClrSky_LW_Observ_Vector is Array[31] of:						
Number of observations for clear sky LW, daily	66	N/A	TBD	31	8	935
ClrSky_SW_Observ_Vector is Array[31] of:						
Number of observations for clear sky SW, daily	67	N/A	TBD	31	8	966
Hourly_Observations						
TOA_Observations_Hourly						
LW_Vector_Hourly is Array[24] of:						
Number of observations for LW, hourly	68	N/A	TBD	24	8	997
SW_Vector_Hourly is Array[24] of:						
Number of observations for SW, hourly	69	N/A	TBD	24	8	1021

Table B-2. Concluded

Description	Parameter Number	Units	Range	Elements/ Record	Bits/ Elem	Elem Num
Surface_Observations_Hourly						
Surface_LW_Vector_Hourly is Array[24] of:						
Number of observations for surface LW, hourly	70	N/A	TBD	24	8	1045
Number of observations for surface net SW, hourly	73	N/A	TBD	24	8	1117
Surface_SW_Vector_Hourly is Array[24] of:						
Number of observations for surface SW, hourly	71	N/A	TBD	24	8	1069
Surface_Net_LW_Vector_Hourly is Array[24] of:						
Number of observations for surface net LW, hourly	72	N/A	TBD	24	8	1093
Surface_Net_SW_Vector_Hourly is Array[24] of:						
Surface_H2OV_Vector_Hourly is Array[24] of:						
Number of observations for surface water vapor, hourly	74	N/A	TBD	24	8	1141
ClrSky_Observations_Hourly						
ClrSky_LW_Observ_Vector_Hourly is Array[24] of:						
Number of observations for clear sky LW, hourly	75	N/A	TBD	24	8	1165
ClrSky_SW_Observ_Vector_Hourly is Array[24] of:						
Number of observations for clear sky SW, hourly	76	N/A	TBD	24	8	1189
Geographical scene type	77	N/A	1 .. 5	1	8	1213

Total Meta Bits/File:	40064
Total Data Bits/Record:	16832
Total Records/File:	13737
Total Data Bits/File:	231221184
Total Bits/File :	231261248

ERBE-Like Science Product 4 Gridded (ES-4G)

The ES-4G data product stores the same time and space averages as the ES-4 science data product, with the difference being the arrangement of the data. While the ES-4 is arranged by region, the ES-4G file presents a gridded data product with all regions for a given data parameter grouped together. The regional presentation of the data is in the same order as that described for the ES-4 product. The 2.5 degree regional parameters are presented as 10368-element vectors, the 2.5 nested to 5.0 degree data is presented as 2592-element vectors, and the 5.0 nested to 10.0 degree data is presented as 648-element vectors. The 2.5, 5.0, and 10.0 degree zonal data is presented as 72, 26, and 18-element vectors, respectively. The global data are presented as 3-element vectors.

Level: 3
Type: Archival
Frequency: 1/month

Time Interval Covered
File: Month
Record: Month

Portion of Globe Covered
File: Global, zonal, regional
Record: Global, zonal, regional

Portion of Atmosphere Covered
File: Surface to TOA

Table B-3. ERBE-Like Science Product 4 Gridded (ES-4G)

Description	Parameter Number	Units	Range	Elements/ Record	Bits/ Elem	Elem Num
ES-4G						
Regional,Zonal_and_Global_Averages						
Multifile_Format						
ES-4G_32-bit_Data						
Monthly_Averages_Day						
MthAvg_Day_Solar_Incidence is Array[10368] of:						
Monthly average solar incidence	1	W-h-m^{-2}	0 .. 500000	10368	32	1
MthAvg_Day_Net is Array[10368] of:						
Monthly net flux	2	W-m^{-2}	-200 .. 200	10368	32	10369
MthAvg_Day_Clear_Sky_Net is Array[10368] of:						
Monthly average clear sky net flux	3	W-m^{-2}	-200 .. 200	10368	32	20737
MthAvg_Day_Clear_Sky_Solar_Incidence is Array[10368] of:						
Monthly average clear sky solar incidence	4	W-h-m^{-2}	0 .. 500000	10368	32	31105
Monthly_Averages_Hour						
MthAvg_Hour_Net is Array[10368] of:						
Monthly average net flux	5	W-m^{-2}	-200 .. 200	10368	32	41473
MthAvg_Hour_Solar_Incidence is Array[10368] of:						
Monthly average solar incidence	6	W-h-m^{-2}	0 .. 500000	10368	32	51841
MthAvg_Hour_Clear_Sky_Net is Array[10368] of:						
Monthly average clear sky net flux	7	W-m^{-2}	-200 .. 200	10368	32	62209
MthAvg_Hour_Clear_Sky_Solar_Incidence is Array[10368] of:						
Monthly average clear sky solar incidence	8	W-h-m^{-2}	0 .. 500000	10368	32	72577
Monthly_Averages_Daily_32 is Array[321408] of:						
Monthly average solar incidence (daily)	9	W-h-m^{-2}	0 .. 500000	321408	32	82945
Monthly_Averages_Hourly						
MthAvg_Hourly_Solar_Incidence is Array[248832] of:						
Monthly average solar incidence (hourly)	10	W-h-m^{-2}	0 .. 500000	248832	32	404353
MthAvg_Hourly_Clear_Sky_Solar_Incidence is Array[248832] of:						
Monthly average clear sky solar incidence (hourly)	11	W-h-m^{-2}	0 .. 500000	248832	32	653185
ES-4G_16-bit_Data						
Monthly_Averages_Day						
MthAvg_Day_LW_Flux is Array[10368] of:						
Monthly average LW flux (day)	12	W-m^{-2}	0 .. 800	10368	16	902017
MthAvg_Day_SW_Flux is Array[10368] of:						
Monthly average SW flux (day)	13	W-m^{-2}	0 .. 400	10368	16	912385
MthAvg_Day_Albedo is Array[10368] of:						
Monthly average albedo (day)	14	N/A	0 .. 1	10368	16	922753
MthAvg_Day_Clear_Sky_LW_Flux is Array[10368] of:						
Monthly average clear sky LW flux (day)	15	W-m^{-2}	0 .. 800	10368	16	933121
MthAvg_Day_Clear_Sky_SW_Flux is Array[10368] of:						
Monthly average clear sky SW flux (day)	16	W-m^{-2}	0 .. 400	10368	16	943489
MthAvg_Day_Clear_Sky_Albedo is Array[10368] of:						
Monthly average clear sky albedo	17	N/A	0 .. 1	10368	16	953857
MthAvg_Day_Surface_Data						
MthAvg_Day_Surface_SW_Flux is Array[10368] of:						
Monthly average day surface SW flux	18	W-m^{-2}	TBD	10368	16	964225
MthAvg_Day_Surface_SW_Net_Flux is Array[10368] of:						
Monthly average day surface SW net flux	19	W-m^{-2}	TBD	10368	16	974593
MthAvg_Day_Surface_LW_Flux is Array[10368] of:						
Monthly average day surface LW flux	20	W-m^{-2}	50 .. 400	10368	16	984961
MthAvg_Day_Surface_LW_Net_Flux is Array[10368] of:						
Monthly average day surface LW net flux	21	W-m^{-2}	50 .. 400	10368	16	995329
MthAvg_Day_Surface_Parameters is Array[10368] of:						
Monthly average day surface water vapor	22	cm	TBD	10368	16	1005697
Monthly_Averages_Hour						

Table B-3. Continued

Description	Parameter Number	Units	Range	Elements/ Record	Bits/ Elem	Elem Num
MthAvg_Hr_LW_Flux is Array[10368] of:						
Monthly average LW flux (hour)	23	W-m^{-2}	0 .. 800	10368	16	1016065
MthAvg_Hr_SW_Flux is Array[10368] of:						
Monthly average SW flux (hour)	24	W-m^{-2}	0 .. 400	10368	16	1026433
MthAvg_Hr_Albedo_ES-4G is Array[10368] of:						
Monthly average albedo (hour)	25	N/A	0 .. 1	10368	16	1036801
MthAvg_Hr_Clear_Sky_LW_Flux is Array[10368] of:						
Monthly average clear sky LW flux (hour)	26	W-m^{-2}	0 .. 800	10368	16	1047169
MthAvg_Hr_Clear_Sky_SW_Flux is Array[10368] of:						
Monthly average clear sky SW flux (hour)	27	W-m^{-2}	0 .. 400	10368	16	1057537
MthAvg_Hr_Clear_Sky_Albedo is Array[10368] of:						
Monthly average clear sky albedo (hour)	28	W-m^{-2}	0 .. 1	10368	16	1067905
MthAvg_Hour_Surface_Data						
MthAvg_Hour_Surface_SW_Flux is Array[10368] of:						
Monthly average hour surface SW flux	29	W-m^{-2}	TBD	10368	16	1078273
MthAvg_Hour_Surface_SW_Net_Flux is Array[10368] of:						
Monthly average hour surface SW net flux	30	W-m^{-2}	TBD	10368	16	1088641
MthAvg_Hour_Surface_LW_Flux is Array[10368] of:						
Monthly average hour surface LW flux	31	W-m^{-2}	50 .. 400	10368	16	1099009
MthAvg_Hour_Surface_LW_Net_Flux is Array[10368] of:						
Monthly average hour surface LW net flux	32	W-m^{-2}	50 .. 400	10368	16	1109377
MthAvg_Hour_Surface_Parameters is Array[10368] of:						
Monthly average hour surface water vapor	33	cm	TBD	10368	16	1119745
Monthly_Averages_Daily						
MthAvg_Dly_LW_Flux is Array[321408] of:						
Monthly average LW flux (daily)	34	W-m^{-2}	0 .. 800	321408	16	1130113
MthAvg_Dly_SW_Flux is Array[321408] of:						
Monthly average SW flux (daily)	35	W-m^{-2}	0 .. 400	321408	16	1451521
MthAvg_Dly_Albedo_ES-4G is Array[321408] of:						
Monthly average albedo (daily)	36	N/A	0 .. 1	321408	16	1772929
MthAvg_Dly_Clear_Sky_LW_Flux is Array[321408] of:						
Monthly average clear sky LW flux (daily)	37	W-m^{-2}	0 .. 800	321408	16	2094337
MthAvg_Dly_Clear_Sky_SW_Flux is Array[321408] of:						
Monthly average clear sky SW flux (daily)	38	W-m^{-2}	0 .. 400	321408	16	2415745
MthAvg_Dly_Clear_Sky_Albedo is Array[321408] of:						
Monthly average clear sky albedo (daily)	39	N/A	0 .. 1	321408	16	2737153
MthAvg_Daily_Surface_Data						
MthAvg_Daily_Surface_SW_Flux is Array[321408] of:						
Monthly average daily surface SW flux	40	W-m^{-2}	TBD	321408	16	3058561
MthAvg_Daily_Surface_SW_Net_Flux is Array[321408] of:						
Monthly average daily surface SW net flux	41	W-m^{-2}	TBD	321408	16	3379969
MthAvg_Daily_Surface_LW_Flux is Array[321408] of:						
Monthly average daily surface LW flux	42	W-m^{-2}	50 .. 400	321408	16	3701377
MthAvg_Daily_Surface_LW_Net_Flux is Array[321408] of:						
Monthly average daily surface LW net flux	43	W-m^{-2}	50 .. 400	321408	16	4022785
MthAvg_Daily_Surface_Parameters is Array[321408] of:						
Monthly average daily surface water vapor	44	cm	TBD	321408	16	4344193
Monthly_Averages_Hourly						
MthAvg_Hrly_LW_Flux is Array[248832] of:						
Monthly average LW flux (hourly)	45	W-m^{-2}	0 .. 800	248832	16	4665601
MthAvg_Hrly_SW_Flux is Array[248832] of:						
Monthly average SW flux (hourly)	46	W-m^{-2}	0 .. 400	248832	16	4914433
MthAvg_Hrly_Albedo_ES-4G is Array[248832] of:						

Table B-3. Continued

Description	Parameter Number	Units	Range	Elements/ Record	Bits/ Elem	Elem Num
Monthly average albedo (hourly)	47	N/A	0 .. 1	248832	16	5163265
MthAvg_Hrly_Clear_Sky_LW_Flux is Array[248832] of:						
Monthly average clear sky LW flux (hourly)	48	$W\text{-}m^{-2}$	0 .. 800	248832	16	5412097
MthAvg_Hrly_Clear_Sky_SW_Flux is Array[248832] of:						
Monthly average clear sky SW flux (hourly)	49	$W\text{-}m^{-2}$	0 .. 400	248832	16	5660929
MthAvg_Hrly_Clear_Sky_Albedo is Array[248832] of:						
Monthly average clear sky albedo (hourly)	50	N/A	0 .. 1	248832	16	5909761
MthAvg_Hourly_Surface_Data						
MthAvg_Hourly_Surface_SW_Flux is Array[248832] of:						
Monthly average hourly surface SW flux	51	$W\text{-}m^{-2}$	TBD	248832	16	6158593
MthAvg_Hourly_Surface_SW_Net_Flux is Array[248832] of:						
Monthly average hourly surface SW net flux	52	$W\text{-}m^{-2}$	TBD	248832	16	6407425
MthAvg_Hourly_Surface_LW_Flux is Array[248832] of:						
Monthly average hourly surface LW flux	53	$W\text{-}m^{-2}$	50 .. 400	248832	16	6656257
MthAvg_Hourly_Surface_LW_Net_Flux is Array[248832] of:						
Monthly average hourly surface LW net flux	54	$W\text{-}m^{-2}$	50 .. 400	248832	16	6905089
MthAvg_Hourly_Surface_Parameters is Array[248832] of:						
Monthly average hourly surface water vapor	55	cm	TBD	248832	16	7153921
ES-4G_8-bit_Data						
Number_of_Observations_Daily						
Number_of_Observations_LW_Flux is Array[321408] of:						
Number of observations LW flux (daily)	56	N/A	TBD	321408	8	7402753
Number_of_Observations_SW_Flux is Array[321408] of:						
Number of observations SW flux (daily)	57	N/A	TBD	321408	8	7724161
Number_of_Observations_Clear_Sky_LW_Flux is Array[321408] of:						
Number of observations clear sky LW flux	58	N/A	TBD	321408	8	8045569
Number_of_Observations_Clear_Sky_SW_Flux is Array[321408] of:						
Number of observations clear sky SW flux (daily)	59	N/A	TBD	321408	8	8366977
Number_of_Observations_Daily_Surface_Data						
Obsrv_Daily_Surface_SW_Flux is Array[321408] of:						
Number observations daily surface SW flux	60	N/A	N/A	321408	8	8688385
Obsrv_Daily_Surface_SW_Net_Flux is Array[321408] of:						
Number observations daily surface SW net flux	61	N/A	TBD	321408	8	9009793
Obsrv_Daily_Surface_LW_Flux is Array[321408] of:						
Number observations daily surface LW flux	62	N/A	TBD	321408	8	9331201
Obsrv_Daily_Surface_LW_Net_Flux is Array[321408] of:						
Number observations daily surface LW net flux	63	N/A	TBD	321408	8	9652609
Number_of_Observations_Daily_Surface_Parameters is Array[321408] of:						
Number observations daily surface water vapor	64	N/A	TBD	321408	8	9974017
Number_of_Observations_Hourly						
Number_of_Observations_Hrly_LW_Flux is Array[248832] of:						
Number of observations LW flux (hourly)	65	N/A	TBD	248832	8	10295425
Number_of_Observations_Hrly_SW_Flux is Array[248832] of:						
Number of observations SW flux (hourly)	66	N/A	TBD	248832	8	10544257
Number_of_Observations_Hrly_ClrSky_LW_Flux is Array[248832] of:						
Number of observations clear sky LW flux (hourly)	67	N/A	TBD	248832	8	10793089
Number_of_Observations_Hrly_ClrSky_SW_Flux is Array[248832] of:						
Number of observations clear sky SW flux (hourly)	68	N/A	TBD	248832	8	11041921
Number_of_Observations_Hourly_Surface_Data						
Obsrv_Hourly_Surface_SW_Flux is Array[248832] of:						
Number observations hourly surface SW flux	69	N/A	TBD	248832	8	11290753
Obsrv_Hourly_Surface_SW_Net_Flux is Array[248832] of:						
Number observations hourly surface SW net flux	70	N/A	TBD	248832	8	11539585

Table B-3. Concluded

Description	Parameter Number	Units	Range	Elements/ Record	Bits/ Elem	Elem Num
Obsrv_Hourly_Surface_LW_Flux is Array[248832] of:						
Number observations hourly surface LW flux	71	N/A	TBD	248832	8	11788417
Obsrv_Hourly_Surface_LW_Net_Flux is Array[248832] of:						
Number observations hourly surface LW net flux	72	N/A	TBD	248832	8	12037249
Number_of_Observations_Hourly_Surface_Parameters is Array[248832] of:						
Number observations hourly surface water vapor	73	N/A	TBD	248832	8	12286081
Geotype_Instances is Array[10368] of:						
Geotype - surface type for current region	74	N/A	0 .. 5	10368	8	12534913
Total Meta Bits/File:	0					
Total Data Bits/Record:	174016512					
Total Records/File:	7					
Total Data Bits/File:	1218115584					
Total Bits/File :	1218115584					

ERBE-Like Science Product 9 (ES-9)

The ES-9 stores data for each 2.5 degree region observed during a month. There are 10368 possible regions and a given region is viewed by the scanner several times as the spacecraft passes overhead. For each region, data is stored by the hour for each hour of each day in the month. Stored data includes the mean estimates of shortwave and longwave radiant flux at the top of the atmosphere, the standard deviations of these estimates, the maximum and minimum estimate, and scene information or cloud condition. Similar parameters are determined for those scanner measurements that were identified as viewing clear sky areas. New with the CERES instrument are the surface downward shortwave flux, the surface downward longwave flux, the net shortwave and longwave flux at the surface, and water vapor data. Daily, monthly hourly, and monthly averages are also stored.

Level: 3
Type: Archival
Frequency: 1/month

Time Interval Covered
File: 1 month
Record: Hour box data

Portion of Globe Covered
File: Global
Record: Regional

Portion of Atmosphere Covered
File: Surface to TOA

Table B-4. ERBE-Like Science Product 9 (ES-9)

Description	Parameter Number	Units	Range	Elements/ Record	Bits/ Elem	Elem Num
ES-9						
ES-9_File_Header is Array[9] of:						
File header is currently a 9-word vector used for validation		N/A		9	32	
ES-9_Record_Level_Data_Scaling is Array[66] of:						
A scale factor vector with scale factors to be applied to the record data		N/A		66	32	
ES-9_Data_Records is Array[10368] of:						
Region number for the current data record	1	N/A	1..10368	1	16	1
Geographic scene for this region	2	N/A	1 .. 5	1	16	2
Scene_Fraction_Data is Array[4] of:						
Scene fraction histogram	3	N/A		4	16	3
Monthly_Averages_Day						
SW flux	4	$W\text{-}m^{-2}$	0 .. 1200	1	16	7
SW flux minimum value	5	$W\text{-}m^{-2}$	0 .. 1200	1	16	8
SW flux maximum value	6	$W\text{-}m^{-2}$	0 .. 1200	1	16	9
SW flux standard deviation	7	$W\text{-}m^{-2}$	TBD	1	16	10
SW flux number of days with at least one sample	8	day	TBD	1	16	11
LW flux	9	$W\text{-}m^{-2}$	50 .. 400	1	16	12
LW flux minimum value	10	$W\text{-}m^{-2}$	50 .. 400	1	16	13
LW flux maximum value	11	$W\text{-}m^{-2}$	50 .. 400	1	16	14
LW flux standard deviation	12	$W\text{-}m^{-2}$	TBD	1	16	15
LW flux number of days with at least 1 sample	13	day	TBD	1	16	16
Mean albedo	14	N/A	0 .. 1	1	16	17
Mean net flux	15	$W\text{-}m^{-2}$	TBD	1	16	18
MthAvg_Day_Solar_Incidence is Array[2] of:						
Monthly total integrated solar incidence	16	N/A	TBD	2	16	19
Clear sky SW flux	17	$W\text{-}m^{-2}$	0 .. 1200	1	16	21
Clear sky SW flux minimum value	18	$W\text{-}m^{-2}$	0 .. 1200	1	16	22
Clear sky SW flux maximum value	19	$W\text{-}m^{-2}$	0 .. 1200	1	16	23
Clear sky SW flux standard deviation	20	$W\text{-}m^{-2}$	TBD	1	16	24
Clear sky SW flux number of days with at least 1 sample	21	day	TBD	1	16	25
Clear sky LW flux average flux	22	$W\text{-}m^{-2}$	50 .. 400	1	16	26
Clear sky LW flux minimum value	23	$W\text{-}m^{-2}$	50 .. 400	1	16	27
Clear sky LW flux maximum value	24	$W\text{-}m^{-2}$	50 .. 400	1	16	28
Clear sky LW flux standard deviation	25	$W\text{-}m^{-2}$	TBD	1	16	29
Clear sky LW flux number of days with at least 1 sample	26	day	TBD	1	16	30
Clear sky albedo	27	N/A	0 .. 1	1	16	31
Clear sky net radiant flux	28	$W\text{-}m^{-2}$	TBD	1	16	32
MthAvg_Day_ClrSky_Solar_Incidence is Array[2] of:						
Clear sky solar incidence	29	N/A	TBD	2	16	33
Surface SW downward flux	30	$W\text{-}m^{-2}$	0 .. 1200	1	16	35
Surface SW downward flux minimum value	31	$W\text{-}m^{-2}$	0 .. 1200	1	16	36
Surface SW downward flux maximum value	32	$W\text{-}m^{-2}$	0 .. 1200	1	16	37
Surface SW downward flux standard deviation	33	$W\text{-}m^{-2}$	TBD	1	16	38
Surface SW downward flux number of days with at least 1 sample	34	day	TBD	1	16	39
Surface SW net flux	35	$W\text{-}m^{-2}$	0 .. 1200	1	16	40
Surface SW net flux minimum value	36	$W\text{-}m^{-2}$	0 .. 1200	1	16	41
Surface SW net maximun value	37	$W\text{-}m^{-2}$	0 .. 1200	1	16	42
Surface SW net standard deviation	38	$W\text{-}m^{-2}$	TBD	1	16	43
Surface SW net number of days with at least 1 sample	39	day	TBD	1	16	44
Surface LW downward flux	40	$W\text{-}m^{-2}$	50 .. 400	1	16	45
Surface LW downward flux minimum value	41	$W\text{-}m^{-2}$	50 .. 400	1	16	46

Table B-4. Continued

Description	Parameter Number	Units	Range	Elements/ Record	Bits/ Elem	Elem Num
Surface LW downward flux maximum value	42	$W-m^{-2}$	50 .. 400	1	16	47
Surface LW downward flux standard deviation	43	$W-m^{-2}$	TBD	1	16	48
Surface LW downward flux number of days with at least 1 sample	44	day	TBD	1	16	49
Surface LW net flux	45	$W-m^{-2}$	50 .. 400	1	16	50
Surface LW net flux minimum value	46	$W-m^{-2}$	50 .. 400	1	16	51
Surface LW net flux maximum value	47	$W-m^{-2}$	50 .. 400	1	16	52
Surface LW net flux standard deviation	48	$W-m^{-2}$	TBD	1	16	53
Surface LW net flux number of days with a least 1 sample	49	day	TBD	1	16	54
Water vapor data (monthly average - day)	50	cm	TBD	1	16	55
Water vapor data minimum value	51	cm	TBD	1	16	56
Water vapor data maximum value	52	cm	TBD	1	16	57
Water vapor data standard deviation	53	cm	TBD	1	16	58
Water vapor data number of days with a least 1 sample	54	day	TBD	1	16	59
Monthly_Averages_Hour						
SW flux	55	$W-m^{-2}$	0 .. 1200	1	16	60
SW flux minimum value	56	$W-m^{-2}$	0 .. 1200	1	16	61
SW flux maximum value	57	$W-m^{-2}$	0 .. 1200	1	16	62
SW flux standard deviation	58	$W-m^{-2}$	TBD	1	16	63
SW flux number of days with at least 1 sample	59	day	TBD	1	16	64
LW flux	60	$W-m^{-2}$	50 .. 400	1	16	65
LW flux minimum value	61	$W-m^{-2}$	50 .. 400	1	16	66
LW flux maximum value	62	$W-m^{-2}$	50 .. 400	1	16	67
LW flux standard deviation	63	$W-m^{-2}$	TBD	1	16	68
LW flux number of days with at least 1 sample	64	day	TBD	1	16	69
Albedo	65	N/A	0 .. 1	1	16	70
Net flux	66	$W-m^{-2}$	TBD	1	16	71
MthAvg_Hr_Solar_Incidence is Array[2] of:						
Solar incidence	67	N/A	TBD	2	16	72
Clear sky SW flux	68	$W-m^{-2}$	0 .. 1200	1	16	74
Clear sky SW flux minimum value	69	$W-m^{-2}$	0 .. 1200	1	16	75
Clear sky SW flux maximum value	70	$W-m^{-2}$	0 .. 1200	1	16	76
Clear sky SW flux standard deviation	71	$W-m^{-2}$	TBD	1	16	77
Clear sky SW flux number of days with at least 1 sample	72	day	TBD	1	16	78
Clear sky LW flux	73	$W-m^{-2}$	50 .. 400	1	16	79
Clear sky LW flux minimum value	74	$W-m^{-2}$	50 .. 400	1	16	80
Clear sky LW flux maximum value	75	$W-m^{-2}$	50 .. 400	1	16	81
Clear sky LW flux standard deviation	76	$W-m^{-2}$	TBD	1	16	82
Clear sky LW flux number of days with at least 1 sample	77	day	TBD	1	16	83
Clear sky albedo	78	N/A	0 .. 1	1	16	84
Clear sky net flux	79	$W-m^{-2}$	TBD	1	16	85
MthAvg_Hr_ClrSky_Solar_Incidence is Array[2] of:						
Clear sky solar incidence	80	N/A	TBD	2	16	86
Surface SW downward flux	81	$W-m^{-2}$	0 .. 1200	1	16	88
Surface SW downward flux minimum value	82	$W-m^{-2}$	0 .. 1200	1	16	89
Surface SW downward flux maximum value	83	$W-m^{-2}$	0 .. 1200	1	16	90
Surface SW downward flux standard deviation	84	$W-m^{-2}$	TBD	1	16	91
Surface SW downward flux number of days with at least 1 sample	85	day	TBD	1	16	92
Surface SW net flux	86	$W-m^{-2}$	0 .. 1200	1	16	93
Surface SW net flux minimum value	87	$W-m^{-2}$	0 .. 1200	1	16	94
Surface SW net flux maximum value	88	$W-m^{-2}$	0 .. 1200	1	16	95
Surface SW net flux standard deviation	89	$W-m^{-2}$	TBD	1	16	96
Surface SW net flux no days with at least 1 sample	90	day	TBD	1	16	97
Surface LW downward flux	91	$W-m^{-2}$	50 .. 400	1	16	98

Table B-4. Continued

Description	Parameter Number	Units	Range	Elements/ Record	Bits/ Elem	Elem Num
Surface LW downward flux minimum value	92	W-m^{-2}	50 .. 400	1	16	99
Surface LW downward flux maximum value	93	W-m^{-2}	50 .. 400	1	16	100
Surface LW downward flux standard deviation	94	W-m^{-2}	TBD	1	16	101
Surface LW downward flux no days with at least 1 sample	95	day	TBD	1	16	102
Surface LW net flux	96	W-m^{-2}	50 .. 400	1	16	103
Surface LW net flux minimum value	97	W-m^{-2}	50 .. 400	1	16	104
Surface LW net flux maximum value	98	W-m^{-2}	50 .. 400	1	16	105
Surface LW net flux standard deviation	99	W-m^{-2}	TBD	1	16	106
Surface LW net flux no days with at least 1 sample	100	day	TBD	1	16	107
Surface water vapor data	101	cm	TBD	1	16	108
Surface water vapor data minimum value	102	cm	TBD	1	16	109
Surface water vapor data maximum value	103	cm	TBD	1	16	110
Surface water vapor data standard deviation	104	cm	TBD	1	16	111
Surface water vapor data number of days with at least 1 sample	105	day	TBD	1	16	112
Monthly_Averages_Daily is Array[31] of:						
Solar constant, distance corrected	106	W-m^{-2}	1364 .. 1400	31	16	113
SW flux	107	W-m^{-2}	0 .. 1200	31	16	144
SW flux minimum value	108	W-m^{-2}	0 .. 1200	31	16	175
SW flux maximum value	109	W-m^{-2}	0 .. 1200	31	16	206
SW flux standard deviation	110	W-m^{-2}	TBD	31	16	237
SW flux number of days with at least 1 sample	111	day	TBD	31	16	268
LW flux	112	W-m^{-2}	50 .. 400	31	16	299
LW flux minimum value	113	W-m^{-2}	50 .. 400	31	16	330
LW flux maximum value	114	W-m^{-2}	50 .. 400	31	16	361
LW flux standard deviation	115	W-m^{-2}	TBD	31	16	392
LW flux number of days with at least 1 sample	116	day	TBD	31	16	423
Albedo	117	N/A	0 .. 1	31	16	454
MthAvg_Dly_Solar_Incidence is Array[2] of:						
Solar incidence	118	N/A	TBD	62	16	485
Clear sky SW flux	119	W-m^{-2}	0 .. 1200	31	16	487
Clear sky SW flux minimum value	120	W-m^{-2}	0 .. 1200	31	16	518
Clear sky SW flux maximum value	121	W-m^{-2}	0 .. 1200	31	16	549
Clear sky SW flux standard deviation	122	W-m^{-2}	TBD	31	16	580
Clear sky SW flux number of days with at least 1 sample	123	day	TBD	31	16	611
Clear sky LW flux	124	W-m^{-2}	50 .. 400	31	16	642
Clear sky LW flux minimum value	125	W-m^{-2}	50 .. 400	31	16	673
Clear sky LW flux maximum value	126	W-m^{-2}	50 .. 400	31	16	704
Clear sky LW flux standard deviation	127	W-m^{-2}	TBD	31	16	735
Clear sky LW flux number of days with at least 1 sample	128	day	TBD	31	16	766
Clear sky albedo	129	N/A	0 .. 1	31	16	797
Surface SW downward flux	130	W-m^{-2}	0 .. 1200	31	16	828
Surface SW downward flux minimum value	131	W-m^{-2}	0 .. 1200	31	16	859
Surface SW downward flux maximum value	132	W-m^{-2}	0 .. 1200	31	16	890
Surface SW downward flux standard deviation	133	W-m^{-2}	TBD	31	16	921
Surface SW downward flux number of days with at least 1 sample	134	day	TBD	31	16	952
Surface SW net flux	135	W-m^{-2}	0 .. 1200	31	16	983
Surface SW net flux minimum value	136	W-m^{-2}	0 .. 1200	31	16	1014
Surface SW net flux maximum value	137	W-m^{-2}	0 .. 1200	31	16	1045
Surface SW net flux standard deviation	138	W-m^{-2}	TBD	31	16	1076
Surface SW net flux number of days with at least 1 sample	139	day	TBD	31	16	1107
Surface LW downward flux	140	W-m^{-2}	50 .. 400	31	16	1138
Surface LW downward flux minimum value	141	W-m^{-2}	50 .. 400	31	16	1169
Surface LW downward flux maximum value	142	W-m^{-2}	50 .. 400	31	16	1200

Table B-4. Continued

Description	Parameter Number	Units	Range	Elements/ Record	Bits/ Elem	Elem Num
Surface LW downward flux standard deviation	143	$W-m^{-2}$	TBD	31	16	1231
Surface LW downward flux number of days with at least 1 sample	144	day	TBD	31	16	1262
Surface LW net radiant flux	145	$W-m^{-2}$	50 .. 400	31	16	1293
Surface LW net radiant flux minimum value	146	$W-m^{-2}$	50 .. 400	31	16	1324
Surface LW net radiant flux maximum value	147	$W-m^{-2}$	50 .. 400	31	16	1355
Surface LW net radiant flux standard deviation	148	$W-m^{-2}$	TBD	31	16	1386
Surface LW net radiant flux number of days with at least 1 sample	149	day	TBD	31	16	1417
Surface water vapor data	150	cm	TBD	31	16	1448
Surface water vapor data minimum value	151	cm	TBD	31	16	1479
Surface water vapor data maximum value	152	cm	TBD	31	16	1510
Surface water vapor data standard deviation	153	cm	TBD	31	16	1541
Surface water vapor number of days with at least 1 sample	154	day	TBD	31	16	1572
Monthly_Averages_Hourly is Array[24] of:						
SW flux	155	$W-m^{-2}$	0 .. 1200	24	16	1603
SW flux minimum value	156	$W-m^{-2}$	0 .. 1200	24	16	1627
SW flux maximum value	157	$W-m^{-2}$	0 .. 1200	24	16	1651
SW flux standard deviation	158	$W-m^{-2}$	TBD	24	16	1675
SW flux number of days with at least 1 sample	159	day	TBD	24	16	1699
MthAvg_Hrly_SW_Stats_Sum is Array[2] of:						
SW sum of estimates	160	N/A	TBD	48	16	1723
MthAvg_Hrly_SW_Stats_Sum_Squared is Array[2] of:						
SW sum of estimates squared	161	N/A	TBD	48	16	1725
LW flux	162	$W-m^{-2}$	50 .. 400	24	16	1727
LW flux minimum value	163	$W-m^{-2}$	50 .. 400	24	16	1751
LW flux maximum value	164	$W-m^{-2}$	50 .. 400	24	16	1775
LW flux standard deviation	165	$W-m^{-2}$	TBD	24	16	1799
LW flux number of days with at least 1 sample	166	day	TBD	24	16	1823
MthAvg_Hrly_LW_Stats_Sum is Array[2] of:						
LW flux sum of estimates	167	N/A	TBD	48	16	1847
MthAvg_Hrly_LW_Stats_Sum_Squared is Array[2] of:						
LW sum of estimates squared	168	N/A	TBD	48	16	1849
Albedo	169	N/A	0 .. 1	24	16	1851
MthAvg_Hrly_Solar_Incidence is Array[2] of:						
Solar incidence	170	N/A	TBD	48	16	1875
Clear sky SW flux	171	$W-m^{-2}$	0 .. 1200	24	16	1877
Clear sky SW flux minimum value	172	$W-m^{-2}$	0 .. 1200	24	16	1901
Clear sky SW flux maximum value	173	$W-m^{-2}$	0 .. 1200	24	16	1925
Clear sky SW flux standard deviation	174	$W-m^{-2}$	TBD	24	16	1949
Clear sky SW flux number of days with at least 1 sample	175	day	TBD	24	16	1973
MthAvg_Hrly_ClrSky_SW_Stats_Sum is Array[2] of:						
Clear sky SW sum of estimates	176	N/A	TBD	48	16	1997
MthAvg_Hrly_ClrSky_SW_Stats_Sum_Squared is Array[2] of:						
Clear sky SW sum of estimates squared	177	N/A	TBD	48	16	1999
Clear sky LW flux	178	$W-m^{-2}$	50 .. 400	24	16	2001
Clear sky LW flux minimum value	179	$W-m^{-2}$	50 .. 400	24	16	2025
Clear sky LW flux maximum value	180	$W-m^{-2}$	50 .. 400	24	16	2049
Clear sky LW flux standard deviation	181	$W-m^{-2}$	TBD	24	16	2073
Clear sky LW flux number of days with at least 1 sample	182	day	TBD	24	16	2097
MthAvg_Hrly_ClrSky_LW_Sum is Array[2] of:						
Clear sky LW sum of estimates	183	N/A	TBD	48	16	2121
MthAvg_Hrly_ClrSky_LW_Sum_Squared is Array[2] of:						
Clear sky LW sum of estimates squared	184	N/A	TBD	48	16	2123
Clear sky albedo	185	N/A	0 .. 1	24	16	2125

Table B-4. Continued

Description	Parameter Number	Units	Range	Elements/ Record	Bits/ Elem	Elem Num
MthAvg_Hrly_ClrSky_Solar_Incidence is Array[2] of:						
Clear sky solar incidence	186	N/A	TBD	48	16	2149
Surface SW downward flux	187	$W\text{-}m^{-2}$	0 .. 1200	24	16	2151
Surface SW downward flux minimum value	188	$W\text{-}m^{-2}$	0 .. 1200	24	16	2175
Surface SW downward flux maximum value	189	$W\text{-}m^{-2}$	0 .. 1200	24	16	2199
Surface SW downward flux standard deviation	190	$W\text{-}m^{-2}$	TBD	24	16	2223
Surface SW downward flux number of days with at least 1 sample	191	day	TBD	24	16	2247
Surface SW net flux	192	$W\text{-}m^{-2}$	0 .. 1200	24	16	2271
Surface SW net flux minimum value	193	$W\text{-}m^{-2}$	0 .. 1200	24	16	2295
Surface SW net flux maximum value	194	$W\text{-}m^{-2}$	0 .. 1200	24	16	2319
Surface SW net flux standard deviation	195	$W\text{-}m^{-2}$	TBD	24	16	2343
Surface SW net flux no days with at least 1 sample	196	day	TBD	24	16	2367
Surface LW downward flux	197	$W\text{-}m^{-2}$	50 .. 400	24	16	2391
Surface LW downward flux minimum value	198	$W\text{-}m^{-2}$	50 .. 400	24	16	2415
Surface LW downward flux maximum value	199	$W\text{-}m^{-2}$	50 .. 400	24	16	2439
Surface LW downward flux standard deviation	200	$W\text{-}m^{-2}$	TBD	24	16	2463
Surface LW downward flux number of days with at least 1 sample	201	day	TBD	24	16	2487
Surface LW net flux	202	$W\text{-}m^{-2}$	50 .. 400	24	16	2511
Surface LW net flux minimum value	203	$W\text{-}m^{-2}$	50 .. 400	24	16	2535
Surface LW net flux maximum value	204	$W\text{-}m^{-2}$	50 .. 400	24	16	2559
Surface LW net flux standard deviation	205	$W\text{-}m^{-2}$	TBD	24	16	2583
Surface LW net flux no days with at least 1 sample	206	day	TBD	24	16	2607
Surface water vapor data	207	cm	TBD	24	16	2631
Surface water vapor data minimum value	208	cm	TBD	24	16	2655
Surface water vapor data maximum value	209	cm	TBD	24	16	2679
Surface water vapor data standard deviation	210	cm	TBD	24	16	2703
Surface water vapor data no days with at least 1 sample	211	day	TBD	24	16	2727
Number of hour boxes	212	Hour boxes	1 .. 744	24	16	2751
MthAvg_Hrly_Spare_values is Array[14] of:						
Spares	213	N/A	N/A	336	16	2775
Hourly_Per_Day is Array[744] of:						
Hour box number	214	N/A	1 .. 744	744	16	2789
Hrly_Per_Day_Date is Array[2] of:						
Whole part of Julian date	215	day	2449353..2458500	1488	16	3533
Fractional part of Julian day	216	day	0 .. 1	744	16	3535
Hrly_Per_Day_Scene_Fraction is Array[4] of:						
Scene fraction	217	N/A	TBD	2976	16	4279
Hrly_Per_Day_Albedo is Array[4] of:						
Albedo vector	218	N/A	0 .. 1	2976	16	4283
Cosine of the solar zenith angle	219	N/A	0 .. 1	744	16	4287
Satellite zenith angle	220	deg	0 .. 90	744	16	5031
Azimuth angle	221	deg	0 .. 360	744	16	5775
Solar incidence	222	N/A	TBD	744	16	6519
SW flux	223	$W\text{-}m^{-2}$	0 .. 1200	744	16	7263
SW flux minimum value	224	$W\text{-}m^{-2}$	0 .. 1200	744	16	8007
SW flux maximum value	225	$W\text{-}m^{-2}$	0 .. 1200	744	16	8751
SW flux standard deviation	226	$W\text{-}m^{-2}$	TBD	744	16	9495
SW flux number of days with at least 1 sample	227	day	TBD	744	16	10239
LW flux	228	$W\text{-}m^{-2}$	50 .. 400	744	16	10983
LW flux minimum value	229	$W\text{-}m^{-2}$	50 .. 400	744	16	11727
LW flux maximum value	230	$W\text{-}m^{-2}$	50 .. 400	744	16	12471
LW flux standard deviation	231	$W\text{-}m^{-2}$	TBD	744	16	13215
LW flux number of days with at least 1 sample	232	day	TBD	744	16	13959

Table B-4. Concluded

Description	Parameter Number	Units	Range	Elements/ Record	Bits/ Elem	Elem Num
SW flux maximum difference	233	$W\text{-}m^{-2}$	TBD	744	16	14703
LW flux maximum difference	234	$W\text{-}m^{-2}$	TBD	744	16	15447
Clear sky albedo	235	N/A	0 .. 1	744	16	16191
Clear sky LW flux	236	$W\text{-}m^{-2}$	50 .. 400	744	16	16935
Clear sky LW flux standard deviation	237	$W\text{-}m^{-2}$	TBD	744	16	17679
Clear sky LW flux number samples	238	N/A	TBD	744	16	18423
Surface SW downward flux	239	$W\text{-}m^{-2}$	0 .. 1200	744	16	19167
Surface SW net flux	240	$W\text{-}m^{-2}$	0 .. 1200	744	16	19911
Surface LW flux	241	$W\text{-}m^{-2}$	50 .. 400	744	16	20655
Surface LW net flux	242	$W\text{-}m^{-2}$	50 .. 400	744	16	21399
Water vapor data	243	cm	TBD	744	16	22143

Total Meta Bits/File:	2400
Total Data Bits/Record:	498528
Total Records/File:	10368
Total Data Bits/File:	873771008
Total Bits/File :	873773408

REPORT DOCUMENTATION PAGE

Form Approved
OMB No. 0704-0188

1. AGENCY USE ONLY *(Leave blank)*	2. REPORT DATE	3. REPORT TYPE AND DATES COVERED
	December 1995	Reference Publication

4. TITLE AND SUBTITLE
Clouds and the Earth's Radiant Energy System (CERES) Algorithm Theoretical Basis Document. *Volume II—Geolocation, Calibration, and ERBE-Like Analyses (Subsystems 1–3)*

5. FUNDING NUMBERS
WU 148-65-41-01

6. AUTHOR(S)
CERES Science Team

7. PERFORMING ORGANIZATION NAME(S) AND ADDRESS(ES)
NASA Langley Research Center
Hampton, VA 23681-0001

8. PERFORMING ORGANIZATION REPORT NUMBER
L-17521

9. SPONSORING/MONITORING AGENCY NAME(S) AND ADDRESS(ES)
National Aeronautics and Space Administration
Washington, DC 20546-0001

10. SPONSORING/MONITORING AGENCY REPORT NUMBER
NASA RP-1376, Volume II

11. SUPPLEMENTARY NOTES

12a. DISTRIBUTION/AVAILABILITY STATEMENT
Unclassified–Unlimited
Subject Category 47
Availability: NASA CASI (301) 621-0390

12b. DISTRIBUTION CODE

13. ABSTRACT *(Maximum 200 words)*

The theoretical bases for the Release 1 algorithms that will be used to process satellite data for investigation of the Clouds and Earth's Radiant Energy System (CERES) are described. The architecture for software implementation of the methodologies is outlined. Volume II details the techniques used to geolocate and calibrate the CERES scanning radiometer measurements of shortwave and longwave radiance to invert the radiances to top-of-the-atmosphere (TOA) and surface fluxes following the Earth Radiation Budget Experiment (ERBE) approach, and to average the fluxes over various time and spatial scales to produce an ERBE-like product. Spacecraft ephemeris and sensor telemetry are used with calibration coefficients to produce a chronologically ordered data product called bidirectional scan (BDS) radiances. A spatially organized instrument Earth scan product is developed for the cloud-processing subsystem. The ERBE-like inversion subsystem converts BDS radiances to unfiltered instantaneous TOA and surface fluxes. The TOA fluxes are determined by using established ERBE techniques. Hourly TOA fluxes are computed from the instantaneous values by using ERBE methods. Hourly surface fluxes are estimated from TOA fluxes by using simple parameterizations based on recent research. The averaging process produces daily, monthly-hourly, and monthly means of TOA and surface fluxes at various scales. This product provides a continuation of the ERBE record.

14. SUBJECT TERMS
Earth Observing System; Clouds and the Earth's Radiant Energy System; Earth radiation budget; Clouds satellite measurements; Surface radiation; Atmospheric radiative divergence

15. NUMBER OF PAGES
136

16. PRICE CODE
A07

17. SECURITY CLASSIFICATION OF REPORT	18. SECURITY CLASSIFICATION OF THIS PAGE	19. SECURITY CLASSIFICATION OF ABSTRACT	20. LIMITATION OF ABSTRACT
Unclassified	Unclassified	Unclassified	